Random matrices and chaos in nuclear physics: Nuclear structure

H. A. Weidenmüller

Max-Planck-Institut für Kernphysik, D-69029 Heidelberg, Germany

G. E. Mitchell

North Carolina State University, Raleigh, North Carolina 27695, USA
and Triangle Universities Nuclear Laboratory, Durham, North Carolina 27706, USA

(Published 8 May 2009)

Evidence for the applicability of random-matrix theory to nuclear spectra is reviewed. In analogy to systems with few degrees of freedom, one speaks of chaos (more accurately, quantum chaos) in nuclei whenever random-matrix predictions are fulfilled. An introduction into the basic concepts of random-matrix theory is followed by a survey over the extant experimental information on spectral fluctuations, including a discussion of the violation of a symmetry or invariance property. Chaos in nuclear models is discussed for the spherical shell model, for the deformed shell model, and for the interacting boson model. Evidence for chaos also comes from random-matrix ensembles patterned after the shell model such as the embedded two-body ensemble, the two-body random ensemble, and the constrained ensembles. All this evidence points to the fact that chaos is a generic property of nuclear spectra, except for the ground-state regions of strongly deformed nuclei.

DOI: 10.1103/RevModPhys.81.539 PACS number(s): 24.60.Lz, 25.70.Gh, 21.60.Cs, 21.60.Ev

CONTENTS

I. INTRODUCTION

In the 1970s, chaos became a household word for physicists. Chaos had been known to mathematicians, astrophysicists, and other specialists since the early years of the 20th century. It took the advent of the personal computer to make chaos generally known: The exponential divergence of the trajectories of a chaotic system with Hamiltonian dynamics could easily be simulated. Many Hamiltonian systems, especially those with few degrees of freedom, have been analyzed since. The subject has been reviewed, for instance, by Gutzwiller (1990).

In the wake of this development, physicists in several fields became interested in quantum manifestations of classical chaos ("quantum chaos"). Again, this caused a flurry of activity, especially in the study of systems with few degrees of freedom; see McDonald and Kaufman (1979), Casati *et al.* (1980), and Berry (1981). The work culminated in the Bohigas-Giannoni-Schmit (1984) conjecture. The conjecture connects the spectral fluctuation properties of quantum systems that are chaotic in the classical limit with predictions of random-matrix theory (RMT). A summary of these developments has been given by Haake (2001).

Independently of these developments and preceding them, RMT had been developed in the framework of nuclear physics by Wigner and Dyson—see Porter (1965). Data accumulated in the 1960s and analyzed in the 1980s provided evidence that nuclear spectra follow RMT predictions. The wide interest enjoyed by RMT in the 1980s among practitioners of quantum chaos had repercussions on nuclear physics: Nuclei are many-body systems, and chaos manifests itself here in ways different from those of few-degrees-of-freedom systems. At the same time, nuclei are paradigmatic for the applicability of RMT to fermionic many-body systems and for the occurrence of chaos in such systems. Thus much work was done to establish RMT and to analyze and interpret quantum chaos in nuclei.

The present review is the first part of a two-part series dealing with RMT and chaos in nuclear physics. It focuses on spectral properties of nuclei, while the second part will deal with RMT and chaos in nuclear reactions. Topics such as compound-nucleus scattering, Ericson fluctuations, isobaric analog resonances, and parity violation in epithermal neutron scattering are not dealt with here. The paper is intended as an introductory review to the field. It is aimed mainly at two groups of physicists, those who work on quantum chaos in fields different from nuclear physics, and nuclear physicists who wish to learn about RMT and chaos in nuclei. We assume accordingly no prior knowledge of RMT and chaos nor do we assume any detailed knowledge of nuclear physics. We aim at giving a comprehensive survey that is focused on concepts and illustrative examples while derivations and formulas are kept to a minimum. The last comprehensive review of the field was given in *Reviews of Modern Physics* over 25 years ago by Brody *et al.* (1981); a short review was later published by Bohigas and Weidenmüller (1988). Wherever possible, we have avoided giving a large number of references in favor of citing review articles: Readability of the article was our primary concern, followed by completeness.

In Sec. II, we motivate RMT and introduce those concepts of RMT that are frequently used in nuclear physics. We pay particular attention to the Gaussian orthogonal ensemble (GOE) of random matrices. We establish the connection between RMT and quantum chaos. In Sec. III, we describe those applications of RMT to nuclear spectra that do not make use of specific nuclear-structure concepts. Comparison between RMT predictions and spectroscopic data is used to establish the domain of applicability of RMT to nuclear spectra. Special attention is devoted to the breaking of isospin symmetry, and to a test of time-reversal invariance. The role of RMT and chaos in nuclear models is described in Sec. IV. We focus attention on the two most important nuclear-structure models, namely, the spherical shell model and the collective model in two of its versions, but also mention a number of other applications of RMT. Nuclei (and other fermionic many-body systems) are governed by the mean field (in nuclei, the shell model) and a residual interaction dominated by two-body forces. In such systems, the structure of the Hamiltonian is very different from that of a typical GOE matrix. That difference has given rise to a number of random-matrix ensembles that are closer in structure to the mean-field approach than is the GOE. These are treated in Sec. V. Section VI contains a summary and conclusions.

II. RANDOM MATRICES

A. Why random matrices?

Random matrices were introduced to nuclear physics in the 1960s by Wigner [see Wigner's papers in Porter (1965)]. That step was preceded (and probably motivated) by Bohr's insight that nuclei are systems of great complexity. It is useful to recall the arguments that led Bohr (1936) to this insight.

Experiments in the 1930s, especially by Fermi and his group in Rome on neutron scattering by light nuclei, had revealed the existence of numerous narrow resonances (Fermi *et al.*, 1934, 1935). We show in Fig. 1 data of a similar type taken in the 1950s by Rainwater and his group at Columbia University (Garg *et al.*, 1964). That group used time-of-flight spectroscopy of slow neutrons to measure the total neutron cross section on a number of heavy even-even nuclei (nuclei with even numbers of protons and neutrons). The cross section versus neutron energy E_n shown in Fig. 1 for the target nucleus ^{232}Th displays narrow resonances with widths <1 eV and spacings of about 20 eV. The target nucleus ^{232}Th has spin 0 and positive parity; the incident slow neutrons carry zero angular momentum and have spin $\frac{1}{2}$. Therefore, the

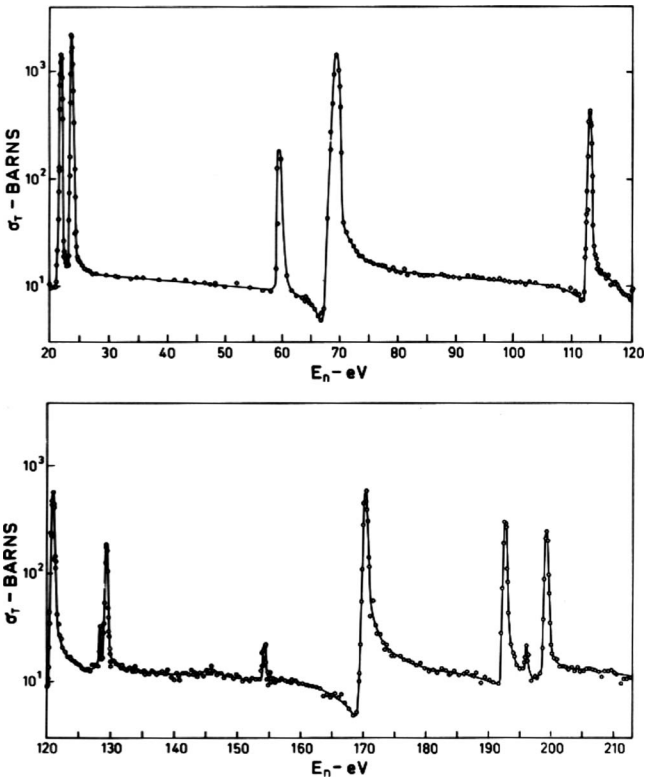

FIG. 1. The total neutron cross section on ^{232}Th vs neutron energy E_n in eV. From Neutron Cross Section, 1964, as reproduced in Bohr and Mottelson, 1969, Vol. 1, p. 178.

resonances all have spin/parity $1/2^+$. These resonances correspond to excited states of the "compound nucleus" ^{233}Th with an excitation energy slightly above the neutron separation energy of 4.786 MeV (the "neutron threshold"). The number of resonances observed in each compound nucleus was limited by the resolution of the spectrometer and was never much larger than 200. Similar data on proton resonances at the Coulomb barrier in lighter nuclei were later taken by the Triangle Universities group (Wilson *et al.*, 1975). Together these data form what has been called the "nuclear data ensemble" by Haq *et al.* (1982) and Bohigas *et al.* (1983).

Bohr argued that the existence of numerous narrowly spaced and narrow compound-nucleus resonances was incompatible with independent-particle motion and was due to strong nucleon-nucleon interactions. Indeed, assuming an independent-particle model with a nuclear radius of about 5 fm and a potential well depth of several 10 MeV, one finds that the single-particle states have a typical spacing of several hundred keV and widths of the order of 10 keV or larger, in complete disagreement with the data. To account qualitatively for the data, Bohr proposed his compound-nucleus model (Fig. 2): The incident nucleon carries kinetic energy (as indicated by the billiard cue), collides with the nucleons in the target, and shares its energy with many nucleons. In units of the time for passage of the nucleon through the nuclear interior, it takes the system a long time until one of its constituent nucleons acquires sufficient energy to be reemitted from the system.

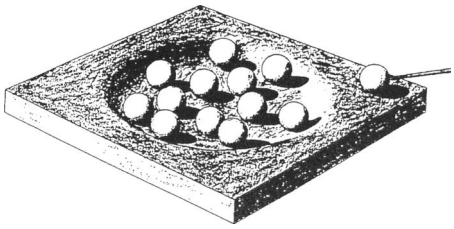

FIG. 2. Bohr's wooden toy model of the compound nucleus. From Nature, 1936.

Bohr's idea that the nucleus is a complex, strongly interacting system was adopted by the community and held sway until the discovery of the nuclear shell model in 1949. Bohr's idea almost certainly motivated Wigner to introduce random matrices. To explain the spirit of the approach, we focus attention on nuclear levels with the same quantum numbers (total spin J, parity Π, and, at least in light nuclei, total isospin T) and ask the following: Can we identify generic spectral properties of a system with strong interactions? Figure 3 shows six spectra, all having the same total number of levels, and spanning the same total energy interval, and therefore having the same average level spacing. The spectra differ only in the way the spacings between neighboring levels are distributed. For the one-dimensional harmonic oscillator (the rightmost spectrum), all spacings are identical. The spacing distributions differ more and more from a delta function as we go ever more to the left. The random-matrix approach characterizes spectra by their fluctuation properties: The distribution of spacings of nearest neighbors is the first and obvious measure for spectral

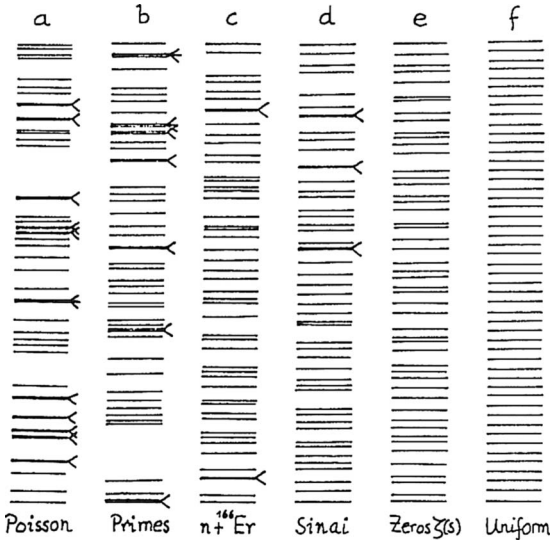

FIG. 3. Six spectra with 50 levels each and the same mean level spacing. From right to left: The one-dimensional harmonic oscillator, a sequence of zeros of the Riemann zeta function, a sequence of eigenvalues of the Sinai billiard (see Sec. II.F), a sequence of resonances seen in neutron scattering on ^{166}Er, a sequence of prime numbers, and a set of eigenvalues obeying Poisson statistics (see Sec. II.F). From Bohigas and Giannoni, 1984.

fluctuations. It is referred to as the nearest-neighbor spacing (NNS) distribution. There are other measures such as the correlation between nearest spacings, between next-nearest spacings, etc. Some of these are introduced below.

To implement this approach, we need to develop a statistical theory of spectra. Random matrices provide the tool to do so. Instead of considering the actual nuclear Hamiltonian (which was not known in the 1950s), we consider an ensemble of Hamiltonians (each given in matrix form). The ensemble is defined in terms of some probability distribution for the matrix elements, hence the name random matrices. The ensemble is chosen in such a way that the member Hamiltonians incorporate generic features. The spectral distribution functions are calculated as averages over the ensemble and are compared with the actual fluctuation properties of nuclear spectra.

Canonical random-matrix theory (RMT) as developed by Wigner and Dyson [see Porter (1965)] classifies systems by their symmetry properties. Nuclei are invariant under time reversal. The matrix representation of the nuclear Hamiltonian can accordingly be chosen real and symmetric. The random-matrix ensemble, which is considered almost exclusively in this review, is therefore an ensemble of real and symmetric matrices.

The random-matrix approach does not aim at calculating individual spectra and at comparing them with data. Rather, one determines the joint probability distribution of the eigenvalues and from here calculates certain spectral fluctuation measures such as the NNS distribution as averages over the ensemble. RMT contains one (or, in the general case, a number of) input parameter(s). In the case of spectral fluctuations, that input parameter is the average nuclear level spacing. The fluctuation measures predicted by RMT are scaled by the average level spacing and are thus parameter-free. If the observed spectral fluctuation properties agree with RMT predictions, and if no further information on the system is available, one concludes that the system is generic. This implies that no information beyond the average nuclear level spacing can be deduced from the available spectral information. If, on the other hand, the data do not agree with RMT predictions, this indicates that the spectrum is not generic and the available spectral information may be used to deduce further properties of the system. The harmonic oscillator in one dimension is a case in point.

The random-matrix approach to spectral fluctuations (and to other properties of complex systems) has some similarity to classical thermodynamics. There one is also interested in a generic description of systems in terms of a few parameters. These parameters (specific heat, magnetic susceptibility, etc.) are system specific, but within the framework of classical thermodynamics they need not be determined from the system's Hamiltonian. In that sense, classical thermodynamics and random-matrix theory are phenomenological theories that do not refer to an underlying system-specific Hamiltonian. The random-matrix approach differs fundamentally from the dynamical approach used in most fields of physics where one integrates the equations of motion and fits a few parameters of an (otherwise known) Hamiltonian to the data. Similar to classical thermodynamics, the random-matrix approach has been applied to many systems beyond nuclear physics (Guhr *et al.*, 1998).

B. The Gaussian orthogonal ensemble

In Secs. II.B and II.C, we define the Gaussian orthogonal ensemble (GOE) and collect and interpret a number of results for this ensemble. We also introduce the Gaussian unitary ensemble (GUE). Proofs may be found in Porter (1965) and Mehta (2004). For the GOE, we consider real and symmetric Hamiltonian matrices H in a Hilbert space of dimension N. With $\mu,\nu=1,\ldots,N$, the matrix elements obey $H_{\mu\nu}=H_{\nu\mu}=H_{\mu\nu}^*$. For realistic systems Hilbert space is infinite dimensional, so we consider the limit $N\to\infty$ in what follows. The ensemble is defined in terms of an integration over matrix elements. The volume element in matrix space,

$$d[H]=\prod_{\mu\leqslant\nu} dH_{\mu\nu}, \tag{1}$$

is the product of the differentials $dH_{\mu\nu}$ of the independent matrix elements (i.e., of the matrix elements not connected by symmetry). The ensemble is defined by the probability density $\mathcal{P}(H)$ of the matrices H,

$$\mathcal{P}(H)d[H]=\mathcal{N}_0\exp\left\{-\frac{N}{4\lambda^2}\mathrm{Tr}(H^2)\right\}d[H]. \tag{2}$$

Here $\mathcal{N}_0$ is a normalization factor and λ is a parameter. This parameter defines the average level density [see Eq. (14)]. In applications of the GOE to data, λ is determined by the empirical average level density. The spectral fluctuation properties of the GOE are then predicted in a parameter-free fashion.

The Gaussian weight factor is a cutoff that ensures convergence of the ensemble averages of observables for large values of the integration variables. We use the symmetry of the matrices to write the trace in the exponent as $\Sigma_{\mu<\nu}2H_{\mu\nu}^2+\Sigma_\mu H_{\mu\mu}^2$. Then the probability density

$$\mathcal{P}(H)d[H]=\mathcal{N}_0\prod_\mu \exp\left\{-\frac{N}{4\lambda^2}H_{\mu\mu}^2\right\}dH_{\mu\mu} \times\prod_{\rho<\sigma}\exp\left\{-\frac{N}{2\lambda^2}H_{\rho\sigma}^2\right\}dH_{\rho\sigma} \tag{3}$$

is a product of terms each of which depends only on a single matrix element. Therefore, the GOE has the following properties: The independent matrix elements are uncorrelated Gaussian-distributed random variables with zero mean value and a second moment given by

$$\overline{H_{\mu\nu}H_{\rho\sigma}}=\frac{\lambda^2}{N}(\delta_{\mu\rho}\delta_{\nu\sigma}+\delta_{\mu\sigma}\delta_{\nu\rho}). \tag{4}$$

Here the overbar denotes the ensemble average. Defining the GOE by these properties is equivalent to the definition (2).

While the form of the probability measure in Eq. (2) is fixed by symmetry requirements, the Gaussian cutoff in that equation seems completely arbitrary. However, using plausible assumptions one can actually derive that factor. Rosenzweig and Porter (1960) have shown that the distribution (2) is obtained when one assumes that the ensemble is orthogonally invariant, and that matrix elements not connected by symmetry are statistically independent. Also Balian (1968) has derived the distribution (2) from a maximum entropy principle.

In the GOE, every state in Hilbert space is connected to itself and to every other state by a matrix element of H. Since all nondiagonal matrix elements have the same first and second moments, every state is coupled to all other states with equal average strength. This results in level repulsion between any pair of levels, and in a complete mixing of states in Hilbert space. The importance of such coupling is seen when we consider a more general ensemble with probability density

$$\mathcal{P}_\alpha(H)d[H] = \tilde{\mathcal{N}}_0 \prod_\mu \exp\left\{-\frac{N}{4\lambda^2}H_{\mu\mu}^2\right\} dH_{\mu\mu} \times \prod_{\rho<\sigma} \exp\left\{-\frac{N}{2\alpha\lambda^2}H_{\rho\sigma}^2\right\} dH_{\rho\sigma}, \tag{5}$$

where the positive parameter α ranges from 0 to 1. For $\alpha=0$, all nondiagonal elements vanish, and the ensemble (5) consists of diagonal matrices with independent, Gaussian-distributed diagonal elements. The shape of the average spectrum is Gaussian, there is no level repulsion, and the spectral fluctuations are Poissonian (see Sec. II.F). For $\alpha=1$, the ensemble coincides with the GOE. For values of α between these two limits, the shape of the spectrum and the spectral fluctuations interpolate between those two limiting cases. Significant mixing between levels occurs when the mean-square mixing matrix element $\overline{H_{\mu\nu}^2}$ with $\mu\neq\nu$ is roughly equal to the square of the mean level spacing. Taking for the latter the GOE value $d=\pi\lambda/N$ at the center of the semicircle [see Eq. (14)], we find that significant mixing occurs when α is of order $1/\sqrt{N}$. We see that for $N\to\infty$, mixing sets in as soon as α differs from zero. These observations are used in Secs. III.D.1 and III.D.4.

Reality and symmetry of the matrices $H_{\mu\nu}$ are preserved under orthogonal transformations of the basis. The ensemble (2) is chosen accordingly in such a way that it is invariant under such transformations: With each matrix H belonging to the ensemble, all matrices obtained from H by orthogonal transformations also belong to the ensemble. As a consequence, there does not exist a preferred direction in Hilbert space, and the ensemble is generic. Because of that invariance and the Gaussian cutoff, the ensemble is referred to as the Gaussian orthogonal ensemble of random matrices.

Instead of the $N(N+1)/2$ integration variables $H_{\mu\nu}$ with $\mu\leqslant\nu$ used in Eq. (2), we may use the N eigenvalues E_μ of the matrices H and the $N(N-1)/2$ generators of the orthogonal transformation O, which diagonalizes H. Then the volume element dH takes the form

$$dH = dO \prod_{\mu<\nu} |E_\mu - E_\nu| \prod_\rho dE_\rho. \tag{6}$$

The factor dO represents the Haar measure of the orthogonal group in N dimensions. [The Haar measure is the unique invariant measure that can be assigned to every compact group and that is used to define integrals over that group (Conway, 1990).] The probability density $\mathcal{P}(H)$ takes the form

$$\mathcal{P}(H)d[H] = \mathcal{N}_0 dO \exp\left\{-\frac{N}{4\lambda^2}\sum_\mu E_\mu^2\right\} \times \prod_{\rho<\sigma} |E_\rho - E_\sigma| \prod_\nu dE_\nu. \tag{7}$$

The right-hand side of Eq. (7) is the product of two factors. One factor depends only on the eigenvalues, and the other only on the diagonalizing matrices. It follows that the eigenvalues and the eigenvectors of the matrices H are uncorrelated random variables. In the limit $N\to\infty$, the projections of the eigenvectors onto an arbitrary direction in Hilbert space have a Gaussian distribution. Some properties of the eigenvalue distribution can be read off directly from Eq. (7). The factor $\Pi_{\mu<\nu}|E_\mu - E_\nu|$ stems from the volume element in matrix space and reflects the orthogonal invariance of the ensemble. It causes the probability density for the eigenvalues to go to zero as two eigenvalues approach each other. This is a manifestation of level repulsion, a basic feature of quantum mechanics.

Another property of the GOE is displayed when we write the probability density in the form

$$\mathcal{P}(H)d[H] = \mathcal{N}_0 dO \prod_\mu dE_\mu \exp\left\{-\frac{N}{4\lambda^2}\sum_\nu E_\nu^2 + \sum_{\rho<\sigma} \ln|E_\rho - E_\sigma|\right\}. \tag{8}$$

For the interpretation of the eigenvalue distribution in Eq. (8), we use an analogy to classical statistical mechanics. We consider the eigenvalues E_μ as position coordinates of N particles in one dimension. The probability density of the eigenvalues in Eq. (8) then has the form of the canonical partition function (integrated over the momentum variables) of a gas of N classical point particles with repulsive two-body interactions ("Coulomb gas") moving in a common harmonic-oscillator potential at inverse temperature $\beta=1$. The particles will tend to keep apart as much as is consistent with the overall harmonic-oscillator potential. This property leads to the "spectral stiffness" of the GOE discussed below.

Besides the GOE, there exist two more canonical random-matrix ensembles: The Gaussian unitary ensemble (GUE) and the Gaussian symplectic ensemble (GSE). The GUE is the Gaussian ensemble of Hermitian (but not necessarily real) matrices. This ensemble plays a role for systems that are not time-reversal invariant. If that invariance does not hold, the Hamiltonian matrix is Hermitian but cannot in general be chosen real

and symmetric. In nuclear physics, the GUE is used for tests of time-reversal invariance. It is also used as a theoretical testing ground because the calculation of ensemble averages over observables is typically simpler for the GUE than for the GOE. For these reasons, we briefly introduce the GUE in the next paragraphs. The GSE applies to systems with half-integer spin that are invariant under time reversal but not rotationally invariant. The GSE does not apply to nuclei directly [see, however, Lombardi *et al.* (1994)] and is not discussed in this review. In addition to the three canonical ensembles introduced by Dyson [see Porter (1965)] and often distinguished by the label β with $\beta=1$ for the GUE, $\beta=2$ for the GOE, and $\beta=4$ for the GSE, there exist seven more random-matrix ensembles that are defined in terms of invariance requirements (Altland and Zirnbauer, 1997); their construction is based upon Cartan's classification of Lie groups [see Chevalley (1946)]. Some of these ensembles play a role in the low-energy behavior of quantum field theories and find application in lattice QCD, the discretized form of quantum chromodynamics. Others relate to the scattering of electrons off the interphase between a normal conductor and a superconductor.

For the GUE, the independent variables are the real and imaginary parts of the complex elements $H_{\mu\nu}^{\mathrm{GUE}}$ of the Hamiltonian (a matrix of dimension N). The invariant measure has the form

$$d[H^{\mathrm{GUE}}] = \prod_{\mu<\nu} d[\mathrm{Re}\, H_{\mu\nu}^{\mathrm{GUE}}] d[\mathrm{Im}\, H_{\mu\nu}^{\mathrm{GUE}}] \prod_{\sigma} dH_{\sigma\sigma}^{\mathrm{GUE}}. \tag{9}$$

With this definition, the equation for the probability density of the GUE is similar to Eq. (2) and reads

$$\mathcal{P}(H^{\mathrm{GUE}}) d[H^{\mathrm{GUE}}] = \mathcal{N}_0 \exp\left\{-\frac{N}{2\lambda^2}\mathrm{Tr}(H^{\mathrm{GUE}})^2\right\} d[H^{\mathrm{GUE}}]. \tag{10}$$

The GUE is invariant under unitary transformations of Hilbert space. The real and imaginary parts of the matrix elements are uncorrelated random variables with equal Gaussian probability distributions centered at zero. The factors in the exponent are chosen in such a way that the second moments have the values

$$\overline{H_{\mu\nu}^{\mathrm{GUE}} H_{\rho\sigma}^{\mathrm{GUE}}} = \frac{\lambda^2}{N}\delta_{\mu\sigma}\delta_{\nu\rho}. \tag{11}$$

Level repulsion in the GOE is linear; see Eqs. (7) and (19). This is a consequence of orthogonal invariance. In the GUE, the transformation to eigenvectors and eigenvalues as new integration variables involves a unitary transformation $\mathcal{U}$ and yields

$$\mathcal{P}(H^{\mathrm{GUE}}) d[H^{\mathrm{GUE}}] = \mathcal{N}_0 d\mathcal{U} \exp\left\{-\frac{N}{2\lambda^2}\sum_{\mu} E_\mu^2\right\} \times \prod_{\rho<\sigma} (E_\rho - E_\sigma)^2 \prod_{\nu} dE_\nu. \tag{12}$$

Here $d\mathcal{U}$ denotes the Haar measure of the unitary group in N dimensions. Instead of the factor $|E_\rho - E_\sigma|$ occurring in Eq. (7), Eq. (12) contains the factor $(E_\rho - E_\sigma)^2$. As a result, level repulsion for the GUE is quadratic. That difference between GOE and GUE is easily understood: In the GOE, the coupling of any pair of levels is described by a single parameter, namely, the real coupling matrix element. For two levels to have a small spacing, the value of that parameter must be small. In the GUE, the coupling is described by two parameters, namely, the real and imaginary parts of the coupling matrix element. For two levels to have a small spacing, both parameters must be small, and the probability of small spacings is reduced accordingly.

As concerns the GUE analog of Eq. (8), the form of the volume element in matrix space leads to a different inverse temperature $\beta=2$, while for the GSE we have $\beta=4$. The "Dyson parameter" β with $\beta=1$, 2, and 4 is often used to label the three canonical random-matrix ensembles GUE, GOE, and GSE.

C. Properties of the GOE

1. Average level density

A central property of the GOE is the mean level density $\rho(E)$, a function of the energy E. It is defined as

$$\rho(E) = \overline{\sum_{\mu} \delta(E - E_\mu)} \tag{13}$$

and, for $N\to\infty$, given by

$$\rho(E) = \frac{N}{\pi\lambda}\sqrt{1 - \left(\frac{E}{2\lambda}\right)^2}. \tag{14}$$

The average spectrum extends from -2λ to $+2\lambda$. This confinement of the spectrum to a finite stretch of the energy axis is a consequence of the Gaussian cutoff (or, for that matter, of any other sufficiently strong cutoff factor), and of the factor N in the exponent of Eq. (2). When plotted versus $E/4\lambda$, $\rho(E)$ has the shape of a semicircle. (That shape is specific for the Gaussian cutoff.) That is why Eq. (14) is often referred to as "Wigner's semicircle law." The factor N on the right-hand side of Eq. (14) ensures that $\rho(E)$ is normalized to the total number of levels. The mean level spacing $d(E)$ is defined by

$$d(E) = \rho^{-1}(E) \tag{15}$$

and tends to zero as $N\to\infty$ because we fit a spectrum of N eigenvalues into a finite energy interval of length 4λ. At the center of the spectrum, we have $d(0)=\pi\lambda/N$.

2. Universality

The form of the spectrum is due to the Gaussian cutoff factor. That form is obviously totally unrealistic: Hardly any real physical system possesses such a spectrum. While reality and symmetry of the matrices $H_{\mu\nu}$ reflect time-reversal invariance and are thus a consequence of quantum theory, the Gaussian cutoff is not, although the arguments of Rosenzweig and Porter (1960) and of Balian (1968) lend some plausibility to its use. The Gaussian cutoff is preferred from a practical point of view, of course, because of the ease with which Gaussian integrals can be performed. But the GOE is physically interesting only if it furnishes information that is independent of the form of the cutoff factor. That property is guaranteed by the universality of the GOE.

In using the GOE, we are usually not interested in the overall shape of the spectrum. Interest focuses rather on local spectral fluctuation properties such as the NNS distribution or correlations between level spacings. These are predicted in a parameter-free fashion. That means that all local spectral fluctuation properties are functions of a dimensionless parameter s, which is the ratio of the actual level spacing and the mean level spacing. Local spectral fluctuations characterize properties of the spectrum on an energy scale that in the limit $N\to\infty$ is negligibly small compared to the length 4λ of the spectrum. On that scale, the spectral fluctuations are universal: As functions of the parameter s, they have the same form for both the GOE and all non-Gaussian cutoff factors, as long as the latter are orthogonally invariant and confine the spectrum to a finite singly connected piece of the energy axis (Hackenbroich and Weidenmüller, 1995).

Non-Gaussian cutoffs that obey that proviso modify the overall shape of the spectrum. In fact, for any given form of the spectrum it is always possible to find a cutoff factor such that the resulting random-matrix ensemble has an average spectrum of that form. The local fluctuation properties are unaffected by such a choice: In the limit $N\to\infty$, the local fluctuation properties separate from the global spectral properties and become universal.

3. Ergodicity

Theoretical predictions of the GOE are obtained as averages over the ensemble. How can we compare such predictions in a meaningful way with data that, after all, are taken from a physical system with a single Hamiltonian (and not from an ensemble of Hamiltonians)? That question is answered by the property of ergodicity of the GOE. Spectral data on a given system can be used to calculate spectral measures such as the mean level spacing or the NNS distribution as running averages over the spectrum. We denote such a running average by angular brackets. We would like to ascertain that $\bar{O}=\langle O\rangle$ holds true for all members of the ensemble and for all observables O that describe local spectral properties. That equation cannot be proved in general because there is no way to evaluate $\langle O\rangle$ in the framework of the GOE. It is possible, however, to prove the slightly weaker statement (Brody *et al.*, 1981)

$$\overline{(\bar{O}-\langle O\rangle)^2}=0. \tag{16}$$

The proof is made possible because all terms on the left-hand side are ensemble averages. The statement says that for almost all members of the ensemble [with the exception of a set of measure zero and the measure defined in Eq. (1)], the running average of an observable O (calculated for a single member of the ensemble) is equal to the ensemble average of the observable. That property is referred to as ergodicity. The name derives from the formal similarity of the statement with ergodicity in classical statistical mechanics (equality of phase-space average and time average along a single trajectory).

4. Information content of GOE spectra

Equation (3) shows that in the GOE every state in Hilbert space is coupled to every other one by a Gaussian-distributed random-matrix element: In the GOE, all states in Hilbert space are completely mixed with each other. Choosing the parameters N and λ and drawing all independent matrix elements from the resulting Gaussian distribution generates a random GOE matrix. Diagonalizing that matrix yields a GOE spectrum. By construction, that spectrum contains no information beyond the input parameters N and λ. In particular, the spectral fluctuations are void of physical information. If the spectral fluctuations of an experimental spectrum agree with GOE predictions, and if there is no further information on that system, then the spectral data alone cannot be used to extract any physical information on the system beyond the mean level density.

That conclusion is also reached when we ask the following: How many pieces of spectral data are needed to determine the underlying Hamiltonian H? In the case of a GOE spectrum, counting shows that we need all N eigenvalues and all N orthonormal eigenfunctions to determine the $N(N+1)/2$ independent matrix elements of H. This must be compared with the usual dynamical approach to physical systems where the Hamiltonian is given in terms of a few (say n) parameters. Then n pieces of data suffice to determine the Hamiltonian. Further data can be used to check the consistency of the underlying theory.

D. GOE fluctuation measures

1. Porter-Thomas distribution

We recall that in the GOE eigenvalues and eigenfunctions are uncorrelated random variables. For $N\to\infty$, the projections of the eigenfunctions onto an arbitrary vec-

tor in Hilbert space have a Gaussian distribution centered at zero. Therefore, the squares ψ^2 of such projections have a χ^2 distribution with one degree of freedom. We introduce the variable

$$y = \psi^2/\overline{\psi^2}. \tag{17}$$

The resulting distribution is also known as the Porter-Thomas distribution and has the form

$$P(y) = \frac{1}{\sqrt{2\pi y}} \exp(-y/2). \tag{18}$$

The function $P(y)$ is given in terms of the mean value $\Gamma = \overline{\psi^2}$. That parameter is an input parameter that is not predicted by random-matrix theory. The distribution can be checked experimentally: Transition probabilities of nuclear levels to a fixed final state and decay widths to a fixed channel are proportional to squares of matrix elements containing the nuclear wave functions. These matrix elements can be read as projections of the wave functions onto a particular vector in Hilbert space.

It may happen that the mean value Γ undergoes a secular variation. This is the case, for instance, for doorway states. Then it is necessary to "unfold" the fluctuations by scaling the intensities properly; see Sec. II.G.

2. Nearest-neighbor-spacing distribution and Δ_3 statistic

It takes substantial theoretical effort to work out the spectral fluctuation measures in the GOE. That is not described here. We confine ourselves to introducing two fluctuation measures that have found wide application in the analysis of experimental data: The nearest-neighbor-spacing (NNS) distribution $P(s)$ and the Δ_3 statistic due to Dyson and Mehta. These are obtained in the limit $N \to \infty$. Prior to using these measures for data analysis, it is necessary to unfold the experimental spectra; see Sec. II.D.3.

The NNS distribution $P(s)$ depends on s, which is the ratio of the actual level spacing and the mean level spacing d. It cannot be given in closed form. An excellent approximation due to Wigner is known as the Wigner surmise,

$$P(s) = \frac{\pi}{2} s \exp(-\pi s^2/4). \tag{19}$$

The linear increase with s for small s is due to GOE level repulsion as displayed in Eq. (7). Universality shows that the Gaussian falloff is not related to the Gaussian cutoff factor defining the GOE and simply accounts for the fact that very large spacings are unlikely to occur. The exact expression for $P(s)$ was first derived by Gaudin (1961). $P(s)$ is displayed in Fig. 4.

The NNS distribution describes the distribution of level spacings but does not contain information about their correlations. Such information is contained in another fluctuation measure, the Δ_3 statistic. The number staircase function

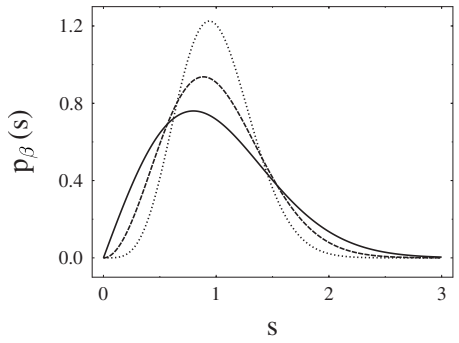

FIG. 4. The nearest-neighbor-spacing (NNS) distribution of the GOE (solid line) vs s, the ratio of the actual level spacing and the mean level spacing. For comparison, we also show the NNS distributions for the GUE (dashed line) and the GSE (dotted line). The parameter β is the Dyson index with $\beta=1$, 2, and 4 for GUE, GOE, and GSE, respectively.

$$\mathcal{N}(E) = \int_{-\infty}^{E} dE' \sum_{\mu} \delta(E' - E_\mu) \tag{20}$$

counts the number of eigenvalues below energy E. With increasing energy, it increases by unity as E passes a (nondegenerate) eigenvalue and is otherwise constant. The number of eigenvalues in the energy interval $[E_0, E_0+L]$ is given by $n(E_0,L) = \mathcal{N}(E_0+L) - \mathcal{N}(E_0)$. By definition of the mean level spacing $d(E)$, we have $\overline{n(E_0,L)} = L/d(E_0)$. [We use that, for $N \to \infty$, $d(E)$ is constant (independent of E) in any energy interval containing a finite number of levels.] The number variance $\Sigma^2_\beta(L) = \overline{n^2(E_0,L)} - (\overline{n(E_0,L)})^2$ is a fluctuation measure that contains information about correlations between level spacings. Suppose, for instance, that actual GOE spectra can be constructed by drawing spacings at random from the NNS distribution. In this case, $\Sigma^2_\beta(L)$ would grow linearly with L. In fact $\Sigma^2_\beta(L)$ is, for large L, proportional to $\ln L$. The slow growth indicates that large spacings and small spacings do not follow each other at random but almost alternate, and reflects the "stiffness" of GOE spectra; see the text below Eq. (8). For the three canonical ensembles, the number variance is shown in Fig. 5. The number variance is seldom used in nuclear physics because it fluctuates too strongly; one uses the Δ_3 statistic by Dyson and Mehta instead. The latter is defined by

$$\Delta_3(L) = \min_{a,b} \frac{1}{L} \left\langle \int_{E_0}^{E_0+L} dE' \overline{[\mathcal{N}(E') - a - bE']^2} \right\rangle_{E_0}. \tag{21}$$

We integrate the ensemble average of the square of the difference between the number staircase function and the straight line $(a+bE')$ over an energy interval, divide by the length L of that interval, and minimize the result with respect to the parameters a and b of the straight line. The angular brackets denote an average over the initial point E_0. It can be shown that $\Delta_3(L)$ can be written as an integral over the number variance $\Sigma^2_\beta(L)$.

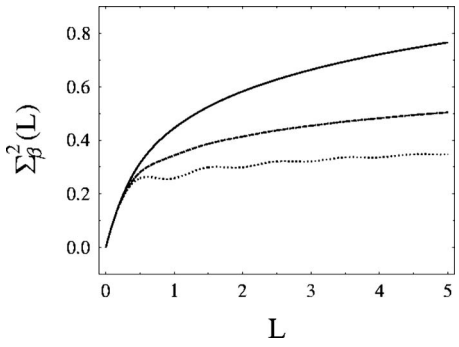

FIG. 5. The number variance vs the length L of the interval (L is in units of the mean level spacing) for the three canonical ensembles. Top curve, GOE; middle curve, GUE; bottom curve, GSE. The parameter β is the Dyson index; see Fig. 4. From Guhr *et al.*, 1998.

Therefore, Δ_3 is much smoother than $\Sigma^2_\beta(L)$ and is better suited for data analysis. Similar to $\Sigma^2_\beta(L)$, $\Delta_3(L)$ grows logarithmically with L. For large L,

$$\Delta_3(L) \approx \frac{1}{\pi^2}\{\ln L - 0.0687\}. \tag{22}$$

Similar to Σ^2, the Δ_3 statistic reflects the stiffness of GOE spectra and is often referred to as spectral stiffness. Figure 6 shows $\Delta_3(L)$ vs L for the GOE.

3. Unfolding of spectra: Purity and completeness

In the limit $N\to\infty$, the average level density $\rho(E)$ of the GOE in Eq. (14) is constant in every energy interval containing a finite number of levels, and the same is true of the average level spacing d. In nuclei, the situation differs: The level density grows nearly exponentially with energy. In many cases, even a fairly short stretch of levels displays this fact: The spacings of the lowest-lying levels are consistently larger than those of the highest-lying ones. That fact distorts the spectral fluctuation measures and must be taken into account prior to comparing data with GOE predictions. This is done by unfolding the spectra: The actual spectrum is modified such that the average level spacing is constant. GOE predictions relate to spectra consisting of levels with identical quantum numbers. Spectra obtained experimentally may be incomplete [i.e., miss levels (especially those with small or very large widths)], or not be pure (i.e., may contain levels with uncertain or incorrect quantum number assignments). It is important to know how lack of completeness and/or purity affects the comparison of data with GOE predictions.

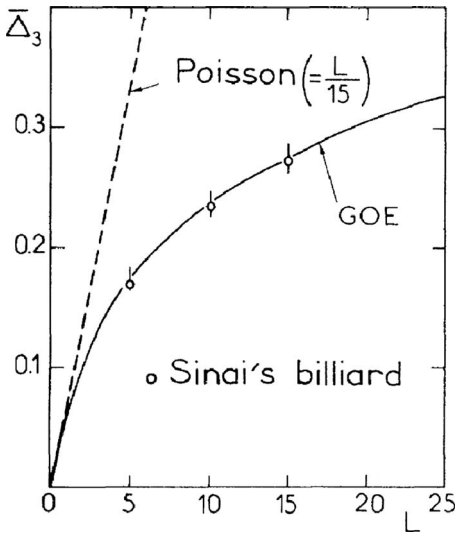

FIG. 6. The Δ_3 statistic for the Sinai billiard (open circles), the GOE prediction (solid line), and the Poisson result (dashed line). From Bohigas *et al.*, 1984.

Unfolding requires knowledge of the average level density $\rho(E)$ for the data at hand. The situation is easy if a theoretical prediction for the average level density is available. This is the case, for instance, in billiards (where a point particle moving in two dimensions is scattered elastically on some surface). Here the Weyl formula [see Baltes and Hilf (1976)] gives the average level density in closed form in terms of the area enclosed by the surface and the length of the boundaries of that surface. Given $\rho(E)$, the spectrum (or the spectra) is subsequently unfolded by mapping the eigenvalues E_μ onto new eigenvalues ε_μ by the prescription

$$\varepsilon_\mu = \int_{-\infty}^{E_\mu} dE\rho(E). \tag{23}$$

By construction, the new eigenvalues are dimensionless and have an average level spacing equal to unity. The ε_μ can be used to construct the NNS distribution and the Δ_3 statistic. We observe that the right-hand side of Eq. (23) is the average of the staircase function defined in Eq. (20). The unfolded eigenvalues ε_μ are the values of that function taken at E_μ. Usually, however, the exact form of the average level density is not known. If the data are obtained by numerical simulation of an ensemble (diagonalization of many matrices), the average level density is best found by numerically averaging over the ensemble. If we deal with an empirical spectrum of, say, several tens of levels, it is advantegeous to use the data to construct the staircase function rather than the level density (the representation of the latter in the form of a histogram depends on the bin width chosen), and to fit a low-order polynomial to that function. The unfolded eigenvalues are again given by the values of the fitted staircase function taken at the original eigenvalues E_μ.

How does the omission of levels affect spectral fluctuation properties? If a fraction f of levels is removed at random from a complete sequence (no missing levels, no levels with wrong quantum numbers), then the resulting correlation functions can easily be related to the correlation functions of the complete sequence (Bohigas and Pato, 2004). As a consequence, in the limit of large level numbers the information on spectral correlations is fully preserved provided f is known. In nuclei, levels with small widths are hard to detect and easily missed. But widths are theoretically predicted to be uncorrelated with the positions of eigenvalues. The removal of levels

with small widths is thus a random process, and the analysis of Bohigas and Pato (2004) applies. The fraction f can be estimated using the Porter-Thomas distribution and the experimental detection efficiency. The admixture to a complete sequence of levels with wrong quantum numbers can be treated similarly (Bohigas and Pato, 2004).

E. Discussion

The random-matrix approach described above is based on a few general principles: invariance of the system under time reversal (which leads to an ensemble of real and symmetric matrices), absence of a preferred direction in Hilbert space (which makes the ensemble generic and implies orthogonal invariance), and confinement of the spectrum to a singly connected finite stretch of the energy axis (which is realized for the Gaussian cutoff as well as for many other cutoff factors).

The GOE is universal: Cutoff factors different from the Gaussian cutoff but subject to the conditions formulated in Sec. II.C.2 lead to different forms of the average spectrum but to identical predictions for the local spectral fluctuation measures. GOE predictions of local spectral fluctuation measures are useful for the analysis of data because the ensemble is ergodic: For almost all members of the ensemble, the fluctuation measure calculated as an average over the ensemble equals the result obtained by taking a running average over the spectrum of that member.

It is rather amazing that the few principles just mentioned lead to parameter-free quantitative predictions for the local spectral fluctuation measures. Equation (18) gives the distribution law relevant for transition matrix elements and decay widths. Equations (19) and (22) present the two measures that are most frequently used for the analysis of spectral data. Needless to say, other fluctuation measures have also been worked out [see Brody *et al.* 1981].

Random-matrix theory predicts fluctuation properties in terms of mean values. In the examples treated so far, the input mean value has been the average of the squares of the projected wave functions as in Eq. (18), or the local average level density $\rho(E)$ (or the average level spacing d) as in Eqs. (19) and (22). Both parameters must be determined from the data. Then the theory predicts the distribution of the relevant observables. In case the level density changes significantly over the length of the given spectrum, an unfolding of the spectrum must precede the comparison with GOE predictions.

F. Random matrices and chaos

There exists a close connection between random matrices and quantum chaos. The latter term refers to quantum systems that are chaotic in the classical limit. In classical mechanics, chaos is a dynamical property characterized by the exponential divergence in time of trajectories starting in close-lying points of phase space. The phase space of a fully chaotic system is filled with such chaotic trajectories and is void of islands with regular dynamics. The analysis of chaos in classical conservative systems uses the existence of periodic orbits and was pioneered by Gutzwiller. The results are summarized in his book (Gutzwiller, 1990). Periodic-orbit theory has been successfully applied to many systems with few degrees of freedom (including systems that are not fully chaotic). To the best of our knowledge, a similarly complete understanding of chaos in classical many-body systems with their high-dimensional phase space does not exist. Atomic nuclei pose the additional difficulty that the matter density is very high. Even in the classical limit, it is not possible to neglect the fact that neutrons and protons are fermions. This fact leads to complications regarding periodic-orbit theory [see, for instance, Sommermann and Weidenmüller (1993), Weidenmüller (1993), and Sakhr and Whelan (2003)].

Since the late 1970s, much effort has been devoted to identifying the dynamical properties of quantum systems that are fully chaotic in the classical limit [see Gutzwiller (1990) and Haake (2001)]. There were two lines of development: Some looked for signals of classical chaos in the time evolution of wave packets, others focused attention on the fluctuation properties of eigenvalues and eigenfunctions of closed systems (which possess a discrete spectrum). Here we confine ourselves to the latter development, which has had repercussions in nuclear physics. Mounting numerical evidence from classically chaotic few-degrees-of-freedom systems due to McDonald and Kaufman (1979), Casati (1980), Berry (1981), and others culminated in the work of the Orsay group (Bohigas *et al.*, 1984) on the Sinai billiard: A point particle moving in two dimensions is scattered elastically by the interior surface of a square and by the exterior surface of a circle inscribed into the square. That system is fully chaotic and invariant under time reversal. Solving the Schrödinger equation for the Sinai billiard numerically, the Orsay group accumulated a sequence of about 1000 consecutive eigenvalues belonging to eigenfunctions of the same symmetry class. For a meaningful evaluation of the spectral fluctuation measures, their numerical accuracy had to be much better than the average level spacing. It was also important to make sure that no eigenvalue was missed. The Weyl formula [see Baltes and Hilf (1976)] was used to unfold the spectrum. The number of eigenvalues was large enough to evaluate for the first time the Δ_3 statistic (in addition to the NNS distribution, which had been used before). The results are shown in Figs. 6 and 7.

In the figures, the data on the Sinai billiard are compared with GOE predictions and with the Poisson distribution. The latter has an exponential form, is typical for regular (or integrable) systems (Berry and Tabor, 1977), and is explained below. The figures show excellent agreement between the results for the Sinai billiard and the GOE predictions. This agreement led Bohigas *et al.* (1984) to formulate the following conjecture [the Bohigas-Giannoni-Schmit (BGS) conjecture]: The spectral fluctuation properties of a quantum system that is fully chaotic in the classical limit coincide with those of

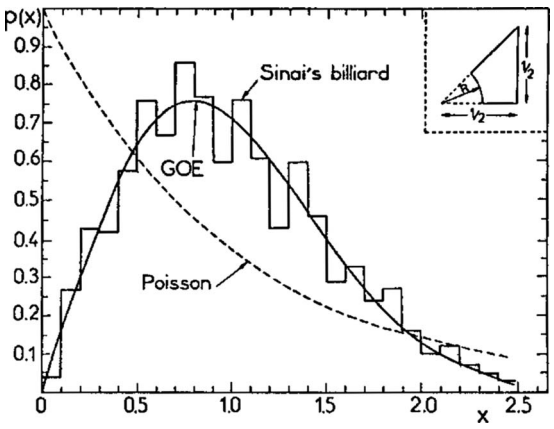

FIG. 7. The NNS distribution for the Sinai billiard (histogram), the GOE prediction (solid line), and the Poisson result (dashed line). While the theoretical literature commonly uses the label s for the actual level spacing in units of the mean level spacing, that quantity is usually referred to as x when RMT predictions are compared with data. We follow that usage here. Inset: The eigenvalues must be selected according to the symmetries of the eigenfunctions. From Bohigas *et al.*, 1984.

the canonical random-matrix ensemble having the same symmetry. Massive numerical evidence on other few-degrees-of-freedom systems has given extensive support to the conjecture. Attempts to prove the conjecture analytically have been based partly on periodic-orbit theory (which has been important all along in the understanding of classical chaos) and the semiclassical approximation. Berry (1985) established a connection between classical chaos and the Δ_3 statistic. More recently and for a special fluctuation measure (the two-point function, a quantity intimately related to the Δ_3 statistic), the conjecture was proved, or, to use a mathematically less demanding term, demonstrated by Heusler *et al.* (2007). The argument uses generic properties of periodic orbits in classically chaotic systems with few degrees of freedom.

The semiclassical arguments used by Heusler *et al.* (2007) do not apply directly to chaos in classical or quantum many-body systems. This point was made at the beginning of this section and is discussed again in Sec. III.C.1. For the time being, we also adopt the BGS conjecture for many-body systems. Thus we speak of quantum chaos (or of chaos) whenever in a many-body system such as the nucleus the spectral fluctuation measures introduced above agree with GOE predictions. We have to keep in mind that the NNS distribution is a less safe indicator of quantum chaos than the Δ_3 statistic. To see this, we consider (Rosenzweig and Porter, 1960) a real symmetric matrix with diagonal entries that are eigenvalues of a regular system with average level spacing d and with nondiagonal elements of typical strength v [see the example in Eq. (5)]. The parameter that rules the regular-to-chaos transition is v/d. As we increase that parameter from very small values, neighboring levels begin to repel, and the NNS distribution of the GOE is approached. This happens before the long-range stiffness of the spectrum as manifest in the Δ_3 statistic is attained.

In classical mechanics, the case of complete chaos is a limiting one. Another limiting case is that of completely regular motion. In quantum mechanics, regular motion corresponds to the existence of a complete set of quantum numbers that label every state. There is no level repulsion, and no correlation between levels. As shown by Berry and Tabor (1977), this case generically yields a spectrum where the spacings have an exponential distribution ("Poisson spectrum"); see Fig. 7. The general case in classical mechanics is the one in which phase space consists of islands of regular trajectories separated by domains filled with chaotic trajectories. There does not seem to exist a generic description of the distribution of level spacings for that case. The Brody distribution defined in Eq. (28) below is a purely heuristic (and not the only) interpolation formula between the Poisson distribution and the Wigner surmise.

G. Doorway states

As explained in Sec. II.B, the GOE yields the generic description of spectra of bound quantum systems. It offers the best first guess of spectral properties if we have no specific knowledge of the system except for the fact that it is invariant under time reversal. There are cases, however, where we possess some limited additional dynamical information. We may then look for a theoretical description that takes that information fully into account but is otherwise generic. Doorway states are a case in point. Other examples for this type of approach are described in Sec. III.D.

We consider a particular mode of excitation of the system. To be specific, we take the electric dipole operator D acting on the ground state $|g\rangle$ of an even-even nucleus in the long-wavelength limit. With H the Hamiltonian, we shift for simplicity the energy such that the ground state has energy zero, $H|g\rangle=0$. We choose the normalization of the dipole mode $|0\rangle=D|g\rangle$ such that $\langle 0|0\rangle=1$. Then the expectation value $E_0=\langle 0|H|0\rangle$ gives the mean excitation energy of the dipole mode. In general, the dipole mode is not an eigenstate of H. Therefore, the variance of H with respect to the dipole mode, i.e., $\Delta H^2=\langle 0|H^2|0\rangle-E_0^2=\Sigma_{\mu\geqslant 1}(H_{0\mu})^2$, does not vanish. (Here μ labels states with the same quantum numbers as, but orthogonal to, the dipole mode.) As a consequence, the cross section for dipole absorption possesses a large number of sharp lines, each occurring at an eigenstate of H. (Here we disregard the fact that for most nuclei E_0 is greater than the threshold for particle emission, so that the sharp lines actually become more or less broad resonances.) We observe that $(1/N)\Delta H^2=(1/N)\Sigma_{\mu\geqslant 1}(H_{0\mu})^2$ represents the mean coupling strength of the dipole mode with the other states of the system. The ratio of that expression and the mean level spacing (taken at E_0) is a measure of the length of the energy interval over which the dipole mode is strongly mixed with other states. Within that interval, the peak

heights of the dipole absorption lines are enhanced, and an average of the cross section for dipole excitation (taken with a Lorentzian weight function whose width is larger than the mean level spacing) displays a resonance at or near the energy E_0. This is the giant dipole resonance. Dipole absorption may be viewed as a two-step process. First the dipole mode is formed. The ground states of even-even nuclei have spin 0 and positive parity, and the dipole operator is the z component of a vector. Therefore, in these nuclei the dipole mode has spin 1 and negative parity. Subsequently, that mode decays into the eigenstates of H with the same quantum numbers. It is obvious that that same picture applies to many other nuclear reactions: neutrons impinging on a nucleus give rise to a single-particle mode, protons generate isobaric analog modes, etc. The picture can likewise be used to describe the distribution of simple configurations such as one-particle one-hole states over the eigenstates of the system. Early summaries of the doorway state idea may be found in Bohr and Mottelson (1969) and Mahaux and Weidenmüller (1969). For a recent discussion that goes beyond the standard model described next, see Zelevinsky *et al.* (1996) and De Pace *et al.* (2007).

We turn to the standard description of a doorway state within random-matrix theory. To this end, we define the following extension of the GOE. With E_0 the mean excitation energy of the doorway state, and with $H_{0\mu}$ (where $\mu=1,\ldots,N$) the coupling matrix elements of the doorway state with the other states of the system, the Hamiltonian matrix H for the doorway-state model takes the form

$$H=\begin{pmatrix} E_0 & H_{0\nu} \\ H_{\mu 0} & H_{\mu\nu} \end{pmatrix}. \tag{24}$$

Here $H_{\mu\nu}$ is a GOE matrix of dimension N. With $|0\rangle$ the doorway state, we have $\langle 0|H|0\rangle=E_0$ and $(1/N)\Delta H^2=(1/N)\Sigma_\mu (H_{0\mu})^2$. Because of the distinct role of the doorway state, the doorway model of Eq. (24) is not orthogonally invariant. It does possess that invariance, however, in the subspace of states carrying labels $\mu\geqslant 1$. That statement implies that ensemble averages of observables cannot depend on the individual coupling matrix elements $H_{0\mu}$ but depend only on the orthogonal invariant $(1/N)\Sigma_\mu (H_{0\mu})^2$, the mean-square coupling matrix element.

Every random-matrix model that incorporates additional dynamical information does so at the expense of complete orthogonal invariance. That invariance is extremely helpful in working out the spectral properties of the GOE. Therefore, noninvariant extensions of the GOE are often difficult to handle. This is not the case for the model of Eq. (24) because we add only a single state to the GOE. As a consequence, in the limit $N\to\infty$ both the spectral statistics and the Porter-Thomas distribution of the Hamiltonian (24) coincide with those of the GOE. The only distinct feature of the model is the strength function for the doorway state. It is defined as the ensemble average of $\Sigma_\tau |\langle 0|\tau\rangle|^2\delta(E-E_\tau)$ and gives the probability per unit energy interval to find the doorway state admixed to the eigenstates $|\tau\rangle$ of H with eigenvalues E_τ. Stated differently, the strength function is the average value of the level density weighted with the square of the overlap matrix element. In form, the strength function is closely related to the local density of states used in condensed-matter physics. Because of the ensemble average, the strength function is a smooth function of energy E and has the form

$$\overline{\sum_\tau |\langle 0|\tau\rangle|^2\delta(E-E_\tau)}=\frac{1}{2\pi}\frac{\Gamma^\downarrow}{(E-E_0)^2+(1/4)(\Gamma^\downarrow)^2}. \tag{25}$$

Here

$$\Gamma^\downarrow=2\pi\left((1/N)\sum_\mu (H_{0\mu})^2\right)\rho(E) \tag{26}$$

is the spreading width of the doorway state, with $\rho(E)=1/d$ the average level spacing of the GOE at energy E. Since $(1/N)\Delta H^2/d=\Gamma^\downarrow/2\pi$, the spreading width measures the length of the energy interval within which the eigenstates of H carry significant admixtures of the door way state. The notation for the spreading width with a down arrow is a reminder of the fact that the spreading width does not account for a decay process into some open channel (with the ensuing probability flux of particles at large distance), but for the mixing of a particular mode with other bound states.

The Lorentzian form of the strength function applies approximately for $\Gamma^\downarrow\ll\lambda$, where 2λ is the radius of the semicircle. For small coupling, Eq. (26) has the form of Fermi's Golden Rule. In the framework of random-matrix theory, the result (26) is valid beyond the perturbative regime, however, and holds even if $\Gamma^\downarrow\rho(E)\gg 1$. Integrating the left-hand side of Eq. (25) and using completeness, we obtain unity. That same statement applies to the right-hand side, and the strength function is properly normalized. The Lorentzian form (25) does not apply when the energy E_0 of the doorway state is close to one of the end points of the semicircle, or when the spreading width becomes very large (i.e., comparable with the radius of the semicircle); see Kota (2001), De Pace *et al.* (2007), and numerical examples given, for instance, in Zelevinsky *et al.* (1996).

The spreading width $\Gamma^\downarrow$ has a remarkable property that makes it a useful measure for the spreading of a doorway state. We ask the following: How does the mean-square matrix element $(1/N)\Sigma_\mu (H_{0\mu})^2$ change with the average level density of the GOE states? That question arises in the nuclear context because doorway phenomena are encountered at various excitation energies and in nuclei with widely different mass numbers for which the nuclear level density differs markedly. An intuitive answer is obtained by noting that a significant increase of the level density implies a significant increase in the complexity of the wave functions making up the GOE states. Therefore, each of the matrix elements $H_{0\mu}$ connecting the doorway state with the GOE states is strongly reduced, and so is the mean square matrix element. But in the expression (26) for the spreading width,

this strong reduction of the mean-square matrix element is essentially compensated by the increase of the average level density. That compensation is exact in simple models (Brody *et al.*, 1981) and is expected to hold to a good degree of approximation in realistic cases. An experimental verification of this expectation comes from investigations of the spreading width for isospin mixing (Harney *et al.*, 1986) not discussed in this review. We conclude that, in contrast to the exponential dependence of the average level density on excitation energy and mass number, the spreading width is expected to be a slowly varying function of these parameters and is thus a useful measure for the spreading of a doorway state.

If the model (24) applies in reality, a doorway state has hardly any influence on spectral properties of the system: The average level density of the states that carry the same quantum numbers as the doorway state is unchanged, their spectral fluctuation properties are the same as for the GOE, and their partial widths for decays different from electric dipole decay to the ground state have the same Porter-Thomas distribution as for the GOE. The only difference to the pure GOE case is the Lorentzian enhancement (25) of the strength function for dipole absorption. This is the only trace left of the doorway state after we take account of its mixing with the complicated states. Dividing the partial widths for dipole absorption of the eigenstates of H by the value of the strength function (taken at the corresponding eigenvalue) removes that trace and should yield quantities that have a pure Porter-Thomas distribution.

III. APPLICATION OF RMT TO NUCLEAR SPECTRA

A. General remarks

Nuclear energy levels are characterized by quantum numbers that reflect the symmetries of the nuclear Hamiltonian: total spin (J) reflects rotational symmetry, parity (Π) reflects invariance under mirror reflection, and isospin (T) reflects proton-neutron symmetry. We exhibit the consequences of such symmetries for the application of RMT to nuclear spectra.

The total Hilbert space is spanned by many-body wave functions that carry the quantum numbers J,Π,T. These can be arranged in such a way that the matrix representation of the nuclear Hamiltonian has block structure,

$$H=\begin{pmatrix} H^{J_1\Pi_1T_1} & 0 & 0 & \cdots \\ 0 & H^{J_2\Pi_2T_2} & 0 & \cdots \\ \vdots & \vdots & \ddots & \cdots \end{pmatrix}. \tag{27}$$

Here $\{J_1\Pi_1T_1\}\neq\{J_2\Pi_2T_2\}\neq\cdots$, and each of the matrices $H^{J\Pi T}$ couples only many-body states that carry the same quantum numbers. If in addition the nuclear dynamics is chaotic, then the BGS conjecture (see Sec. II.F) implies that each of the matrices $H^{J\Pi T}$ is a member of a random-matrix ensemble. Since nuclei obey time-reversal invariance, the suitable ensemble is the GOE. In the framework of RMT, Hamiltonian matrices referring to different sets of quantum numbers are assumed to be uncorrelated.

To compare RMT predictions on spectral fluctuations with data on nuclear energy levels, sequences of levels carrying the same quantum numbers are needed. The data are subject to three requirements: (i) the sequence(s) should be as long as possible, (ii) the sequence(s) should be pure (i.e., should not contain levels carrying quantum numbers that differ from those of the rest), and (iii) the sequence(s) should be complete (i.e., there should not be any levels that were not detected). The first requirement is needed to ensure that the running average over the actual spectrum is as close as possible to the running average over the complete spectrum, the latter by ergodicity (Sec. II.C.3) being equal to the GOE ensemble average. The two other requirements guarantee that the statistical predictions of RMT can meaningfully be applied to the data; see Sec. II.D.3 and the discussion in Sec. III.D. Unfortunately, the number of nuclear data sets of sufficient quality to provide detailed tests of RMT is fairly limited. This is primarily due to the requirements of purity and completeness imposed by the sensitivity of the standard fluctuation measures.

In many cases, nuclear levels are observed as narrow particle-unstable resonances; see Fig. 1. Then a multilevel R-matrix fit (Lane and Thomas, 1958) is used to determine the positions the levels would have if they were stable under particle decay. These positions are used to calculate level spacings and to test GOE predictions. (In R-matrix theory, the nucleus is thought to be enclosed by a ficticious boundary that lies some distance beyond the nuclear radius. Boundary conditions on that surface and the nuclear Hamiltonian jointly define a set of discrete states within the boundary. These states appear as resonances in the scattering matrix S. Approximations to the resulting formal expression for S serve as the basis of the fits to data.)

In comparing nuclear data with GOE predictions for the NNS distribution and/or the Δ_3 statistic, one faces the following difficulty: Both distributions are parameter free, and it is difficult to assess the significance of the usual tests for goodness of fit such as the χ^2 test when one is far from these limiting cases. Therefore, one uses measures that interpolate between the GOE prediction and the case of a totally regular system. These do have free parameters, and the goodness-of-fit tests are easily interpreted. The NNS distribution has the form of the Wigner surmise (19) for the GOE and is proportional to $\exp(-s)$ (Poisson distribution) for regular systems (Berry and Tabor, 1977). An expression that interpolates between both is the Brody distribution (Brody *et al.*, 1981). It depends on a single parameter ω and is given by

$$P_\omega(s)=(1+\omega)\alpha s^\omega \exp(-\alpha s^{1+\omega}), \tag{28}$$

where s is the actual level spacing in units of the mean level spacing, and the constant $\alpha=[\Gamma\{(2+\omega)/(1+\omega)\}]^{1+\omega}$ is fixed by normalization. For $\omega=0(\omega=1)$, the Brody distribution equals the Poisson distribution (the Wigner dis-

tribution), respectively. For all $\omega>0$, the Brody distribution vanishes at $s=0$. The Brody formula is only one of several formulas that interpolate between the Poisson and the Wigner distribution. Another example is the Berry-Robnik distribution (Berry and Robnik, 1984).

For the GOE, the Δ_3 statistic has the logarithmic dependence on the length L of the energy interval shown in Eq. (22), while for a regular system it is linear in L. A parameter-dependent measure for deviations from the GOE is obtained by considering a spectrum that is a superposition of k independent GOE spectra. For $k\gg 1$, the Δ_3 statistic approaches the linear dependence of the regular case. [Apparently this was first noticed by Gurevich and Pevsner (1957).] The deviation from the GOE prediction is significant already for $k=2$; see Fig. 16.

The predictions of RMT on fluctuation properties of nuclear wave functions can only be tested in terms of the distribution of matrix elements (either for decay into open channels or for electromagnetic transitions, weak interaction matrix elements not being numerous enough for such a test). Here the size of the sample again is important. In addition, there is usually an experimental cutoff for small matrix elements so that only part of the Porter-Thomas distribution can be tested.

Two properties of nuclei are central for tests of RMT. (i) In every nucleus, the average level density increases roughly exponentially with excitation energy. Thus, while typical level spacings near the ground state are several hundred keV, spacings of levels having the same spin and parity (a subset of all levels) at neutron threshold in heavy nuclei are typically 10 eV; see Fig. 1. For fixed excitation energy, the level density increases likewise with mass number A (save for corrections due to nuclear shell structure; see Sec. IV.A.1). The requirements on experimental energy resolution increase with increasing level density and, in general, limit nuclear spectroscopy except for fortuitous situations such as those leading to the data in Fig. 1. (ii) Levels below the threshold for particle emission have only small widths (in comparison with the mean level spacing) due to beta or gamma decay. Above particle threshold, the total widths of the nuclear resonances increase rapidly with increasing excitation energy. This is because the number of open channels for particle decay increases rapidly (the number of states available for decay in the daughter nuclei increases roughly exponentially with excitation energy in these nuclei). As a consequence, isolated resonances as shown in Fig. 1 are observed only just above the lowest particle threshold. A few hundred keV above that threshold, resonances begin to overlap (the mean level spacing decreases, the average total width increases), and it is no longer possible to investigate spectral fluctuations. Rather, this is the domain of statistical nuclear reaction theory. Thus tests of GOE predictions in nuclear spectra are limited to the energy interval between the ground state and an energy somewhat above the first particle threshold.

In describing the application of RMT to nuclear data, we first discuss the experimental methods that have been used to obtain the relevant spectral information (Sec. III.B). We then review the results of comparing the data with GOE predictions on spectral fluctuations (Sec. III.C). RMT can be extended to deal with violations of symmetry or invariance. This is described in Sec. III.D.

B. Experimental methods

1. Neutron resonances

The early tests of RMT involved neutron resonances, as shown in Fig. 1. The scattering of slow neutrons enables the study of individual resonances in a narrow window of energies at high excitation energy in the compound nucleus—typically 5–7 MeV. At these energies, the level density in medium-weight and heavy nuclei is very large. However, the angular momentum barrier for the incident neutron severely restricts the neutron's orbital angular momentum and thus the spins J of the compound nuclear resonances that contribute to the scattering. For slow neutrons, only s- and p-wave resonances are usually observed.

The experimental method of choice is a time-of-flight measurement. Longer flight paths allow for better energy resolution (essential to resolve the resonances), but reduce the counting rate because of the smaller detector solid angle. Thus high-intensity neutron sources are required. Today the most intense neutron beams are produced at spallation sources.

The most common experiment is a transmission measurement. The transmission of the neutron beam through a target with nuclei of mass number A determines the total cross section for the $n+A$ reaction. Neutron capture followed by γ emission is also helpful in determining the resonance parameters. Analysis of the resonance data is normally performed with the Lane and Thomas version of the Wigner-Eisenbud R-matrix formalism (Lane and Thomas, 1958). The classic monograph on neutron resonance reactions has been given by Lynn (1968).

For a comparison with RMT predictions, the levels in a sequence must have the same quantum numbers. Thus one key issue is to determine the spin J and parity Π of each resonance. This is done using the angular momentum ℓ of the scattered neutron. For spin-0 targets, all s-wave resonances have $J^{\Pi}=1/2^{+}$. For slow neutrons, the difference in penetrabilities for $\ell=0$ and $\ell=1$ is so large that at first sight ℓ can be assigned by inspection—strong resonances are s wave and weak resonances are p wave. One normally formalizes this with a Bayesian analysis (Bollinger and Thomas, 1968, 1970), but this approach is not reliable in the gray area between weak s-wave and strong p-wave resonances. Of course other experiments can be used to improve the spin and parity assignments. We mention neutron capture with high-resolution γ-ray spectroscopy or with calorimeters (where for each capture reaction the total number and individual energies of the emitted gamma rays are registered). However, these are very time consuming.

In addition to the issue of spurious resonances (incorrect spin or parity assignments), the other major problem is missing levels. The missing levels are expected to be the weakest levels, hence the focus on signal-to-noise ratios and energy resolution in resonance measurements. The Porter-Thomas distribution predicts many weak resonances. Assuming that distribution, one can estimate the fraction of missing levels. Unfortunately this nearly universally used correction method can be misleading if nonstatistical effects are present. An alternative approach utilizing the NNS distribution was developed only recently (Agvaanluvsan *et al.*, 2003). Bohigas and Pato (2004) extended the investigation of the effects of missing levels to other level fluctuation measures.

Almost all of the neutron resonance data suitable for detailed comparison with RMT are obtained for spin-0 targets. Most of the neutron resonance data used in the early evaluation of RMT were obtained by Rainwater's group at Columbia (Liou, Camarda, Wynchank, *et al.*, 1972; Liou, Camarda, and Rahn, 1972) for a number of nuclei with mass numbers $A>110$. Due to experimental limitations, the number of resonances in each nucleus was never significantly larger than 200.

2. Proton resonances

Due to the Coulomb barrier, proton resonances cannot be studied near zero bombarding energy as neutron resonances are. High-resolution proton resonance measurements are typically taken at bombarding energies corresponding to 60–70 % of the Coulomb barrier. This has two major advantages. First, the Coulomb barrier penetrability serves to narrow the proton widths and makes possible the resolution of individual resonances in rather dense spectra. Second, the addition of Coulomb and nuclear resonance scattering amplitudes leads to striking interference patterns that are used to identify the spin and parity of each resonance. The parity assignment is normally apparent by inspection, since the interference patterns for even and odd orbital angular momenta are quite different. This is important because the proton penetration factors for different orbital angular momenta do not differ as much as for the neutron resonances. As a result, one usually observes *s*-, *p*-, and *d*-wave and sometimes even *f*- and *g*-wave resonances. The primary difficulty consists in determining the J value of the proton resonances. Additional experiments (inelastic scattering or capture) can resolve this problem, but as in the neutron case these experiments are very time consuming and therefore are rarely performed. Although most of the high-quality proton resonance data are also for *s*-wave sequences, there are (in contrast to the neutron case) a few *p*-wave sequences that are considered pure and complete. With very few exceptions, the level density becomes too great for this method to work much beyond mass number $A=60$. Here the typical number of resonances of the same spin and parity is 50 or so. Thus the proton resonance data complement the neutron resonance data; the best results for each set are obtained in quite different mass regions. Almost all of the data used to compare with RMT are for spin-0 targets and from the Triangle Universities Nuclear Laboratory (TUNL) (Wilson *et al.*, 1975; Watson *et al.*, 1981).

In order to observe (nearly) all of the resonances, one needs good beam-energy resolution and high beam intensity. These requirements seem contradictory. One approach is to accept the time-dependent energy fluctuations intrinsic to the accelerator and make a correction later. The most successful correction method solves the resolution-intensity impasse using two beams. One (high-intensity) beam is used to perform the experiment; the other beam is used to generate a feedback signal that follows the beam energy fluctuations; this signal generates a voltage difference that is applied to the target. Thus the time-dependent energy fluctuations are canceled. The method works well for a Van de Graaff accelerator where most of the fluctuations have low frequency. The details have been given by Bilpuch *et al.* (1976).

3. Low-lying levels

The spectroscopy of low-lying levels (excitation energies below 2 MeV or so) has always been a primary object of study in nuclear physics. Many different approaches have been used: various nuclear reactions including inelastic scattering, pickup, and transfer reactions; γ-ray spectroscopy following β or α decay; etc. Almost all of these processes are quite selective. Therefore, one needs to use many different approaches to ensure that all levels (in some energy interval) are observed. One powerful technique uses the neutron capture reaction. Neutron capture on nucleus A is followed by sequences of γ transitions that finally populate the ground state of nucleus $A+1$. The average neutron resonance capture technique (Bollinger and Thomas, 1968) effectively averages over many neutron resonances and is nonselective; it also averages over Porter-Thomas fluctuations, increasing the probability of observing weak transitions. Every low-lying state within some spin range is expected to be populated. The combination of neutron capture and direct reactions has led to a number of complete level schemes at low energies (von Egidy *et al.*, 1986, 1988).

4. High-spin states

The ground states of even-even nuclei have spin 0; those of even-odd, odd-even, and odd-odd nuclei have small spin values. The excitation energy $E(J)$ of the lowest state with given spin J generically increases with J; the function $E(J)$ defines the "yrast line"; see Fig. 8. High-spin states located near the yrast line are typically investigated via the collision of two heavy nuclei ("heavy-ion collisions"). At nonzero impact parameter, the two colliding nuclei with mass numbers A_1 and A_2 typically carry a large angular momentum of relative motion. The high-spin intermediate complex formed by the collision (with spin values as large as $60\hbar$ or so) may

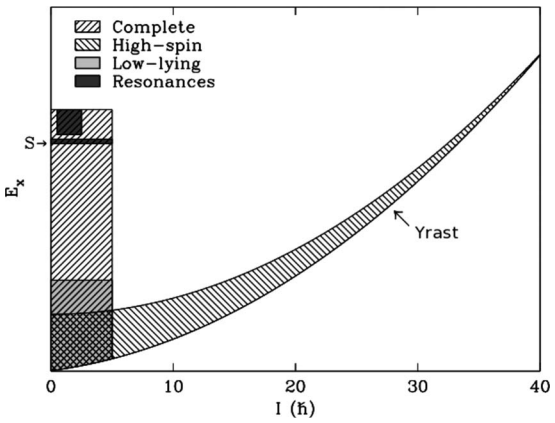

FIG. 8. The yrast line, i.e., the excitation energy $E(J)$ of the lowest state with spin J vs J for an even-even nucleus with mass number around 160 (schematic). The shaded area indicates the domain where spectroscopic information is available; see Døssing *et al.* (1996). The letter S denotes the particle threshold. Depending on A, S typically lies between 5 and 8 MeV.

decay by a sequence of γ transitions (perhaps with intermittent neutron evaporation) to the ground state of a nucleus whose mass number is smaller than but close to A_1+A_2. The γ rays emitted in this process are analyzed using large-scale γ-ray detection arrays. This approach has generated a very large amount of data. These comprise many rotational bands (with many states in each) for a range of heavy nuclei. (Rotational bands are typical for deformed nuclei and are dealt with in Sec. IV.B.1.) The observed states have relatively high spin and rather large excitation energies, but are not far above the yrast line. Some aspects of the method of analysis have been summarized by Døssing *et al.* (1996), where further references may be found.

Unfortunately, the difficulties in obtaining suitable data sets for comparison with RMT are many. One often sees many rotational bands, but of course each band has only one state of a specific spin and parity. Thus one is forced to combine results from many bands and nuclei. Another serious issue is the problem of quantum number assignments. Within a given band with a well-known bandhead, the assignments are reliable; assignments based on interband transitions are more problematic. Until now, levels up to a few 100 keV above the yrast line have been analyzed (Garrett *et al.*, 1997); higher-lying rotational bands cannot be individually resolved. The evidence here points to regular motion; see Sec. III.C.3. Theoretical expectations are that at around 800 keV above the yrast line the spectral fluctuations become chaotic; see Sec. IV.B.2. It is to be hoped that with improved resolution (perhaps attainable with the next generation of large-scale detectors), spectroscopic data in that interesting energy region will become available.

5. Complete level schemes

The ideal is a complete scheme that begins at the ground state and extends into the neutron or proton resonance region, with perfect quantum number assignments to each level. Obtaining such a complete level scheme is exceptionally difficult at best, and impossible in medium-weight to heavy nuclei. The level densities are simply too great. For very light nuclei, on the other hand, the level density is small and the total number of states is not sufficient for a detailed statistical analysis. Only for nuclei in the mass range between 20 and 40 or so does the level density have suitable values. These are essentially the nuclei belonging to the $2s1d$-shell; see Sec. IV.A.1.

It might seem that complete spectra might best be measured using a variety of reactions as done for the spectroscopy of low-lying states. However, this approach meets practical difficulties. Most reactions are not only selective, but also provide information only in a limited energy range. In the approach that was successfully used for two nuclei—^{26}Al and ^{30}P—the properties (quantum numbers, positions, and widths) of a number of proton resonances were determined. The proton capture reaction was then measured for these resonances, which had different quantum numbers. The method essentially guarantees that all levels below the proton separation energy are observed. Quantum numbers are assigned to the observed levels using high-resolution γ-ray spectroscopy, including angular distributions of primary and secondary γ rays. The experimental procedure for ^{30}P has been described by Grossmann *et al.* (2000). The general approach has been summarized by Mitchell and Shriner (2001). With the help of the neutron capture reaction, a "nearly complete" level scheme below 4.3 MeV excitation energy was measured in ^{116}Sn (Raman *et al.*, 1991).

The analysis of the complete spectra must allow for isospin-symmetry breaking and is dealt with in Sec. III.D.1.

6. Low-lying modes of excitation

The emphasis here is not on complete level schemes in a restricted energy range (as in Sec. III.B.3), but rather on phenomena that relate to levels of fixed spin and parity and seem linked to the concept of a doorway state; see Sec. II.G. The primary example of a doorway state is the giant electric dipole resonance, which manifests itself in a large resonancelike structure in the absorption cross section for γ rays. The isobaric analog resonances provide another classic example of a doorway-state phenomenon. The analysis of both types of resonances involves nuclear reaction theory and is not part of this review.

There are several other interesting excitation modes at lower energy—including the low-lying isovector magnetic orbital dipole or scissors mode with $J^\Pi=1^+$ (Bohle *et al.*, 1984; Richter, 1995) and the electric pygmy dipole resonance with $J^\Pi=1^-$ (both spin assignments applying to even-even nuclei). Nuclear resonance fluorescence measurements have been used to generate extensive data sets of 1^+ and 1^- states; the method provides a unique J value of 1 and a probable parity assignment, while measurements with a polarized photon beam pro-

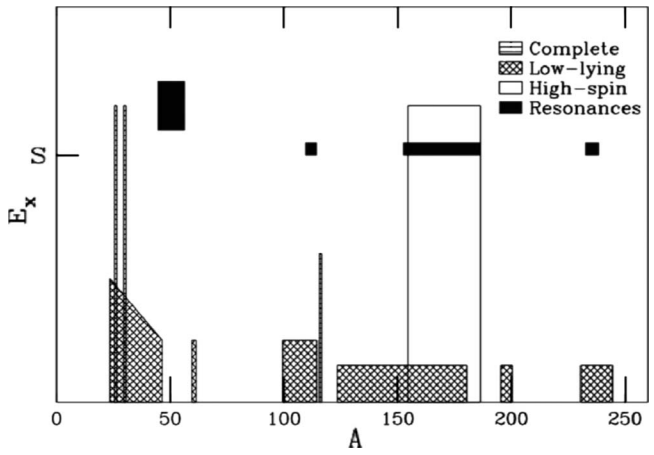

FIG. 9. The domains of excitation energy E_x and mass number A where spectral fluctuations have been investigated are shown for four classes of states (resonances, low-lying states, high-spin states, and states that belong to a complete spectrum). Complete spectra are known for three nuclei only, ^{26}Al, ^{30}P, and ^{116}Sn. The letter S denotes the particle threshold.

vide a definitive parity assignment. Work at Darmstadt has been focused on both the scissors mode (Enders *et al.*, 2000) and the electric pygmy dipole resonance (Enders *et al.*, 2004).

7. Summary

Figure 9 summarizes in a qualitative fashion the domains of excitation energy E_x and mass number A where spectral fluctuations have been investigated. The figure is largely self-explanatory; suffice it to say that the proton resonances around $A=50$ are measured above threshold but below the Coulomb barrier. The figure shows that high-spin states are measured at comparatively high excitation energies. This statement has to be taken with a grain of salt, however. For an even-even nucleus with mass number A around 160 or so, Fig. 8 shows schematically the excitation energy of the lowest state with spin J vs J (the yrast line). The high-spin states that were analyzed so far lie up to a few 100 keV above the yrast line and, for that value of J, represent low-lying excited states. Sequential decay of a rotational band close to the yrast line by repeated emission of γ rays reduces both J and the overall excitation energy, while the distance to the yrast line remains essentially the same.

C. Tests of fluctuation measures

The fluctuation measures described in Sec. II.D have been applied to nuclear data obtained with the experimental methods summarized in Sec. III.B. We emphasize again that, due to the sensitivity of these measures, the quality of the data sequence (the degree of purity and completeness) is of paramount importance; only a small fraction of all nuclear data can be used for such tests.

We mention in passing another measure, the "correlation hole." As a test for spectral fluctuations of the GOE type, it has been applied much more widely in molecular physics (Leviandier *et al.*, 1986; Guhr and Weidenmüller, 1990b; Lombardi *et al.*, 1994) than in nuclear physics (Alhassid and Whelan, 1993). Let $1-Y_2(b)$ denote the probability of finding two levels at a distance b. For completely uncorrelated (Poissonian) spectra one has $Y_2(b)=0$ for all b, while GOE level repulsion implies $Y_2(0)=1$. The Fourier transform of the spectral autocorrelation function (a function of time t) depends on the Fourier transform of Y_2 and is sensitive to the difference between regular and chaotic motion. For chaotic motion, it displays a correlation hole at $t=0$.

1. Neutron and proton resonances

Although the fluctuation measures described in Sec. II.D were proposed to describe neutron resonances in the 1950s, even in the early 1960s there were no neutron data of sufficient quality to provide an adequate test of RMT. For example, Dyson and Mehta (1963) considered the best available neutron resonance data and concluded the data were such that the RMT "model" was neither proved nor disproved. They exhorted experimentalists to improve the data quality.

By the early 1970s, the high-quality neutron resonance data from the Columbia group (Liou, Camarda, and Rahn, 1972, Liou, Camarda, Wynchank, *et al.*, 1972) were available and seemed to confirm the predictions of the GOE version of RMT. However, due to the limited number of resonances (of order 100) for each nucleus, these results were considered suggestive but not definitive. Haq *et al.* (1982) and Bohigas *et al.* (1983) combined neutron resonance data sets from a number of nuclei. This was made possible by scaling level spacings in units of the mean level spacing (the GOE fluctuation measures depend on that scaled parameter only). They also included some of the proton resonance data in their analysis. A complication (relative to the neutron data) here was the much larger energy range needed in order to obtain a reasonable sample size. This larger energy range required a correction (unfolding) of the experimental data in order to transform to a new set of levels with constant mean level spacing; see Sec. II.D.3. The analysis also included suitable spectra for other than s-wave proton resonances. Using all these data, they obtained a set of 1407 levels that they labeled the nuclear data ensemble (NDE). The analysis of the NDE is done by combining an energy average (for every nucleus) with an ensemble average (over all nuclei that are included in the NDE). Both the NNS and the Δ_3 statistic for the NDE agreed well with the GOE predictions; see Figs. 10 and 11. A number of later tests with other measures also agreed well with GOE predictions [see, for instance, Lombardi *et al.* (1994)] even though the presence of nonstatistical effects can never be excluded (Koehler *et al.*, 2007).

The analyses by Haq *et al.* (1982) and Bohigas *et al.* (1983) and some of the subsequent papers mark a turn-

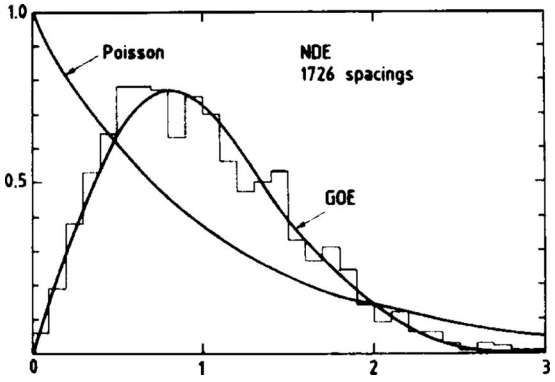

FIG. 10. The NNS distribution for the nuclear data ensemble vs s as in Fig. 4 (histogram) and the GOE prediction (solid line). From Bohigas *et al.*, 1983. (By the time that paper was published, the nuclear data ensemble had grown to 1726 spacings.)

ing point in the history of applications of RMT to nuclear spectra. As a result of these analyses, it became generally accepted that proton and neutron resonances in medium-weight and heavy nuclei agree with GOE predictions. With the later recognition of the connection between spectral RMT fluctuations and quantum chaos (see Sec. II.F), the term "chaos" began to be used by nuclear physicists.

As mentioned in Sec. II.F, chaos in classical many-body systems has not been investigated as thoroughly in terms of periodic-orbit theory as in classical few-degrees-of-freedom systems, not to mention complications due to the exclusion principle. Therefore, the connection between classical chaos and RMT is less well established and the use of the term "chaos" is somewhat more tentative in nuclei. By the same token, the use of semiclassical periodic-orbit theory in nuclei has been basically limited to independent-particle motion. In that

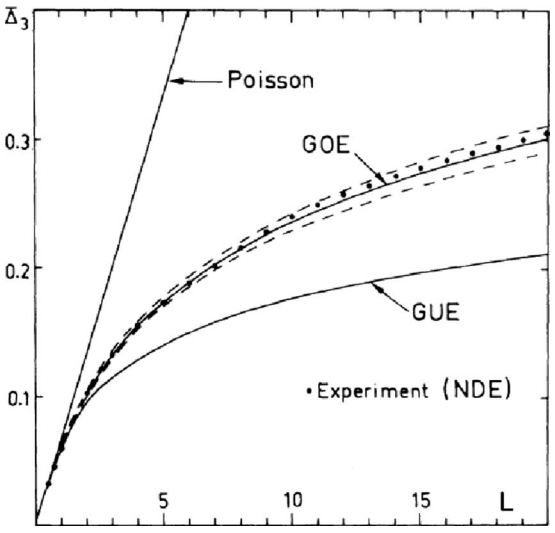

FIG. 11. The Δ_3 statistic for the nuclear data ensemble (data points) and the GOE and GUE predictions (solid lines). The dashed lines estimate the finite-range-of-data errors. From Haq *et al.*, 1982.

domain, it has been very successful. We mention early applications by Strutinsky (1966, 1967, 1968), whose "shell-correction method" is reviewed in Sec. IV.C.1, by Balian and Bloch (1970), and recent work by Bohigas and Leboeuf (2002), Leboeuf and Roccia (2006), and Roccia and Leboeuf (2007).

According to RMT, the eigenvalues and eigenvectors are uncorrelated random variables; see Eq. (6). In nuclei, this prediction was tested by Bohigas *et al.* (1983). The correlation coefficient was found to be 0.017 ± 0.029, the error reflecting the finite number of data points. In microwave billiards, the test yields 0.02 ± 0.05 (Alt *et al.*, 1995). Another test (also giving agreement with the GOE) has been reported in molecules by Lombardi and Seligman (1993).

2. Low-lying levels

After the success of RMT in describing the fluctuation properties of highly excited (resonance) states, it was natural to attempt to extend such analyses to low-lying states. Although there is an enormous amount of experimental information available for states near the ground state, for most nuclides the quantum numbers are known for only a very limited number of low-lying states. In particular, complete and pure sequences of levels with the same spin and parity are typically very short. Therefore, data from several or many nuclei must be combined to generate a sufficiently large ensemble. Moreover, the shortness of the available sequences precludes the study of fluctuation measures other than the NNS distribution. An extensive data set was compiled by von Egidy *et al.* (1986, 1988). An initial analysis of a subset of these data was performed by Abul-Magd and Weidenmüller (1985). A more extensive analysis of this same data set was performed by Shriner *et al.* (1991). The spacing distributions and their cumulative sums are shown in Fig. 12. The nuclei are grouped into classes according to mass number A. The size of each class was determined by the data available. The cumulative sums have smaller fluctuations. While the agreement with the Wigner distribution looks satisfactory in most cases, clear deviations occur for $150 < A \leqslant 180$ (rare-earth nuclei) and for $230 < A$ (very heavy nuclei). In both ranges of mass numbers, sizable nuclear deformations occur and cause rotational motion; see Sec. IV.B.1. The rotational model is integrable and the motion is therefore regular. The same statement holds for other forms of so-called collective motion; see Sec. IV.B.

The spacing distributions were fit with the Brody distribution (Brody *et al.*, 1981). The overall trend of the Brody parameter ω was to decrease with increasing mass number A—for the lightest region ($A = 25$–50) the average value of ω was about 0.7, while for the heaviest mass region ($A = 225$–250) the value of ω was 0.2. Various theoretical works have attempted to explain this behavior, including Bae *et al.* (1992) and Yoshinaga *et al.* (1993). To exhibit the connection of the NNS distributions with the degree of collectivity, attention was focused on the behavior of the 2^+ and 4^+ states because these states play a

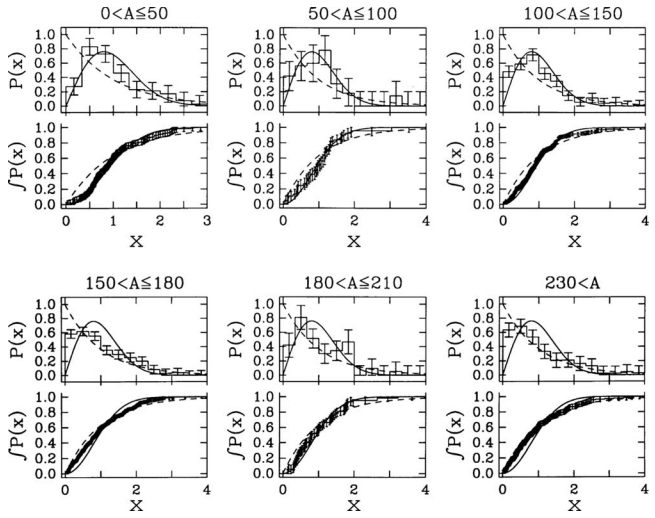

FIG. 12. Level spacing distributions for six different regions. Upper panels: NNS distributions (histograms) are compared with the Wigner distribution (solid lines) and the Poisson distribution (dashed lines) for several ranges of mass numbers. Lower panels: Same for the cumulative distributions (number of spacings smaller than x) (cf. the caption of Fig. 7). The approximate number of levels in each region is as follows: $A=0-50$ ($N=150$), $A=50-100$ ($N=50$), $A=100-150$ ($N=270$), $A=150-180$ ($N=450$), $A=180-210$ ($N=60$), $A>230$ ($N=190$). From Shriner *et al.*, 1991.

prominent role in collective rotations and vibrations of the nucleus. Two types of nuclei were considered: nuclei with approximately spherical ground states and nuclei with strongly deformed ground states; see Sec. IV.B. The transition between both classes was studied. Depending on the model chosen, the motion is chaotic or regular in one but not in the other limit. Figure 13 shows that the experimental results are striking. 2^+ and 4^+ states in strongly deformed nuclei have NNS distributions that agree with the Poisson distribution, while the corresponding states in spherical nuclei have spacing distributions that agree with the Wigner distribution. Unfortunately, the limited amount of data and the corresponding large uncertainties preclude a more detailed assessment of the effects of collectivity.

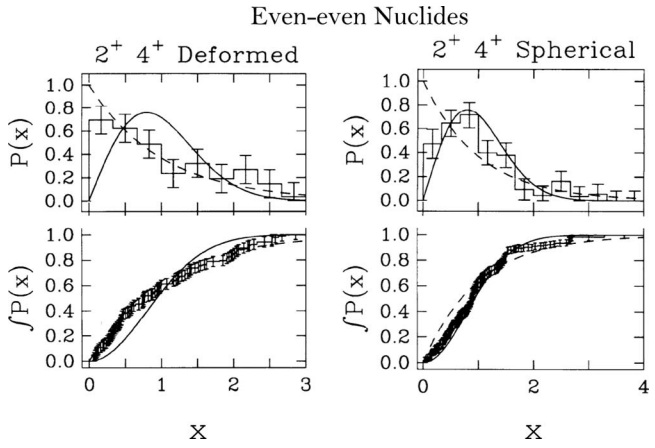

FIG. 13. Comparison of the NNS distributions vs x, the level spacing in units of the mean level spacing, for 2^+ and 4^+ states in strongly deformed (left panel) and in spherical nuclei (right panel). Adapted from Shriner *et al.*, 1991.

Another approach by Abul-Magd *et al.* (2004) focused on specific states (the lowest 2^+ states in even-even nuclei) and collected all complete sequences of low-lying 2^+ states from the nuclear data tables. The sequences are short in most cases. Nuclei are classified by the ratio $R_{4/2}$ of the excitation energy of the lowest 4^+ state over that of the lowest 2^+ state. That ratio is a well-known measure of collectivity. The size of each class is chosen such that it contains a sufficient number of sequences for a meaningful statistical analysis. The NNS distributions are analyzed using a measure different from the Brody distribution and obtained by superposing a number of uncorrelated GOE sequences, each of mean fractional level density f. The parameter f serves as a fit parameter and is referred to as the "chaoticity parameter." In its dependence on $R_{4/2}$, this parameter displays deep minima when $R_{4/2}=2.0$, 2.5, and 3.3. These values correspond to the dynamical symmetries of a specific collective model, the interacting boson model described in Sec. IV.B.1. Whenever one of these symmetries prevails, the motion of the nucleus is integrable and thus regular.

In summary, there is evidence that the nuclear dynamics in the ground-state region is partly chaotic and partly regular. The regular features are dominant whenever collective motion with a high degree of symmetry applies.

3. High-spin states

The only extensive analysis of the statistical properties of high-spin states was performed by Garrett *et al.* (1997). The data set comprised energy levels in deformed nuclei in the range of proton numbers $Z=62-75$ and mass numbers $A=155-185$. The spin values ranged up to $J=40$. The levels were at high excitation energies, but only up to several hundred keV above the yrast line; see Fig. 8. They found that the NNS distribution agreed best with the Poisson distribution. This is consistent with the results for low-lying states in deformed nuclei; see Sec. IV.B.2.

An observed deficiency of small spacings is not well understood. It is possible that right above the yrast line a symmetry related to the K quantum number is partly broken. This quantum number measures the projection of the nuclear spin onto the body-fixed symmetry axis; see Sec. IV.B.1. This might lead to level repulsion at small distances. Hopefully the analysis of similar data will shed more light on that question. We return to the general issue of symmetry breaking and its influence on spectral fluctuation properties in Sec. III.D.1.

4. Analysis of low-lying modes of excitation

At low excitation energies, one observes several modes of excitation. Statistical measures have been used in order to identify the character of the mode in the case

of the scissors mode (Enders *et al.*, 2000) and of the pygmy dipole resonance (Enders *et al.*, 2004).

For the scissors mode (a low-lying isovector magnetic dipole mode), data were generated by nuclear resonance fluorescence measurements (Enders *et al.*, 2000). The spectra of 13 heavy deformed even-even nuclei with neutron numbers in the 82–126 range (corresponding to a major shell) were used to generate an ensemble of 152 scissors-mode states with spin/parity 1^+, all in a range of excitation energy between 2.5 and 4.0 MeV. In each nucleus, the sequence of states used in the analysis was required to contain a minimum number of eight states. After unfolding, the ensemble was analyzed with the standard RMT fluctuation measures. The data agreed well with Poisson statistics. They examined the effects of missing levels on the spacing and width distributions and concluded that missing levels can be ruled out as a cause of this behavior. They concluded that the levels of the scissors mode are excited by a common mechanism. The levels are collective but it is not possible to identify a common doorway. It seems that the underlying microscopic mechanism is not yet fully understood.

The electric pygmy dipole resonance is so named because of its small strength relative to the giant electric dipole resonance. In heavy nuclei, the pygmy resonance is located at excitation energies around 5–7 MeV. Enders *et al.* (2004) studied the statistical properties of this mode in four isotones, all with neutron number 82. They created an ensemble of 184 1^- states in the excitation energy range of 4–8 MeV, along with their dipole transition strengths to the ground state. After unfolding, the spectral fluctuations (strength and spacing distributions) are close to Poissonian. Because of a significant number of missing levels, the analysis is rather involved in this case, however, and they concluded that the weak correlations found point to GOE behavior of the complete spectra. That conclusion is reinforced by an extensive comparison with spectra calculated using a particular nuclear model, the quasiparticle phonon model. These agree with the data but yield GOE behavior for the full spectra (including the levels missing in the data). The fundamental mode of excitation is collective. Many other states exist at the excitation energy where it occurs. These fragment the doorway state and produce a correlated spectrum of GOE type.

In comparing their results for these two modes, they concluded that the key reason for the apparently different statistical behavior is the difference in excitation energy. The higher-energy mode (electric pygmy dipole) is in a region of greater level density. This results in correlated spectra.

5. Eigenvector distribution

The GOE predicts a Gaussian distribution for the projections of the eigenvectors and the Porter-Thomas distribution for their squares; see Sec. II.D.1. While both the NNS distribution and the Δ_3 statistic are strongly affected by missing levels and/or impure sequences, the Porter-Thomas distribution (a probability density and not a correlation function) is expected to be less sensitive to missing or wrongly assigned levels. The experimental data normally used are the reduced widths (for resonances) or the reduced transition strengths (for electromagnetic transitions). Early neutron resonance data appeared to agree with the Porter-Thomas distribution; a frequently quoted example is for neutron resonances on ^{232}Th measured by Rainwater's group at Columbia University [see Garg *et al.* (1964)]. The analysis by the Orsay group of the nuclear data ensemble included a test of the Porter-Thomas distribution for the widths [see Bohigas *et al.* (1983)], and used a total of 1182 measured widths. In addition to a direct comparison with the Porter-Thomas distribution, a search for the best χ^2 distribution was also done. Very good agreement with the GOE prediction was found.

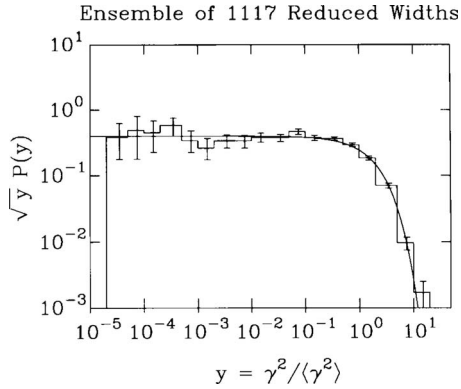

FIG. 14. The distribution $\sqrt{y}P(y)$ for $y=\gamma^2/\overline{\gamma^2}$ for 1117 reduced widths. From Shriner *et al.*, 1987.

Further and more detailed attempts to confirm the Porter-Thomas distribution have run into the following difficulty. For a set of Gaussian-distributed amplitudes $\{\gamma_i\}$, the second and fourth moments are related by $\langle\gamma^4\rangle=3\,\langle\gamma^2\rangle^2$, where the angular brackets denote the running average. According to Harney (1984), the error (square root of the variance) of the ratio $R=\langle\gamma^4\rangle/3\langle\gamma^2\rangle^2$ is $\sqrt{8/3k}$, where k is the number of data points. This is a rather large value. For the often quoted ^{232}Th data, for example, $k=171$, and the error of R is 0.125. Thus this excellent data set only confirms the Gaussian nature of the amplitude distribution at the 12% level.

To overcome this problem, a larger data set seemed useful. An ensemble of 1117 reduced widths was formed with TUNL data (Shriner *et al.*, 1987). With $y=\gamma^2/\langle\gamma^2\rangle$ and $P(y)$ the Porter-Thomas distribution, the result for $\sqrt{y}P(y)$ is shown in Fig. 14. The visual agreement with the GOE prediction is striking. However, the value of R for this ensemble turned out to be 1.26. The problem is that a relatively small number of nonstatistical large widths has a major impact on R because R depends on the fourth moment of the amplitudes.

To overcome that difficulty, a different measure that is less sensitive to a few nonstatistical amplitudes was needed. The normalized linear correlation coefficient

$$\rho(x,x') = \frac{\sum_i (x_i - \langle x\rangle)(x_i' - \langle x'\rangle)}{\left[\sum_i (x_i - \langle x\rangle)^2 \sum_i (x_i' - \langle x'\rangle)^2\right]^{1/2}} \tag{29}$$

for two data sets $\{x_i\}$ and $\{x_i'\}$ is expected to be a sensitive measure of correlations, as it combines information on both the magnitudes and phases of the data points. To test whether two sets of amplitudes $\{a_i\}$ and $\{a_i'\}$ follow the Gaussian distribution, one calculates the amplitude correlation coefficient $\rho(a,a')$ and the width correlation coefficient $\rho(w,w')$, where w represents the square of the amplitude. [Since it is impossible to measure the absolute sign of an amplitude, $\rho(a,a')$ is calculated with the assumption that $\langle a\rangle = 0 = \langle a'\rangle$.] The Gaussian distribution predicts $\rho^2(a,a') = \rho(w,w')$ and this is the relation that is tested.

To work out the correlation coefficients, it is necessary to measure partial width amplitudes including their relative phases. That was done using the inelastic decay of proton resonances. For example, for a spin-0 target with mass number A and a 2^+ first excited state, a proton resonance in the nucleus with mass number $A+1$ and spin/parity $3/2^-$ can decay to the 2^+ state by emitting the proton with angular momentum/spin $p_{1/2}$ or $p_{3/2}$. The relative phase of the two decay amplitudes is determined by measuring the angular distribution of the inelastically scattered protons and the subsequent deexcitation γ rays. Application of this approach has been described by Mitchell *et al.* (1985).

The relation $\rho^2(a,a') = \rho(w,w')$ can be checked for each data set. However, the sample size for each spin value in each nuclide was small, and it was necessary to combine the data sets. To this end, an ambiguity in the definition of the correlation coefficient was used. Instead of writing the amplitudes in terms of the decay channels $p_{1/2}$ and $p_{3/2}$, any two linear combinations of amplitudes obtained by orthogonal transformations from the original set can be used. The correlation coefficient depends on the chosen representation. There is always a representation in which the amplitude correlation coefficient is zero. Each of the data sets was individually transformed to that representation. The resulting width correlations and their uncertainties were combined for all of the data sets in order to obtain a final value for the width correlation. The result was $\overline{\rho(w,w')} = -0.01 \pm 0.03$ (Shriner *et al.*, 1987, 1989), in agreement with the prediction based on the Gaussian distribution. This is the most sensitive test of the Gaussian assumption.

D. Violation of symmetry or invariance

Two of the symmetries mentioned in Sec. III.A hold only approximately: Isospin symmetry is broken by charge effects, and parity conservation is violated by the weak interaction. Is it possible to extend RMT so as to account for such symmetry breaking? And how do the resulting statistical measures compare with data? We answer these questions for the case of isospin symmetry breaking. We apply the results to the complete spectra of ^{26}Al and ^{30}P. Parity violation is a very weak effect that has so far received a statistical analysis only in the framework of nuclear reaction theory.

We have also assumed that nuclei obey time-reversal invariance. One of the most precise tests in nuclei of that assumption applies RMT. We describe how a measure for violation of time-reversal invariance is derived in the framework of RMT and applied to data.

1. Model for isospin violation

Isospin symmetry is violated in nuclei by charge-dependent effects such as the Coulomb interaction between protons, the neutron-proton mass difference, or the mass differences between charged and neutral pions. Needless to say, the isospin-violating interaction is small compared to the strong force. The breaking of isospin symmetry manifests itself differently in different ranges of mass numbers. In nuclei with mass numbers around 40 or more, it leads to the occurrence of fragmented isobaric analog resonances. The typical features of this phenomenon relate to nuclear reaction theory and are not dealt with here. In some light nuclei with mass numbers smaller than 40 or so, the ground state has isospin $T=0$ but the density of states with $T=1$ in the ground-state region is roughly the same as that of states with $T=0$. The charge-dependent forces mix states with $T=0$ and $T=1$. It is for these nuclei that the following random-matrix model applies.

In order to account for isospin violation (and for symmetry breaking in general), the Hamiltonian (27) must be modified. The matrix elements of the isospin-violating interaction couple states with different T-quantum numbers. For simplicity, we consider two diagonal blocks only. The isospin-breaking interaction conserves parity and total spin so these two blocks carry the same quantum numbers J and Π (which we omit) but different isospin quantum numbers T_1 and T_2. The Hamiltonian has the form

$$H = \begin{pmatrix} H_{\mu\nu}^{T_1} & V_{\mu\sigma} \\ V_{\rho\nu} & H_{\rho\sigma}^{T_2} \end{pmatrix}. \tag{30}$$

With N_1 (N_2) the dimensions of the two block-diagonal matrices, the running indices in the first (second) block are $\mu,\nu = 1,\ldots,N_1$ ($\rho,\sigma = N_1+1,\ldots,N_1+N_2$), respectively. We deviate from our earlier systematic notation and denote the coupling matrix elements connecting the two blocks by V.

We use Eq. (30) to define a random-matrix model for symmetry breaking (Rosenzweig and Porter, 1960). We assume that the matrices H^{T_1} and H^{T_2} are each members of a GOE and are uncorrelated. For simplicity, we assume that the two GOEs have identical semicircle radii $2\lambda_1 = 2\lambda_2 = 2\lambda$ and equal dimensions $N_1 = N_2 = N$, although in practice it is necessary to take $N_1 \neq N_2$ in order to account for the fact that the level densities for states with different isospins differ. The (real) matrix elements of V are assumed to be Gaussian-distributed random

variables with zero mean value and a common second moment $\overline{V^2}$. They are not correlated with each other or with the elements of either of the two GOEs. Strictly speaking, the symmetry-breaking interaction also contributes to the diagonal blocks H^{T_1} and H^{T_2}. However, such contributions can be incorporated in the random-matrix description of these blocks and therefore do not appear explicitly in the model.

To define the strength of $\overline{V^2}$, we recall Eq. (4). That equation seems to suggest that we put $\overline{V^2}=\alpha^2\lambda^2/N$, with $\alpha^2 \ll 1$ to account for the weakness of the symmetry-breaking interaction. That is not correct, however, and we must choose $\overline{V^2}=\alpha^2\lambda^2/N^2$, with α a strength parameter that is independent of N in the limit $N\to\infty$. Indeed, without symmetry breaking, the spectra of H^{T_1} and H^{T_2} are uncorrelated. A weak symmetry-breaking interaction induces level repulsion and stiffness among levels with different isospin. That happens when the matrix elements of V are of the order of the mean level spacing $d=\pi\lambda/N$, or when $\overline{V^2}$ is of the order of λ^2/N^2. Hence the ratio of the strength of the symmetry-breaking interaction (average of the square of the matrix elements) over that of the symmetry-conserving interaction vanishes asymptotically as $1/N$ for $N\to\infty$, since the mean level spacing likewise vanishes in that limit. Conversely, symmetry violation becomes detectable in spectral fluctuation measures when the matrix elements of the symmetry-breaking interaction are of the order of the mean level spacing. This condition was already mentioned below Eq. (5) and is met by the isospin-violating matrix elements in light nuclei; see Sec. III.D.2. The same conclusion is reached when we consider the violation of time-reversal invariance in Sec. III.D.4. Apparently Pandey (1981) was the first to note the relevance of such small parameters for violations of symmetry and/or invariance.

The parameter $\overline{V^2}$ suffers from the same shortcoming as discussed in Sec. II.G for the mean-square-matrix element of a doorway state: $\overline{V^2}$ changes strongly with excitation energy and/or mass number. A much smoother measure of symmetry breaking is the spreading width; see Eq. (26). There are two possible definitions for $\Gamma^{\downarrow}$,

$$\Gamma^{\downarrow T_1}=2\pi\overline{V^2}\rho^{T_2},\quad \Gamma^{\downarrow T_2}=2\pi\overline{V^2}\rho^{T_1}, \tag{31}$$

where ρ^T is the level density for the states with isospin T. It is largely a matter of convenience which of these definitions is used. To interpret the spreading widths, we consider without loss of generality the first of Eqs. (31). We use a basis in which both H^{T_1} and H^{T_2} are diagonal. We first assume that the mean level spacing $1/\rho^{T_1}$ of states with isospin T_1 is significantly larger than $\Gamma^{\downarrow T_1}$ and that $\Gamma^{\downarrow T_1}$ is significantly larger than $1/\rho^{T_2}$. Then the arguments of Sec. II.G apply, each state with isospin T_1 acts as an isolated doorway state, and $\Gamma^{\downarrow}$ is the average width of the probability distribution for finding the doorway state mixed into the eigenstates of the full system. We expect that that interpretation remains qualitatively valid also when the inequalities $1/\rho^{T_1}\gg\Gamma^{\downarrow}\gg 1/\rho^{T_2}$ are violated. In other words, $\Gamma^{\downarrow T_1}$ ($\Gamma^{\downarrow T_2}$) is a measure of the width in energy with which every eigenstate of H^{T_1} (of H^{T_2}, respectively) is spread over the eigenstates of the full system.

The random-matrix ensemble (30) lacks the overall orthogonal symmetry of the GOE. By construction, the ensemble is invariant, of course, under orthogonal transformations of the first N_1 (the last N_2) states, respectively. Nonetheless, the analytical treatment of symmetry violation in RMT is much more difficult than treating a single GOE. While analytical results for the ensemble (30) are not available, replacing each of the two block-diagonal GOEs in Eq. (30) by a GUE, and considering the complex matrix elements in the nondiagonal blocks as uncorrelated Gaussian-distributed random variables with zero mean value and common variance $\overline{V^2}$, one arrives at a tractable problem (Guhr and Weidenmüller, 1990a). Although belonging to a different symmetry class, the resulting ensemble is expected to possess features that are qualitatively similar to those of the ensemble (30). Additional information is generated by a numerical analysis of the ensemble (30).

As $\overline{V^2}/d^2\propto\alpha^2$ increases from zero, the spectral fluctuations change from those of two uncorrelated GUEs to those of a single GUE. From $\overline{V^2}/d^2=0$ to $\overline{V^2}/d^2>0$, the change is discontinuous: Level repulsion among states with different T sets in suddenly. For the local spectral fluctuation measures considered by Guhr and Weidenmüller (1990a), the case of a single GUE is attained when $\overline{V^2}/d^2\approx 1$. We expect this statement to apply likewise to other fluctuation measures, and to hold similarly for the ensemble in Eq. (30). The expectation is confirmed by numerical simulations.

2. Complete level schemes

As described in Sec. III.B.5, complete level schemes were determined for the nuclides ^{26}Al and ^{30}P. These odd-odd $N=Z$ nuclei are particularly interesting because here the densities of states with $T=0$ and with $T=1$ are almost equal, starting from the ground state, while in most nuclei the states with higher T are shifted toward higher excitation energies. Thus these nuclei are ideal to study the effect of isospin-symmetry breaking.

A qualitative test for a conserved symmetry is to consider what happens when that symmetry is neglected. As an example, in Fig. 15 the Δ_3 statistic is shown for the states in ^{26}Al. Only the quantum numbers shown at the top of each panel are taken into account in evaluating Δ_3. We note that ignoring the good quantum number J leads to a major increase in Δ_3. Ignoring T, on the other hand, leads to a very small change of Δ_3. This seems to suggest that isospin is not a good quantum number, in apparent contradiction to other evidence that isospin is only slightly broken (at about the 3% level) in this nuclide.

The point is that (as discussed in Sec. III.D.1) the impact of symmetry breaking on Δ_3 depends on the ratio of the symmetry-breaking matrix element to the mean level spacing d and is thus enhanced by small spacings.

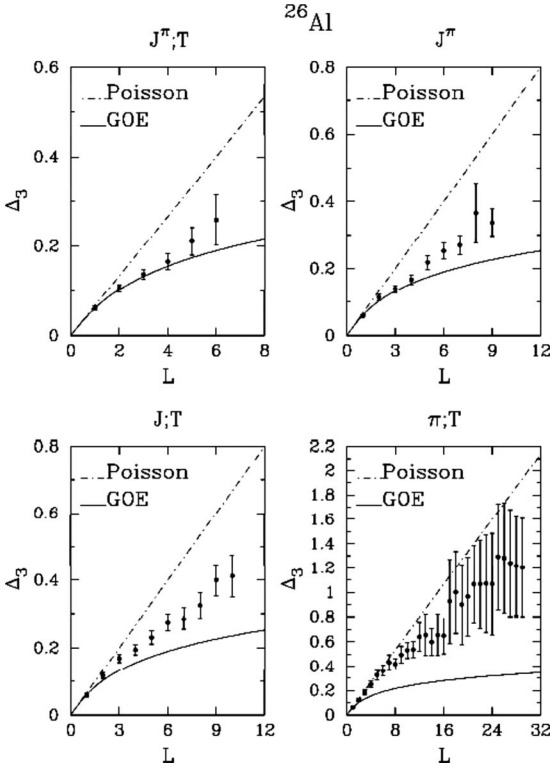

FIG. 15. The Δ_3 statistic shown for the states in ^{26}Al obtained by taking into account only the quantum numbers indicated at the top of each panel.

Hence, a small degree of symmetry breaking can have a large effect on the statistical measures. Somewhat fortuitously, the strength of symmetry breaking in ^{26}Al is such that the Δ_3 statistic lies between the values for a single GOE and for two GOEs; see Fig. 16. More precisely, the root-mean-square value of the symmetry-breaking Coulomb matrix elements in ^{26}Al is a little smaller than, but

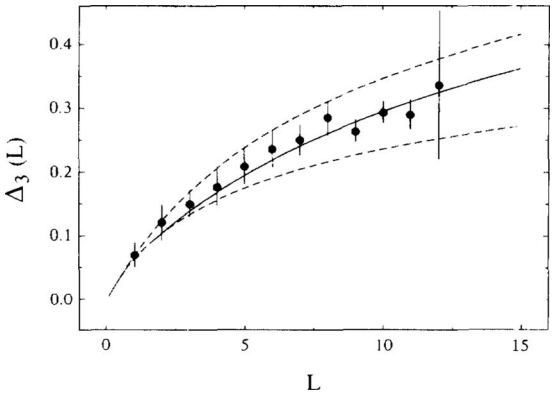

FIG. 16. The spectral rigidity Δ_3 vs L for 75 levels with $T=0$ and 25 levels with $T=1$ measured in ^{26}Al (dots with error bars). The excitation energies lie between 0 and 8 MeV. The lower (upper) dashed line is the prediction for a single GOE (for two uncorrelated GOEs with fractional densities 3/4 and 1/4, respectively). The solid line is the result of a numerical simulation incorporating symmetry breaking. The strength of the symmetry-breaking interaction was fitted to the data. From Guhr *et al.*, 1998.

of the order of, the mean level spacing (Guhr and Weidenmüller, 1990a). The results were consistent with other experimental determinations. Experimental results on isospin violation for ^{30}P were almost identical with the ^{26}Al results (Shriner *et al.*, 2000).

Although these results were consistent with theoretical expectations, they were not considered definitive due to the small sample sizes. Definitive results on symmetry breaking were provided by measurements of acoustic resonances in quartz blocks (Ellegaard *et al.*, 1996) and of electromagnetic resonances in coupled microwave billiards (Alt *et al.*, 1998). In these measurements, the strength of the symmetry breaking force could be effectively varied and much larger sample sizes were obtained. The agreement with the RMT model of Eq. (30) was excellent.

The third nucleus with a "nearly complete" level scheme (for excitation energies below 4.3 MeV) is ^{116}Sn. In that nucleus, the NNS distribution was studied (Raman *et al.*, 1991). Only sequences with a minimum of five levels with the same spin and parity assignments were included in the analysis; there were six such sequences. The histogram for the NNS distribution was fit with the Brody parametrization (28). The fit gave $\omega=0.51\pm0.19$, similar to the best fit in ^{26}Al, which gave $\omega=0.47\pm0.14$. In ^{26}Al, the deviation from GOE predictions is due to isospin symmetry breaking. The cause for the same phenomenon in ^{116}Sn is not clear. The nucleus ^{116}Sn is mentioned in the present section only because of its nearly complete level scheme.

3. Transition strengths

After the studies of isospin symmetry breaking in the complete spectra of ^{26}Al and ^{30}P (see Sec. III.D.2), the effect of symmetry breaking on the eigenvectors in the same systems was also explored. Although there was no formal proof, heuristic arguments predicted that the Porter-Thomas distribution would not be changed by symmetry breaking. The central point of the argument was the complexity of the wave functions of initial and final states of the transitions.

The TUNL group (Adams *et al.*, 1998; Shriner *et al.*, 2000) used the reduced electromagnetic transition probabilities B in these nuclei as the data set. To eliminate issues of scale, subgroups of the transitions were considered. The transition probabilities were classified according to multipolariy (electric dipole $E1$, electric quadrupole $E2$, and magnetic dipole $M1$) and to the isospin difference $\Delta T=0$ or 1 between initial and final states. The parameter $y=B/\bar{B}$ turns out to have a very large dynamic range. Therefore, it is convenient to use $z=\log_{10} y$. In terms of that variable, the upper panels of Fig. 17 show the Porter-Thomas distribution as solid lines. The lower panels give the integrated distributions. The histograms show the data for ^{30}P. Details of the analysis have been given by Adams *et al.* (1998) and Shriner *et al.* (2000). Similar results were obtained for

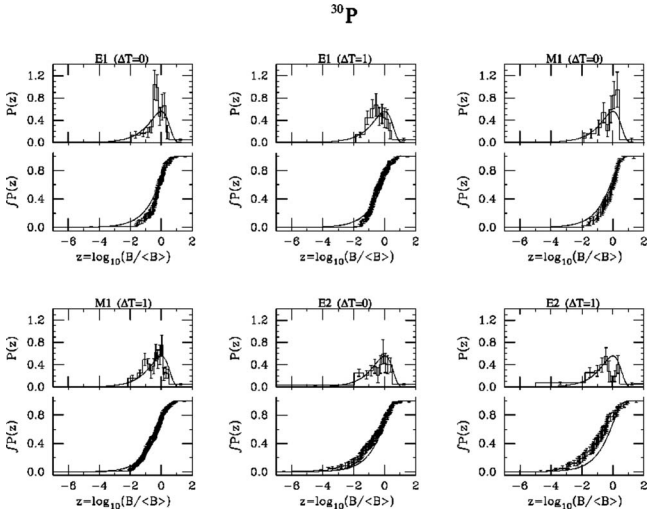

FIG. 17. Comparison between the Porter-Thomas distribution (written in terms of the variable $z=\log_{10} y$) (solid lines) and the data (histograms) for several multipole transitions and isospin differences in ^{30}P. From Shriner *et al.*, 2000.

^{26}Al. It is obvious that the data do not agree with the Porter-Thomas distribution.

It was some years before this somewhat unexpected result was formally analyzed and explained. Barbosa *et al.* (2000) used basically the same approach as for the description of symmetry breaking on the level statistics; see Sec. III.D.1. We only sketch the central point. We consider electromagnetic transitions of a given multipolarity (typically $M1$ or $E2$). The model (30) has to be extended because the electromagnetic transition operator does not, in general, conserve either T or J and connects states with different spins as well as different isospins. For $\overline{V^2}=0$, the eigenfunctions of H are eigenfunctions either of $\mathcal{H}^{J_1T_1}$ or of $\mathcal{H}^{J_2T_2}$. For fixed J_1,J_2, the transition matrix elements belong to one of three classes: (i) those coupling two states with isospin T_1, (ii) those coupling two states with isospin T_2, and (iii) those coupling two states with different isospins. The distribution of matrix elements within each class is expected to be approximately Gaussian, but the three Gaussian distributions may have different heights and widths. Moreover, transitions with different multipolarities behave differently. Therefore, the squares of the transition matrix elements in Fig. 17 cannot have a simple Porter-Thomas distribution even for $\overline{V^2}=0$. As $\overline{V^2}$ increases from zero, the Gaussian distributions get mixed. Details are only accessible numerically. With a somewhat different approach, Hussein and Pato (2000) also predicted a deviation from the Porter-Thomas distribution. Neither group attempted to fit the experimental data in detail. Such an analysis is still missing. We conclude that while the effect of isospin symmetry breaking on the level statistics is a generic phenomenon that can be accounted for completely by a simple extension of RMT in terms of a single parameter (the spreading width), the effect of symmetry breaking on the electromagnetic transition strengths involves additional dynamic elements (classification of the transition matrix elements).

While the size of the data set in ^{26}Al and ^{30}P is limited, experiments using coupled microwave billiards (Dembowski *et al.*, 2005) yielded data with much better statistics. The distribution of transition strengths deviates from the Porter-Thomas distribution. The theory of Barbosa *et al.* (2000) was extended to this case by Dietz *et al.* (2006).

4. Test of time-reversal invariance

Because of the antiunitarity of the time-reversal operator, the modeling of a violation of time-reversal invariance in RMT is fundamentally different from that of a broken symmetry, as discussed in Sec. III.D.1. As explained in Sec. II.A, time-reversal invariance allows us to choose the Hamiltonian matrix as a real and symmetric matrix. The matrix ensemble that models such systems is the GOE. If time-reversal invariance does not hold, the Hamiltonian matrix is Hermitian but cannot, in general, be chosen real and symmetric. The matrix ensemble that models such systems is the GUE; see Sec. II.B. To describe the violation of time-reversal invariance in RMT, we need to construct an ensemble that interpolates between the GOE and the GUE. This is done as follows. Every Hermitian matrix can be written as the sum of a real symmetric matrix and of i times a real antisymmetric matrix. A stochastic model for a Hamiltonian with some violation of time-reversal symmetry is then

$$H=\frac{1}{\sqrt{1+(1/N)\alpha^2}}(H^{\mathrm{GOE}}+N^{-1/2}\alpha iA). \tag{32}$$

Here H^{GOE} represents the GOE, and the elements of the real antisymmetric matrix A are Gaussian-distributed random variables with zero mean value and a second moment given by

$$\overline{A_{\mu\nu}A_{\rho\sigma}}=\frac{\lambda^2}{N}(\delta_{\mu\rho}\delta_{\nu\sigma}-\delta_{\mu\sigma}\delta_{\nu\rho}). \tag{33}$$

The elements of A and H^{GOE} are uncorrelated. The real dimensionless parameter α describes the strength of the violation of time-reversal invariance. For $\alpha=0$ we deal with the GOE, and for $\alpha=N^{1/2}$ we deal with the GUE.

For tests of the violation of time-reversal invariance in nuclei, the central feature of the GUE is level repulsion at small distances (scaled spacing $s\ll 1$). In the case of the GOE, level repulsion leads to a linear dependence of the NNS distribution for small s; see the Wigner surmise (19). In contradistinction, the NNS distribution for the GUE increases quadratically with s for small s. A test for a violation of time-reversal invariance in nuclei is, therefore, based on a detailed examination of the NNS distribution at small spacings (French *et al.*, 1985). As explained below Eq. (5) and, in a different context, in Sec. III.D.1, the mixing of levels (and, thus, the spacing distribution) is sensitive to very small mixing matrix elements that are of the order of the GOE mean level

spacing $d=\pi\lambda/N$. For the perturbation $N^{-1/2}\alpha iA$ in Eqs. (32) and (33), the root-mean-square matrix element has the value $\alpha\lambda/N$. This is comparable to d for $\alpha\approx 1$, which explains the choice of factors $N^{1/2}$ in Eq. (32). As in Sec. III.D.1, the mixing parameter $N^{-1/2}\alpha$ vanishes asymptotically as $1/\sqrt{N}$. The analysis was done (French *et al.*, 1985) for the nuclear data ensemble (see Sec. III.C.1), where typical spacings d are of the order of 10 keV, and yielded an upper bound of about $d/10$ for the time-reversal noninvariant matrix element of the nuclear Hamiltonian. From this result, French *et al.* (1985) inferred an upper bound of about 1% for the time-reversal noninvariant part of the nucleon-nucleon interaction.

IV. CHAOS IN NUCLEAR MODELS

Sections II and III were based almost entirely on concepts of RMT and made little use of the wealth of information on the dynamical behavior of nuclei. We fill this gap in the present section. We discuss the two leading nuclear-structure models which describe phenomenologically the dynamics of nuclei: the shell model (which mostly applies to spherical nuclei) and the collective model (which mostly applies to nuclei with surface deformations). We give an introduction to both models which, in their simplest form, are fully integrable and thus give rise to regular motion. We present evidence that both models also allow for chaotic motion. We then turn to a number of specific applications of RMT that incorporate dynamical aspects.

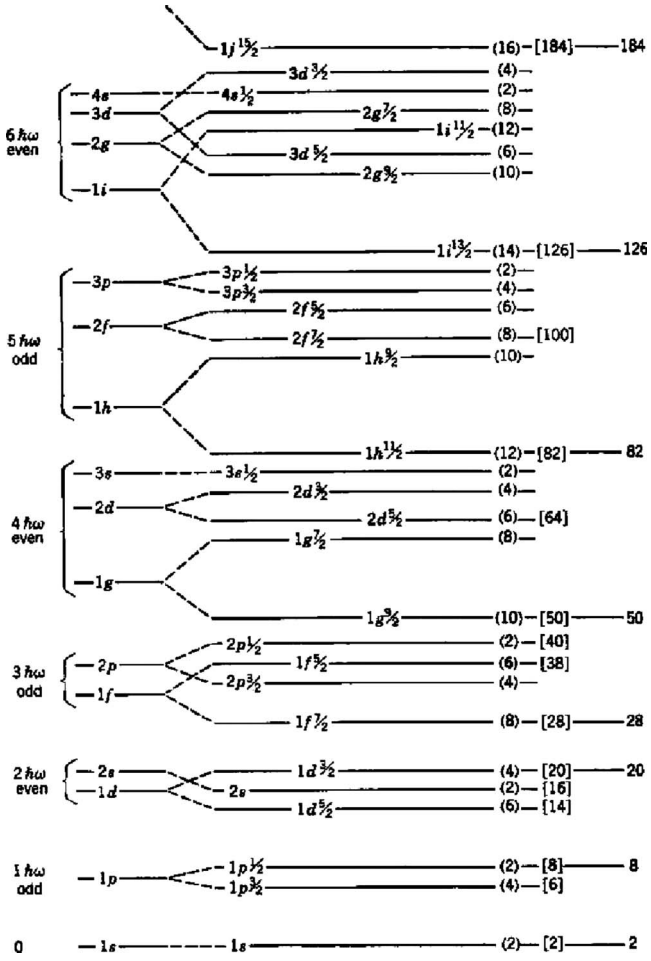

FIG. 18. Level sequence in the nuclear shell model. From Mayer and Jensen, 1955.

A. Spherical shell model

1. The nuclear shell model

In the elementary version of the nuclear shell model, nucleons move independently under the influence of a common mean field. Attempts to introduce a mean field into nuclear theory date back to the 1930s. These attempts were unsuccessful at the time, partly because they lacked an essential ingredient (the strong spin-orbit coupling) and partly because of the success of Bohr's idea of the compound nucleus, which depicted nuclei as systems of strongly interacting particles. The introduction in 1949 of a central single-particle potential with strong spin-orbit coupling by Haxel *et al.* (1949) and Mayer (1949) changed that situation. That model was successful in the description of nuclear properties in the ground-state domain and shifted attention away from the compound-nucleus picture. It gave rise to a burst of spectroscopic activity that lasted for many years and thoroughly validated the model.

The sequence of single-particle levels of the nuclear shell model is shown in Fig. 18. The scheme is fundamentally that of the harmonic oscillator in three dimensions with excitation energies $n\hbar\omega$ and $n=0,1,2,\ldots$. The integer n defines the major shells. Individual levels are denoted by $n+1$, by the single-particle angular momentum ℓ in spectroscopic notation, and by the single-particle total spin j obtained by vector-coupling the angular momentum operator $\vec{\ell}$ and the spin $\vec{s}$. (Here we do not distinguish neutrons and protons and take isospin as a good quantum number. The picture requires some modification for medium-weight and heavy nuclei, which we do not address.) The degeneracy of the single-particle states in each major shell, which is characteristic of the harmonic oscillator, is lifted because the single-particle potential does not have the shape of a harmonic oscillator, and because of the presence of a strong spin-orbit coupling that pushes the states with highest spin in each major shell down into the next-lower major shell (except for the lowest shells, where the spin-orbit interaction is not strong enough). Thus each major shell contains a number of subshells, each of which is characterized by the quantum numbers $(n+1,\ell,j)$. Within a given major shell, the index n is redundant and will often be omitted.

For a nucleus with mass number A, the A nucleons fill the lowest shells in accord with the exclusion principle. The completely filled shells are considered as inert, and

the spectroscopic properties of the low-lying states result from the m "valence nucleons," which partly fill the last shell (the "valence shell"). This scheme accounts for the strong binding energies of nuclei with closed shells, and for the ground-state properties of nuclei differing from closed-shell ones by the addition or removal of a single nucleon. For nuclei with more than one valence nucleon (or more than one hole in the valence shell), an extension of the model is called for because in such cases strong degeneracies occur in the model which are not observed in reality. For instance, two valence nucleons in the $1d_{5/2}$ subshell of the $2s1d$ shell can be coupled to total isospin $T=0$ or 1. For $T=0$ ($T=1$), the possible states have odd (even) total spin values J ranging from $J=0$ to 5. All of these states are degenerate in the elementary shell model.

To remedy that situation, the elementary shell model is viewed as a mean-field theory that takes account of most (but not all) of the nucleon-nucleon interaction. The remaining "residual interaction" must be included to obtain quantitative agreement with data. From the point of view of many-body theory, the residual interaction is an effective interaction. The residual interaction is usually assumed to be a two-body interaction [although there is evidence (Pieper and Wiringa, 2001) that three-body forces are needed in some cases to obtain good fits to the data], to be time-reversal invariant, and to conserve spin and parity. In the spirit of the shell model, it is also assumed that the residual interaction is weak (it does not significantly mix the many-body states belonging to different major shells), so that it effectively acts only among the m valence nucleons in the valence shell.

The input for this model (the full shell model or, in brief, the shell model) consists of the single-particle energies $\varepsilon_{\ell j}$ in the valence shell, and of the matrix elements of the residual interaction in that shell. The residual two-body interaction $V_{\rm res}$ is completely characterized by a finite number of two-body matrix elements. The two-body states $|j_1 j_2 st\sigma\tau\rangle$ are obtained by coupling any two single-particle states $(\ell_1 j_1)$ and $(\ell_2 j_2)$ in the valence shell to total spin s and total isospin t with z components σ and τ. The antisymmetrized two-body matrix elements of $V_{\rm res}$ have the form $\langle j_3 j_4 st|V_{\rm res}|j_1 j_2 st\rangle$. Our notation implies conservation of spin and isospin and takes account of the fact that the values of the matrix elements do not depend on σ and τ. Conservation of parity imposes an additional constraint not explicitly displayed in our notation. For brevity, we refer to these matrix elements by the symbol v_α. The index α enumerates all allowed and distinct (i.e., not connected by symmetry) two-body matrix elements in the valence shell. For the $2s1d$ shell, the range of α is 63, while for the $2p1f$ shell it is 195.

In second quantization, the shell-model Hamiltonian governing the m valence nucleons is then given by

$$\mathcal{H} = \sum_{\ell j} \varepsilon_{\ell j} \sum_{\sigma\tau} a^\dagger_{j\ell\sigma\tau} a_{j\ell\sigma\tau} + \frac{1}{4} \sum_{j_1 j_2 j_3 j_4 st} \langle j_3 j_4 st|V_{\rm res}|j_1 j_2 st\rangle \times \sum_{\sigma\tau} A^\dagger_{j_3 j_4 st\sigma\tau} A_{j_1 j_2 st\sigma\tau}. \quad (34)$$

Here $a^\dagger_{j\ell\sigma\tau}$ creates a nucleon in a state (ℓj) with spin z component σ and isospin z component τ while $A^\dagger_{j_3 j_4 st\sigma\tau}$ creates a pair of nucleons in the state $|j_1 j_2 st\sigma\tau\rangle$. The operators $A^\dagger$ are obtained straightforwardly by vector-coupling products of two operators $a^\dagger_{j\ell\sigma\tau}$ and are not given explicitly.

The eigenvalues and eigenfunctions of $\mathcal{H}$ are identified with the low-lying states of nuclei. For instance, nuclei pertaining to the $2s1d$ shell (the "sd-shell nuclei") have mass numbers $17 \leqslant A \leqslant 39$, and the number of valence nucleons has the range $1 \leqslant m \leqslant 23$. Mass numbers $A=16$ and $A=40$ correspond to the closed-shell nuclei ^{16}O (the $1s$ and $1p$ shells are filled) and ^{40}Ca (the $2s1d$ shell is filled, too). Likewise there are $2f1p$ shell nuclei, etc. (We disregard the $1p$-shell nuclei as they yield too few spectroscopic data for a meaningful statistical analysis.) According to the shell model, the Hamiltonian $\mathcal{H}$ determines the spectral properties of the low-lying states of all nuclei pertaining to the same shell, at least in principle. This claim is subject to a number of provisos. (i) To get good fits to the spectra of all nuclei in a major shell, it may be necessary to allow for a weak dependence of the parameters $\varepsilon_{\ell j}$ and v_α on the number m of valence nucleons. (ii) Non-valence-shell states may be pushed down by the residual interaction into the domain of low excitation energies ("intruder states") and require special treatment. Such states are obtained, for instance, by lifting one or several nucleons from the valence shell into the next higher major shell, or from the inert core into the valence shell, or both. (iii) In its upper part, the spectrum of $\mathcal{H}$ cannot be expected to correspond to reality because the much more numerous non-valence-shell states dominate the actual spectrum and mix with the states in the valence shell. In the studies of chaos reported below, one disregards this fact and confines attention to the valence shell. This is done in order to obtain a manageable numerical problem. There are strong reasons to believe that the results are universal and, thus, also hold when the mixing between major shells is taken into account [see, for instance, Ormand and Broglia (1992)]. (iv) In the form of Eq. (34), the shell model applies to spherical nuclei (although it can be extended to weakly deformed nuclei). Chaos in deformed nuclei is treated in Sec. IV.B.

For purposes of orientation, we cite a few numbers taken from Bohr and Mottelson (1969) and Zelevinsky *et al.* (1996). The spacing between major shells is approximately given by the harmonic-oscillator energy $\hbar\omega \approx 40A^{-1/3}$ MeV. The spin-orbit interaction is $\approx -20(\vec{l}\cdot\vec{s})A^{-2/3}$ MeV. The spacings of adjacent single-particle energies may be as large as a couple of MeV. In the sd shell, for instance, the empirical values in ^{17}O are $\varepsilon_{d5/2} = -4.15$ MeV, $\varepsilon_{s1/2} = -3.28$ MeV, and $\varepsilon_{d3/2}$

=0.93 MeV. With these values and for $m=12$ valence nucleons, the range of the elementary *sd*-shell spectrum would be about 42 MeV. (These values are not completely representative since the $\varepsilon_{\ell j}$s themselves are actually used as fit parameters.) The diagonal matrix elements of the residual interaction may be as large as 1 or 2 MeV in magnitude. This removes some of the degeneracies of the elementary shell model referred to above and stretches the spectrum further. The nondiagonal elements typically amount to several hundred keV in magnitude. These numbers suggest that the residual interaction is able to mix the states in different subshells of the valence shell, while the spectral properties at low excitation energy are essentially determined by valence-shell states (the admixtures of non-valence-shell states are negligible).

Not all parameters of the shell model can be determined equally well by a fit to spectroscopic data. That topic is discussed further in Secs. IV.A.2 and V.B.3. To overcome that difficulty, one uses nuclear many-body theory (i.e., variants of the Bethe-Brueckner-Goldstone expansion) to calculate the two-body matrix elements of $V_{\rm res}$. The results serve as starting values for a fit to the data. In the fit, the two-body matrix elements themselves, or some parameters on which they depend, are varied (Brown and Wildenthal, 1988; Honma *et al.*, 2002). There is evidence that the necessary corrections account mainly for three-body forces (Caurier *et al.*, 2005).

Since $\mathcal{H}$ conserves spin, isospin, and parity, the eigenfunctions of $\mathcal{H}$ are simultaneously eigenfunctions of total spin J, total isospin T, and parity Π. One way to obtain the eigenfunctions of $\mathcal{H}$ with given J,T,Π for m valence nucleons consists in constructing the matrix of $\mathcal{H}$ in a basis of m-body states carrying these quantum numbers and in diagonalizing that matrix. (This is not always the most efficient procedure numerically, but is used here for the sake of argument.) The m-body states needed for this procedure are obtained from the elementary shell model by constructing all Slater determinants of m valence nucleons in the valence shell. These determinants form classes, each class defined by the set $\{m_{\ell j}\}$ where $m_{\ell j}$ is the number of nucleons occupying the subshell (ℓj). The set $\{m_{\ell j}\}$ obviously forms a partition of m so that $\Sigma_{\ell j} m_{\ell j}=m$, where the sum runs over the subshells of the valence shell. The Slater determinants are antisymmetric by construction, but typically are not eigenstates of J and T. The m-body states with good J, T, and Π and fixed $\{m_{\ell j}\}$ are found as linear combinations of the determinants in class $\{m_{\ell j}\}$ and are denoted by $|JT\Pi\mu\rangle$. (We suppress the magnetic quantum numbers and the class index $m_{\ell j}$.) The states $|JT\Pi\mu\rangle$ span a Hilbert space of finite dimension $\mathcal{D}(J,T,\Pi)$, which defines the range of the running index μ. In the $2s1d$ shell and depending on the quantum numbers (J,T), $\mathcal{D}$ ranges from a few to about 7000 in the middle of the shell ($m=12$), while $\mathcal{D}$ attains considerably larger maximum values already in the $2p1f$ shell. This is why the $2s1d$ shell has been the preferred object for theoretical studies of chaos in nuclei. The actual construction of the states $|JT\Pi\mu\rangle$ is cumbersome, involves angular-momentum algebra, and is not given here (De Shalit and Talmi, 1963). In that basis, the matrix elements of $\mathcal{H}$ have the form

$$\mathcal{H}_{\mu\nu}(JT\Pi) \overset{\text{def}}{=} \langle JT\Pi\mu|\mathcal{H}|JT\Pi\nu\rangle = \delta_{\mu\nu}\sum_{\ell j}\varepsilon_{\ell j}m_{\ell j} + \sum_{\alpha} v_{\alpha}C_{\mu\nu}(\alpha;JT\Pi). \quad (35)$$

The first term on the right-hand side of the last of Eqs. (35) is obvious. The form of the second term follows from Eq. (34) except that we have grouped together all matrix elements that are connected by symmetry. Save for this operation, the coefficients $C_{\mu\nu}(\alpha;JT\Pi)$ are matrix elements of the operator $\Sigma_{m\tau}A^{\dagger}_{j_3j_4stm\tau}A_{j_1j_2stm\tau}$ taken between states $|JT\Pi\mu\rangle$ and $|JT\Pi\nu\rangle$. By construction, the matrix $\mathcal{H}_{\mu\nu}$ is real and symmetric.

The form (35) displays explicitly the dependence of the matrix $\mathcal{H}_{\mu\nu}(JT\Pi)$ on the input parameters $\varepsilon_{\ell j}$ and v_{α} of the shell model. We emphasize that the coefficients $C_{\mu\nu}(\alpha;JT\Pi)$ (which for fixed α, J, T, and Π form a real and symmetric matrix in Hilbert space) are determined entirely by the valence shell in which we are working, by the coupling scheme we have used to construct the states $|JT\Pi\mu\rangle$, and by the two-body operator labeled α of which the matrix elements are taken. Except for a set of unitary transformations connecting the coupling scheme we have chosen with any other one, the matrices $C_{\mu\nu}(\alpha)$ are uniquely determined. These matrices reflect the symmetries and invariances of the elementary shell model and are independent of the residual interaction actually considered. In other words, going from one residual interaction with matrix elements v_{α} to another one with matrix elements v'_{α}, all we need to do is to replace the coefficients v_{α} in Eq. (35) by the coefficients v'_{α}, the matrices $C_{\mu\nu}(\alpha)$ remaining the same. We emphasize this simple fact because some properties of the shell-model Hamiltonian $H_{\mu\nu}(JT\Pi)$ are determined by the matrices $C_{\mu\nu}(\alpha)$ alone and are thus generic (i.e., largely independent of the choice of the residual interaction).

It was mentioned before and we emphasize again that the shell model accounts successfully for a vast amount of spectroscopic data in the ground-state domain of spherical nuclei. This is not the place to go into any details. Suffice it to say that some basic features of $V_{\rm res}$ are well established: Pairs of nucleons coupled to isospin $T=1$ have a strong and attractive interaction ("pairing force"). That force leads to spin-0 ground states in even-even nuclei and favors the seniority coupling scheme (De Shalit and Talmi, 1963). In the particle-hole channel, the diagonal elements of $V_{\rm res}$ for pairs of nucleons with isospin $T=0$ (neutron-proton pairs) also show strong attraction, especially for large angular momenta ("quadrupole-quadrupole interaction") and favor nuclear deformations, especially for nuclei far (in mass number) from closed-shell nuclei (see Bohr and Mottelson, 1969). For the *sd* shell, Wildenthal (1984) and Brown and Wildenthal (1988) have established the stan-

dard parameters of the residual interaction ("Brown-Wildenthal interaction") by fitting the 66 parameters (63 two-body matrix elements and 3 single-particle energies) to more than 400 pieces of data. The Brown-Wildenthal interaction may optionally include the Coulomb interaction between protons.

2. Chaos in the shell model

Ever since the shell model was established, a strange dichotomy pervaded nuclear-structure theory. On the one hand, the shell model was extremely successful in describing the properties of low-lying states in many nuclei, and the collective models in their various forms afforded a description of those nuclei that were not accessible to the shell model. Fits to data revealed the basic properties of the residual interaction. Ever more sophisticated measurements widened the data basis. Theoretical efforts were directed both at the determination of $V_{\rm res}$ from the interaction between free nucleons via many-body theory and at the technology to calculate nuclear properties from the shell-model Hamiltonian, including those of deformed nuclei, and thus at understanding collective models. The hope seemed justified that one day one would arrive at a complete understanding of the structure of atomic nuclei. In the 1970s and 1980s, most work in nuclear-structure theory was devoted to that vision.

On the other hand, during the same period the evidence for the applicability of RMT to neutron and proton resonance data grew and was definitively established by 1982; see Sec. III.C.1. But aside from fundamental symmetries, RMT lacks any dynamical structure whatsoever. What did the success of RMT imply for the shell model? Is there an excitation energy (somewhere below neutron threshold but above the energies where shell-model calculations were so successful) beyond which the shell model fails to work and chaos takes over? Or is chaos possible (and perhaps even generic) in the framework of the shell model itself?

In spite of a strong growth of chaos-related research in other fields of physics in the 1980s and early 1990s, these questions did not receive much attention at the time by the nuclear-structure community. The main reason was probably the lack of statistically significant experimental data. In addition, a strong commitment on the part of the community to understand nuclei on a fundamental level perhaps deflected attention away from the issue of chaos. Only a few theoretical papers addressed that issue. Early work by Whitehead *et al.* (1978), Verbaarschot and Brussard (1979), Brown and Bertsch (1984), and Dias *et al.* (1989) addressed the validity of the Porter-Thomas distribution for shell-model eigenfunctions; see comments below. The relation between spectral fluctuations and the shell model was addressed by Weidenmüller (1985). Meredith *et al.* (1988) and Meredith (1993) studied the Lipkin-Meshkov-Glick model: $\mathcal{M}$ fermions occupy a system with three nondegenerate subshells each containing $\mathcal{M}$ degenerate single-particle states. In each subshell, the single-particle states do not carry any further quantum numbers. The two-body interaction acts only between particles in different subshells. All nonzero matrix elements are identical. The Hilbert space has finite dimension. Symmetries reduce the problem to manageable size even when $\mathcal{M}$ is large. The system possesses a classical limit that is attained for coherent states when $\mathcal{M}\to\infty$. Classical chaos can thus be studied in its dependence on the strength of the two-body interaction. As that strength is varied, a close correspondence is numerically established between the transition from regular to chaotic motion and that from Poisson to GOE statistics for the spectral fluctuation measures of the quantum system. The Bohigas-Giannoni-Schmit conjecture was first verified for an interacting many-body system (albeit in the framework of a toy model without characteristic ingredients of the shell model such as conserved quantum numbers). In the 1990s, several (Åberg, 1990; Alhassid *et al.*, 1990; Alhassid and Whelan, 1991; Martinez-Pinedo *et al.*, 1997) addressed chaos in the collective model. This topic is reviewed in Sec. IV.B.

Ormand and Broglia (1992) reported a study of quantum chaos in the shell model for the *sd* shell. That work displayed several features that were also discussed by Zelevinsky *et al.* (1996). We focus on that later, much more extensive paper. They undertook a thorough and systematic theoretical study of chaos in the *sd* shell. They used the well-established Brown-Wildenthal (1988) form of the residual interaction, which is free of random elements. In most of their calculations, Coulomb effects were neglected. They focused attention mainly on nuclei in the middle of the shell ($m=12$) where the dimensions $\mathcal{D}(J,T)$ of the shell-model matrices are manageable and yet sufficiently large for a statistical analysis. (We drop the label Π since all states in the *sd* shell have positive parity.) They calculated spectra and eigenfunctions of the shell-model Hamiltonian numerically and compared the results both with GOE predictions and with thermal averages. The latter were considered because chaos was suspected by Percival (1973) to cause the many-body eigenfunctions all "to look the same," so that concepts such as mean occupation numbers for single-particle states and the Fermi-Dirac distribution may make sense for observables averaged locally over energy.

They used ergodicity (Sec. II.C.3) to compare GOE ensemble averages with running averages over the calculated spectra. To obtain statistically significant results, they used all eigenvalues and/or eigenfunctions pertaining to fixed m and to a pair (J,T) of quantum numbers. As pointed out earlier (Sec. IV.A.1), calculations using only states from the valence shell yield results that are unrealistic in the upper part of the spectrum where non-valence-shell states actually dominate. Therefore, the work of Zelevinsky *et al.* (1996) must be considered a case study of quantum chaos within the shell model in a restricted Hilbert space, rather than a realistic calculation of nuclear properties. While we summarize the results of this work in the present section, we defer a detailed analysis of how chaos is generated in the shell model to Sec. V.B.

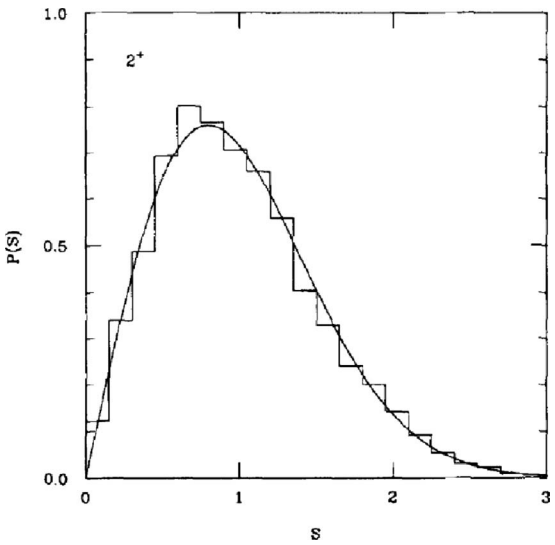

FIG. 19. NNS distribution (histogram) and Wigner surmise (solid line) for the states with $m=12$ and $J=2$, $T=0$ in the *sd* shell. From Zelevinsky *et al.*, 1996.

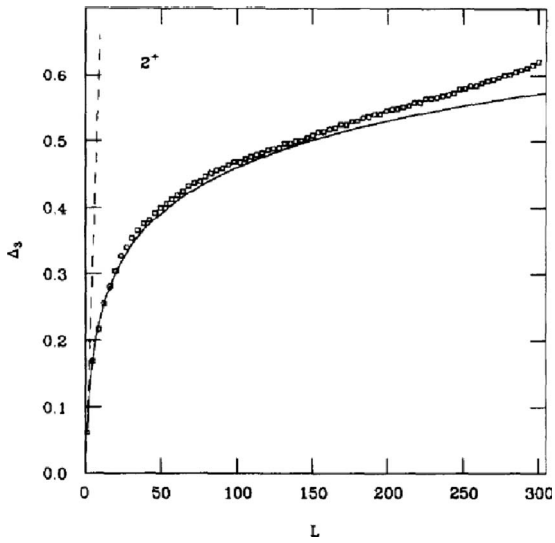

FIG. 20. The Δ_3 statistic (dots) and the GOE prediction (solid line) for states with $m=12$ and $J=2$, $T=0$ in the *sd* shell. From Zelevinsky *et al.*, 1996.

The average level density (calculated from the actual spectrum by smoothing) differs from that of the GOE and has approximately Gaussian shape. That result was anticipated years ago by Mon and French (1975); see also Sec. V.A. The nearly Gaussian shape is an artifact, of course, and due to the restriction to a single major shell; the actual nuclear level density grows nearly exponentially with excitation energy. Results of primary interest in the present context relate to quantum chaos and concern the local spectral fluctuation measures. After unfolding of the spectra, the NNS distribution and the Δ_3 statistic were found to agree well with GOE predictions in the middle of the shell and for sufficiently large values of the matrix dimension $D(J,T)$. For $m=12$ and the states with $J=2$, $T=0$ [$\mathcal{D}(2,0)=3276$], this is shown in Figs. 19 and 20. It is of interest to follow the onset of chaos as the strength of $V_{\rm res}$ is varied. For $V_{\rm res}=0$, the NNS distribution is found to be close to Poissonian, as expected. As the strength is increased, the distribution approaches the Wigner distribution and, within statistics, becomes indistinguishable from that distribution already for strength values amounting to 20% of the actual one. For smaller values of m (^{24}Mg with $m=8$), the NNS distribution at full strength value is still intermediate between the Poisson and the Wigner distribution, even for sizable values of $D(J,T)$ [$D(0,0)=1161$]. Here inclusion of the Coulomb interaction reduces the probability of very small spacings. The Δ_3 statistic in Fig. 20 agrees with the GOE prediction except for large values of L, where it rises above that prediction. That seems to be a systematic trend and is not fully understood at present. It perhaps signals a weakening of GOE-type correlations between eigenvalues with spacings of more than 7 MeV or so and might suggest that strong mixing is restricted to unperturbed shell-model configurations with energies within an energy interval of 10–20 MeV. We return to this point later. [A later evaluation of $\Delta_3(L)$ for the 3^- states showed good agreement with the GOE prediction up to $L\approx 3000$; however, see Zelevinsky (2007).]

Extensive shell-model calculations have also been done for nuclei in the $2p1f$ shell, especially by the Strasbourg-Madrid collaboration (Caurier *et al.*, 2005). We are not aware, however, of an equally thorough analysis of the results with respect to spectral fluctuation measures and other indicators for quantum chaos as done for the *sd* shell by Zelevinsky *et al.* (1996). Kota (2001) analyzed the calculated spectrum of 4^+ states in ^{48}Ca (Martinez-Pinedo *et al.*, 1997; Caurier *et al.*, 1999). Using the 1355 states located in the middle of the spectrum (out of a total of 1755 levels), he found good agreement with the Wigner surmise for the NNS distribution, and with the GOE prediction for the Δ_3 statistic. The latter is reported only for $L\leqslant 60$. Electromagnetic transition intensities and moments for $A\approx 60$ nuclei as calculated by Hamoudi *et al.* (2002) showed good agreement with the Porter-Thomas distribution.

Investigation of the distribution of eigenfunctions offers additional insight and shows the limitations of spectral fluctuation measures in establishing chaos. Here the Porter-Thomas distribution is the standard measure. In early calculations (Whitehead *et al.*, 1978; Verbaarschot and Brussard, 1979; Brown and Bertsch, 1984) for the *sd* shell, it was found that the actual distribution of widths differed from the Porter-Thomas form: There was an overabundance of the largest and smallest widths at the expense of those with values closer to the median. This was ascribed to incomplete mixing of the configurations, especially in the wings of the unperturbed spectrum: Too little mixing leads to admixtures with too small amplitudes and leaves the original states too pure. The issue was followed up by Zelevinsky *et al.* (1996). We denote by $W_{k\mu}$ the square of the amplitude with which an unperturbed shell-model configuration labeled μ is ad-

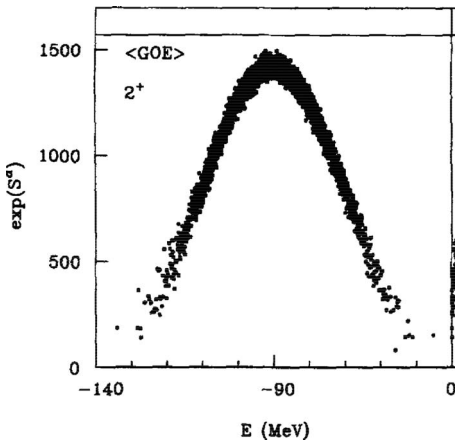

FIG. 21. The exponential of the information entropy (36) vs the energy of the state for the states with $m=12$, $J=2$, and $T=0$ in the *sd* shell (dots). The GOE limit of 1578 is indicated by the horizontal line. From Zelevinsky *et al.*, 1996.

mixed into an eigenstate of the shell-model Hamiltonian. The index k labels the eigenstates such that the associated eigenvalues E_k increase monotonically with k. The measure used was the "information entropy" S_k, which is defined as

$$S_k = -\sum_{\mu} W_{k\mu} \ln W_{k\mu}. \tag{36}$$

For complete mixing and large matrix dimension $\mathcal{D} \gg 1$, wave-function normalization makes us expect $W_{k\mu} \approx 1/\mathcal{D}$ independently of k and μ: On average, all configurations are equally mixed into every eigenstate. This corresponds to a maximum value of $S_k = \ln \mathcal{D}$. That naive estimate does not take into account the Porter-Thomas distribution for the $W_{k\mu}$s. Doing so yields $S_k = \ln(0.48\mathcal{D})$ for the maximum value of S_k (Zelevinsky *et al.*, 1996). We refer to that value as to the GOE limit. Incomplete mixing is bound to reduce that value.

The measure (36) has the advantage that it allows for a detailed study of configurational mixing versus the eigenfunction index k and thus offers more insight than afforded by the Porter-Thomas distribution. This advantage has to be weighed against the shortcoming that the measure depends on the representation chosen for calculating the $W_{k\mu}$'s. (Indeed, S_k is not invariant under orthogonal transformations of the basis of states $\{\mu\}$, while the Porter-Thomas distribution applies to every projection of the eigenvectors of the GOE onto a fixed vector in Hilbert space.) The "natural" representation chosen by Zelevinsky *et al.* (1996) for S_k is defined by the unperturbed shell-model configurations. The implications and limitations of that choice have been discussed by Zelevinsky *et al.* (1996).

Figure 21 shows the exponential of S_k versus k for the same 3276 $J=2$, $T=0$ states as used in Figs. 19 and 20. The GOE limit (1578) is almost reached in the middle of the spectrum. In the wings, the mixing of states is fairly incomplete. That pattern is generic and reinforces earlier findings (Whitehead *et al.*, 1978; Verbaarschot and Brussard, 1979; Brown and Bertsch, 1984; Dias *et al.*, 1989).

The eigenfunctions of the shell-model Hamiltonian are orthogonal and normalized. In the GOE, these conditions impose weak correlations among the expansion coefficients of the eigenfunctions in an arbitrary basis that disappear for $N \to \infty$. The correlations for the expansion coefficients of the shell-model Hamiltonian in the basis of unperturbed shell-model configurations are found to be somewhat larger than those of a GOE with the same dimension, especially in the tails of the spectrum and for the 10 or 20 nearest eigenstates.

In Sec. II.G, we introduced the concept of the strength function for a doorway state. In analogy to Eq. (25), the strength function for an unperturbed shell-model configuration μ with respect to the exact eigenstates of the shell-model Hamiltonian is defined by $\Sigma_k W_{k\mu} \delta(E - E_k)$. Since no ensemble averaging is involved in that definition, it is useful to average over a group of neighboring (in energy) shell-model configurations to get a smooth function. If the eigenstates were complete mixtures of shell-model configurations, the smoothed strength function would be constant (independent of energy E). In fact, the strength functions are peaked with a full width at half maximum of about 20 MeV even for shell-model configurations k in the middle of the unperturbed spectrum. The shape of the strength function is Gaussian near its peak, but only falls off with an exponential tail in the wings. Such exponential decay has been studied by Lewenkopf and Zelevinsky (1994) and Frazier *et al.* (1996).

Another measure, which shows that the eigenfunctions of the shell-model Hamiltonian are not perfect mixtures of the unperturbed shell-model configurations, is provided by the pairing force, an attractive interaction between like nucleons. That force corresponds to a particular linear combination of the interaction operators $\Sigma_{\sigma\tau} A^{\dagger}_{j_3 j_4 s t \sigma\tau} A_{j_1 j_2 s t \sigma\tau}$ appearing in Eq. (34). For a completely mixed system, a plot of the expectation values of that linear combination (taken with respect to the eigenstates of the shell-model Hamiltonian) versus μ is expected to fluctuate about a constant mean value. In fact, the plot shows a systematic enhancement (with respect to the mean value) of about 70% in the ground-state domain at the expense of a corresponding suppression at the upper end of the spectrum, with small fluctuations.

The complete mixing of the eigenfunctions due to chaos may be similar to thermalization. As a test, Zelevinsky *et al.* (1996) calculated the occupation numbers of the three single-particle states $d_{5/2}$, $s_{1/2}$, and $d_{3/2}$ in the exact eigenstates, and plotted the result versus μ. The data have small fluctuations. With the help of a properly defined temperature, the results can be well fitted with the Fermi distribution. The fit parameters are "effective" single-particle energies. These differ by only a few 100 keV from the input parameters (the single-particle energies $\varepsilon_{\ell j}$ of the shell model). This corroborates the picture of thermalization.

In summary, if chaos is measured in terms of the usual spectral fluctuation measures (NNS distribution and Δ_3 statistic), there is evidence that the residual interaction mixes the unperturbed shell-model configurations sufficiently strongly to produce chaos. This is true for nuclei with sufficiently many valence nucleons and in the middle of the spectrum. Chaos is diminished for nuclei with a smaller number of valence nucleons (or of holes in the valence shell). Closer inspection of the eigenvectors offers a more subtle picture. Even for nuclei in the middle of the shell, the mixing of the unperturbed shell-model configurations is not complete, especially in the tails of the spectrum. Small correlations between eigenvector components exist beyond the ones imposed by orthogonality and normalization. The strength functions of the unperturbed shell-model configurations are not constant, but are peaked with a width of 20 MeV or so. The expectation values of the operator of the pairing force are enhanced in the ground-state domain. These deviations from GOE properties may be related to the fact that the Δ_3 statistic shows an upward bend for large values of L. All this shows that within a single major shell chaos is not fully attained for realistic strengths of the interaction, although it would be difficult to detect such deviations experimentally (except for the behavior of Δ_3). In spite of the deviations, thermodynamic concepts apply, and the single-particle occupation numbers follow the Fermi distribution function.

We return to the questions posed at the beginning of this section. From the evidence presented, it seems likely that calculations that would allow for the presence of non-valence-shell states would show that as the excitation energy increases, nuclear levels attain an ever greater similarity to GOE eigenstates. The approach to the GOE limit is probably somewhat faster for nuclei in the middle between two closed shells than for nuclei near closed shells. Chaos thus seems a natural ingredient of the shell model, and not an exclusive alternative to regular motion as seen in the ground-state domain. The results on the strength function for the unperturbed shell-model configurations and on the Δ_3 statistic suggest that at excitation energy E the strong mixing (which is characteristic of quantum chaos) involves only those unperturbed shell-model configurations that are located in an energy interval centered at E and 10–20 MeV wide.

The very success of the shell model, i.e., the ability of the model to account for many basic features of nuclei, implies that many-body states pertaining to different major shells are mixed only weakly. In that sense the residual interaction is weak: It removes the numerous degeneracies of the single-particle model in a manner that causes nearly complete mixing of states within a major shell. However, the residual interaction is not strong enough to destroy the overall shell structure defined by the existence of major shells. In that sense, nuclei are not fully chaotic systems. This point of view has been emphasized by Bunakov (1999).

Chaos does not preclude the existence of regular features. These are seen in the ground-state domain where the mixing of unperturbed shell-model configurations is incomplete, and in the presence of collective modes of excitation which act as doorway states and are seen as giant resonances. Chaos is helpful because it allows for the description of average properties of excited nuclei in terms of concepts of equilibrium statistical mechanics. It remains to show by which mechanism chaos originates in the shell model, and to clarify whether chaos is a generic feature of the shell model or depends upon specific properties of the residual interaction. We return to these questions in Sec. V.B.

An analysis similar to the one in *sd*-shell nuclei described above was carried out for the Ce atom by Flambaum *et al.* (1994) with similar results. This supports the view that chaos is a generic property of self-bound many-body systems.

3. Limits of validity of RMT in nuclei

No real physical system can be expected to possess spectral fluctuation properties that coincide exactly with RMT predictions. Indeed, RMT is based upon a purely stochastic approach, and we must expect that at some point system-specific features dominate spectral properties. Which then are the limitations of RMT in nuclei?

The answer to that type of question is known in systems with few degrees of freedom (Berry, 1985) and in disordered systems (Imry, 2002). For chaotic systems with few degrees of freedom, the limitations of RMT are connected to the shortest periodic orbit in the system. With $\tau_{\min}$ the period of the shortest periodic orbit, $\Delta E = \hbar/\tau_{\min}$ defines the maximum energy interval within which RMT predictions can be expected to hold. In disordered systems, the period $\tau_{\min}$ is replaced by the diffusion time τ_{diff}, and the characteristic energy interval is given by the Thouless energy $E_c = \hbar/\tau_{\text{diff}}$. The dimensionless Thouless conductance g is the ratio of either of these intervals and the average level spacing and gives the number of levels over which RMT predictions are expected to hold.

In nuclei, the situation is not completely clear, and two different schools of thought exist. Bohigas and Leboeuf (2002) used a mean-field approach. It is argued that the mean-field motion is partly chaotic. The shortest periodic orbit at the Fermi energy is used to estimate the characteristic energy interval as $\Delta E = 77.5A^{-1/3}$ MeV. The approach was worked out further by Olofsson *et al.* (2006). However, the mean-field approach addresses single-particle properties only. It is relevant for one-body chaos but is not clearly related to chaos in a many-body system: Without two- or many-body interaction, the eigenvalues of the many-body system are sums of single-particle energies and have a Poisson distribution irrespective of whether the single-particle motion is regular or chaotic.

A different view was taken, for instance, by Bunakov (1999) and Molinari and Weidenmüller (2006), who argued that the independent-particle model gives rise to regular motion, while the residual interaction causes mixing of shell-model configurations and, thus, chaos. The characteristic energy interval over which configura-

tions are strongly mixed (and the range of energies over which RMT predictions apply) is then given by the spreading width. In Sec. IV.A.2 it was shown that in shell-model calculations the spreading width is found to be of the order of 10 MeV. While that number is not substantially different from the estimate obtained within the chaotic mean-field scenario, the origins of both estimates are clearly very different. A test of these predictions is not possible using experimental data. As pointed out, sufficiently long sequences of levels with identical quantum numbers are not known. The shell-model calculations reported on in Sec. IV.A.2 seem to lend substance to the second view.

B. Collective models

1. The collective model of Bohr and Mottelson

Nuclei can undergo shape deformations. This fact became obvious with the discovery of nuclear fission in 1939: A very heavy nucleus splits spontaneously into two fragments of about equal mass. The energy liberated in that process could be roughly understood on the basis of the liquid-drop model. In that model, nuclei are described as charged droplets of an incompressible fluid held together by surface tension. The latter mimics the attractive nuclear force.

A dynamical theory of surface deformations was developed by Bohr (1951, 1952) and Bohr and Mottelson (1952) in the early 1950s. In an expansion of the shape of the nuclear surface in terms of spherical harmonics $Y_{\ell\mu}$, attention is focused on the lowest (in ℓ) nontrivial terms. These are the quadrupole terms $Y_{2\mu}$ (the term with $\ell=0$ is ruled out because of volume conservation and the terms with $\ell=1$ describe the motion of the center of mass). For small values of the five expansion parameters $\alpha_{2\mu}$ with $\mu=-2,-1,0,+1,+2$, the surface has the shape of an ellipsoid. The principal axes of that ellipsoid define an intrinsic ("body-fixed") coordinate system. The five expansion parameters $\alpha_{2\mu}$ can be transformed into the three Euler angles which specify the location of the body-fixed system with respect to the laboratory system, and two parameters (commonly called β and γ) which specify the nuclear shape in the body-fixed system. The potential energy $V(\beta,\gamma)$ defines the static energy of quadrupolar nuclear shape deformations. A dynamical theory is obtained by considering the parameters $\alpha_{2\mu}$ (or their transforms) as dynamical variables that obey bosonic commutation relations. The resulting Hamiltonian ("Bohr Hamiltonian") has a number of parameters [the "masses" connected with the kinetic energy terms and the parameters specifying the potential energy $V(\beta,\gamma)$]. Depending on the values of these parameters, the theory predicts *inter alias* rotational motion and vibrational motion of nuclei. In even-even nuclei, rotational motion manifests itself in the occurrence of rotational bands (sequences of levels with spins $J=0,2,4,\ldots$). The excitation energies (above the bandhead) of the states with spin J in the band are proportional to $J(J+1)$. The eigenfunctions are obtained by projecting the deformed intrinsic state onto fixed angular momentum J. This is done using the Wigner $\mathcal{D}$ functions and integrating over Euler angles. The electromagnetic transitions within the band are electric quadrupole ($E2$) and are strongly enhanced over simple single-particle (i.e., shell-model) estimates. The transition matrix elements are proportional to the static quadrupole moment of the intrinsic deformed state. In Fig. 22, two such rotational bands are displayed. Vibrational motion manifests itself in (nearly) harmonic vibrations of the surface about its equilibrium shape and is characterized by a harmonic-oscillator-like spectrum. The electromagnetic transition matrix elements are also enhanced over single-particle estimates but not as much as in the rotational case. This "collective model" (so named because many nucleons partake in an orderly way in the motion) of Bohr and Mottelson has been extremely successful in accounting for many spectroscopic data (Bohr and Mottelson, 1969). In cases of pure rotational and pure vibrational motion we expect, of course, a predominance of regular features. This view is supported by the empirical evidence reviewed in Secs. III.C.2 and III.C.3.

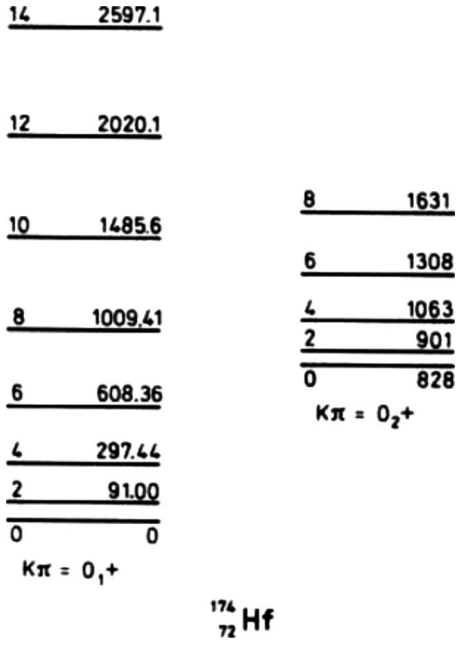

FIG. 22. Two rotational bands in ^{174}Hf. Adapted from Bohr and Mottelson, 1969.

2. Onset of chaos in rapidly rotating nuclei

Studies of chaos in the collective model (Åberg, 1990; Matsuo *et al.*, 1997) have addressed the onset of chaos above the yrast line for states of high spin. (The yrast line is defined in Sec. III.C. As a function of J, it is given by the energy of the lowest level with spin J.) We review first the later, more extensive paper by Matsuo *et al.* (1997) and then the earlier work by Åberg (1990). In both papers, similar techniques were used and similar results were obtained. The starting point is a generalized shell model. Chaos in these approaches is due to the

residual interaction which mixes the basic shell-model configurations. The approach is thus similar to that of Sec. IV.A.1. However, the shell model used differs from the spherical shell model of Sec. IV.A.1. This "Nilsson model" takes into account the fact that rotational motion in medium-weight and heavy nuclei is due to deformations of the nuclear shape. Thus the single-particle Hamiltonian H_{Nilsson} of the Nilsson model contains, in addition to the kinetic energy and a spin-orbit coupling term, a nonspherical, elliptically deformed single-particle potential. The parameters of that potential are obtained by fits to the data. [We mention that deformed single-particle potentials with a pure quadrupole deformation do not give rise to chaotic single-particle motion. An additional octupole deformation is needed. Even then, chaos arises only in the oblate case (Arvieu *et al.*, 1987; Heiss *et al.*, 1994).]

The difficulty with this approach is that by construction H_{Nilsson} is not rotationally invariant. This is not a problem in principle. We recall that according to the collective model (see Sec. IV.B.1) each rotational band is due to a deformed "intrinsic state." The wave function of each band member (which has definite spin J) is obtained by projecting the intrinsic state onto spin J. In the same sense, the many-body eigenstates of H_{Nilsson} (Slater determinants) are viewed as microscopic realizations of intrinsic states. Projection onto states of good total spin will generate from each such Slater determinant the members of a rotational band.

However, in practice projection of Slater determinants is cumbersome, and an approximation (the "cranking model") is used. It is postulated that in the laboratory system the deformed single-particle potential rotates (is "cranked") about some axis with fixed frequency ω. That axis must be perpendicular to the symmetry axis of the potential (since in quantum mechanics rotation about a symmetry axis is not possible). Under a coordinate transformation from the laboratory to the body-fixed frame of reference, the rotating deformed single-particle potential becomes a static deformed potential. As in classical mechanics, that coordinate transformation induces an additional term in the Hamiltonian, and the single-particle Hamiltonian of the cranking model is

$$H_{\text{cranking}} = H_{\text{Nilsson}} - \vec{\omega} \cdot \vec{j}. \tag{37}$$

Here $\vec{\omega}$ points in the direction of the axis of rotation, and $\vec{j}$ is the total spin of the nucleon. The z direction of the body-fixed system is commonly assumed to coincide with the symmetry axis, and the direction of $\vec{\omega}$ is assumed to coincide with the x axis, so that the last term in Eq. (37) (comprising both Coriolis and centrifugal forces) takes the form ωj_x.

The many-body solutions of the cranking Hamiltonian are Slater determinants. Let $|0\rangle$ be the vacuum state, and let $a_i^\dagger$ be the creation operator for the cranked single-particle state labeled $|i(\omega)\rangle$. Then, $|\mu\rangle = \Pi_i a_i^\dagger |0\rangle$ is a Slater determinant of cranked states (all taken at the same frequency ω). The label μ represents a set of occupied orbitals. Different choices of μ correspond to the ground state and to the excited states of the cranking model. It is assumed that the deformed potential is the same for all of these states. This assumption is realistic up to excitation energies of several MeV for nuclei for which the potential energy of deformation displays a deep and stable minimum. The states $|\mu\rangle$ depend on the cranking frequency ω. Taken as functions of ω, the single-particle energies of the cranking model display avoided crossings. At such crossings, the adiabatic single-particle wave functions change abruptly. To obtain states $|\mu\rangle$ that depend smoothly on ω, a diabatic single-particle basis has been used by Åberg (1990) and Matsuo *et al.* (1997).

To generate states of (approximate) total spin J from a given state $|\mu\rangle$, the consistency condition $\langle J_x\rangle(\omega) = J$ is used to determine ω. Here J_x is the x component of the total spin operator (the sum of the spins of all nucleons). In other words, the cranking frequency ω is adjusted so that the system rotates on average with the desired spin J. Matsuo *et al.* (1997) took the thermal average $\langle J_x\rangle$ over all cranked single-particle states with a temperature $T = 0.4$ MeV. This temperature corresponds to the excitation energies of interest (about 2 MeV above yrast). States with different spins generated in this way form a rotational band, with the state $|\mu\rangle$ playing the role of the intrinsic state. This is seen using a Taylor expansion of the expectation value $\langle\mu|H_{\text{cranking}}|\mu\rangle$ in powers of ω. That same expansion is used to transform the intrinsic energies back to the laboratory system.

The states of fixed J generated in this fashion are orthogonal. They are mixed by the residual interaction. Matsuo *et al.* (1997) used a two-body interaction of the surface delta type (the interaction is confined to an infinitely thin layer of the nuclear surface). The interaction strength was determined by previous studies of rotational nuclei. The resulting Hamiltonian contains the eigenvalues of the cranking model in the laboratory system as diagonal elements and the matrix elements of the residual interaction. To obtain a manageable problem, only the lowest 1000 states $|\mu\rangle$ were used. The resulting lowest 300 eigenstates of the total Hamiltonian were found to be rather stable against that truncation. These are used in the statistical analysis. They cover a region of excitation energy up to about 2.4 MeV above yrast.

After unfolding, the spectra were binned. The NNS distribution and the Δ_3 statistic show a gradual transition from near Poissonian behavior in the lowest bin to near GOE behavior in the highest one. For the NNS distribution, this is indicated by the Brody parameter (see Sec. III.A), which increases monotonically with excitation energy U and reaches values close to unity at the upper end of the spectrum. The dependence of the Brody parameter on U is the same for all spin values studied. The Δ_3 statistic agrees with the GOE value only up to a maximum value of L. That value increases with increasing U. Even for the bin containing the 50 states with highest excitation energies, however, this maximum value is as small as 6. This shows that in the cranking model spectral stiffness is a local phenomenon. We recall that similar features (although for much larger val-

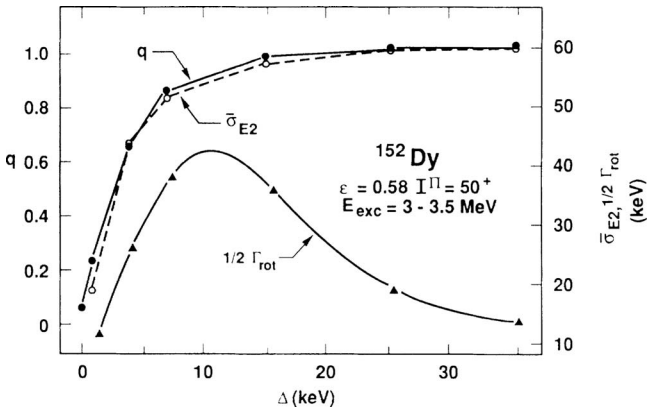

FIG. 23. Mixing parameter q for the Δ_3 statistic (see text) (left-hand scale), average standard deviation $\bar{\sigma}_{E2}$ of the distribution of reduced $E2$ matrix elements (right-hand scale), and half-width at half maximum $\frac{1}{2}\Gamma_{\rm rot}$ (right-hand scale) for the same distribution, all vs Δ, the strength of the two-body interaction which mixes the rotational bands. From Åberg, 1990.

ues of L) are found in the spherical shell model; see Sec. IV.A.2.

Essentially the same model was used by Åberg (1990). However, rather than studying the mixing of rotational bands at fixed interaction strength as a function of excitation energy, the excitation energy was held fixed and the strength Δ of the interaction was varied. This procedure simulates the increase of level density with increasing excitation energy. The results for the Δ_3 statistic were analyzed by writing Δ_3 as the sum of the GOE expression (22) (taken at a scaled length qL with $0<q<1$) and of a term linear in L (as for the Poisson distribution) with relative weight $1-q$. The fit parameter q was determined as a function of the strength Δ of the two-body interaction. The result is shown in Fig. 23. The fragmentation of collective strength was also investigated. The cranking frequency depends upon J and so do, therefore, the single-particle energies of the cranking model. As a result, states with different values of J are mixed differently by the residual interaction. This implies that the collective $E2$ transition strength (which for unmixed rotational bands only connects states within the same band) becomes fragmented. As a measure of the distribution of the reduced matrix elements for $E2$ decay connecting a mother state with spin J and the daughter states with spin $J-2$, the standard deviation is used. An average value $\bar{\sigma}_{E2}$ for the standard deviation is obtained by averaging over 50 mother states. Figure 23 also shows $\bar{\sigma}_{E2}$ versus Δ, the strength of the two-body interaction. Also shown is $1/2\Gamma_{\rm rot}$ (Åberg, 1990; Matsuo *et al.*, 1997), the half-width of the average distribution function of the matrix elements. That function changes from Gaussian to Breit-Wigner form as Δ increases. This fact explains why as a function of Δ, $\frac{1}{2}\Gamma_{\rm rot}$ displays a maximum. We observe that as functions of Δ, q and $\bar{\sigma}_{E2}$ behave very similarly. This shows that the fragmentation of the $E2$ transition strength is an indirect measure of chaos.

The theoretical ideas of Åberg (1990) and Matsuo *et al.* (1997) were applied to data by Stephens *et al.* (2005). A beam of ^{48}Ca ions of 215 MeV hit a target of ^{124}Sn. The resulting isotopes of Yb decay by gamma emission. Pairs of gamma quanta were measured in coincidence. Numerical simulations along the lines described above were compared with the measured spectra. The fits were used to determine the ratio of the strength Δ of the nucleon-nucleon interaction versus the mean level spacing. The ratio covers the range from 0.15 (nearly fully ordered) to 1.5 (nearly fully chaotic), in an energy interval that is consistent with the theoretical work.

Some have proposed (Åberg, 1992; Mottelson, 1992) that at excitation energies of a few MeV above the yrast line, the Coriolis term in Eq. (37) may be rather weak. Then rotational bands would exist with completely mixed wave functions of the GOE type. Nevertheless, the collective $E2$ decay would take place entirely within each band.

On the basis of a representation using both quasiparticles and phonons, order, chaos, and the order-to-chaos transition have been discussed by Soloviev (1995).

3. Chaos in the interacting boson model

The shell model is generally considered the fundamental phenomenological nuclear-structure model (Caurier *et al.*, 2005). However, applications of the model have been restricted in practice to nuclei for which the number of valence nucleons is not too large. This is the case for all nuclei in the $1p$ shell and the $2s1d$ shell and, more recently, for most nuclei in the $2p1f$-shell. For yet heavier nuclei (and thus shells beyond the $2p1f$ shell), the number of valence nucleons for nuclei near the middle of the shells is simply too large, and a shell-model calculation is prohibitively difficult. At the same time, it is in these mass regions that the collective model finds its most successful application. This fact has prompted many to look for a derivation of the collective model from the shell model by introducing suitable collective variables. We mention, in particular, the idea of using a boson expansion within the shell model to obtain a simplified description with built-in collective features. In this approach, pairs of nucleons form bosonlike entities. None of these approaches was truly successful in providing a derivation of the Bohr Hamiltonian from the shell model within controlled approximations. However, in the midst of these efforts, a phenomenological approach emerged that has become eminently successful, namely, the interacting boson model (IBM) of Arima and Iachello (1975). The IBM postulates the existence of s bosons and d bosons. These bosons may be thought of as representing pairs of nucleons coupled to spin 0 and 2, respectively. Alternatively, the d bosons may be viewed as the five quanta of quadrupole surface deformations. The s boson is then an artifice that is used to simplify the mathematics. For each nucleus, the total number N of bosons is fixed in the IBM. In the limit $N\rightarrow\infty$, the solutions of the boson Hamiltonian approach those of the collective model (Dieperinck *et al.*, 1980).

The connection between the IBM and the shell model has been discussed by Iachello and Talmi (1987). The IBM at large has been reviewed by Iachello and Arima (1987).

In the original form of the IBM (often referred to as IBM 1), no distinction is made between nucleon pairs formed of protons and pairs formed of neutrons. This is the form of the IBM for which an analysis with regard to chaotic properties has been performed (Alhassid *et al.*, 1990; Alhassid and Whelan, 1991). To introduce the model, we defined $s^\dagger$ and $d_\mu^\dagger$ as the creation operators for the s boson and the five d bosons, respectively. While $s^\dagger$ is a scalar, $d_\mu^\dagger$ transform under rotations as the components of an irreducible tensor of rank 2. The modified annihilation operators $\tilde{s}=s$ and $\tilde{d}_\mu=(-)^\mu d_\mu$ have the same transformation properties. The symbol $(d^\dagger\times\tilde{d})_\kappa^{(k)}$ denotes the irreducible tensor of rank k with spherical components κ obtained by vector coupling $d^\dagger$ and $\tilde{d}$, and likewise for $s^\dagger$ and $\tilde{s}$. A quadrupole operator $Q(\chi)$ is defined by $Q(\chi)=(d^\dagger\times\tilde{s}+s^\dagger\times\tilde{d})^{(2)}+\chi(d^\dagger\times\tilde{d})^{(2)}$, where χ is a real parameter. Coupling $Q(\chi)$ with itself to an irreducible tensor of rank zero generates the scalar $Q(\chi)\cdot Q(\chi)$. In the spherical representation, the three components of the angular-momentum operator $\vec{L}$ are defined by $\sqrt{10}(d^\dagger\times\tilde{d})_\kappa^{(1)}$, with $\kappa=-1,0,+1$. With $\hat{n}_d$ the number operator for d bosons, the IBM Hamiltonian studied by Alhassid and Whelan (1991) is

$$H=E_0+c_0\hat{n}_d+c_2Q(\chi)\cdot Q(\chi)+c_1\vec{L}^2. \tag{38}$$

The Hamiltonian conserves the total number N of bosons and depends on the four parameters c_0,c_1,c_2, and χ. (The energy E_0 is irrelevant as it only shifts the overall spectrum.) Except for an overall multiplicative scaling factor, only three parameters are relevant for the structure of the spectrum. Aside from the energy of the s boson (which is set equal to zero) and the energy of the d bosons (given by c_0 with $c_0\geqslant 0$ because the energy of the d bosons is generically found not to be below that of the s boson), H contains two scalar boson-boson interaction terms. The parameter χ appearing in Q is empirically restricted by the limiting symmetries described below. Moreover, there is an isomorphism that maps χ onto $-\chi$. Therefore, χ has the range $-\sqrt{7}/2\leqslant\chi\leqslant 0$. The parameters c_0 and c_2 have opposite signs (the quadrupole-quadrupole is attractive). The total angular momentum is a good quantum number; the value of the parameter c_1 only defines the positions of states with different angular momenta with respect to one another and is irrelevant when chaos is investigated. Within the model, quadrupole transition matrix elements are calculated with the help of the same quadrupole operator $Q(\chi)$ that also appears in the Hamiltonian.

The IBM is an algebraic model and therefore easy to solve. Fitting data is also easy because of the small number of parameters in Eq. (38) and in other versions of the model. The fits obtained are very good and cover a wide range of nuclei within a major shell. The parameters change slowly with mass number. The connection between the IBM and the shell model is understood reasonably well, although it has not been possible yet to derive the IBM parameters from the shell model. All this suggests that the IBM encapsulates real properties of nuclei and explains the success and popularity of the model. Studies of chaos have been restricted to the form (38) of the model which applies to even-even nuclei. It is possible, however, to extend both the Bohr-Mottelson model and the interacting boson model to nuclei with an odd number of protons and/or neutrons.

Tests of chaos in the IBM face the same difficulty as do tests of chaos in the nuclear shell model using only a single major shell: The IBM is well established as a tool to describe low-lying states. At higher excitation energies, we expect to find states that cannot be modeled by the IBM. In tests of GOE predictions, one needs large data sets and typically uses the entire spectrum of states of the IBM pertaining to fixed quantum numbers, thereby exceeding the domain of applicability of the IBM to real nuclei.

The IBM has the advantage that domains (in the space of parameters) of full integrability coincide with symmetries of the Hamiltonian. Three such symmetries exist. They are found using group-theoretical arguments. Let $|0\rangle$ denote the vacuum state. The six single-boson states $s^\dagger|0\rangle$ and $d_\mu^\dagger|0\rangle$ span a six-dimensional space. Under the general unitary transformations in six dimensions, i.e., under the group U(6), that space transforms onto itself. The generators of the Lie algebra of U(6) are the operators $b_i^\dagger b_j$, where b_i stands for one of the boson operators s or d_μ. Since H is constructed from scalar quantities involving these operators, H has nonvanishing matrix elements only between pairs of states that belong to the same irreducible representation of U(6). Equivalently, the eigenstates of H form bases of irreducible representations of U(6). We deal with bosons and thus require totally symmetric eigenstates. These belong to the fully symmetric irreducible representations which are characterized by the integer N, the total boson number. The three symmetries of the Hamiltonian correspond to the three chains of subgroups of U(6) given by

$$\begin{aligned}&\mathrm{U}(6)\supset\mathrm{U}(5)\supset\mathrm{O}(5)\supset\mathrm{O}(3)\quad\text{(case I)},\\&\mathrm{U}(6)\supset\mathrm{SU}(3)\supset\mathrm{O}(3)\quad\text{(case II)},\\&\mathrm{U}(6)\supset\mathrm{O}(6)\supset\mathrm{O}(5)\supset\mathrm{O}(3)\quad\text{(case III)}.\end{aligned} \tag{39}$$

Case I is realized for $c_2=0$, case II for $c_0=0$ and $\chi=-\sqrt{7}/2$, and case III for $c_0=0$ and $\chi=0$. Each of the three cases corresponds to a simple dynamical situation. In case I we deal with vibrational nuclei, in case II with rotational nuclei, and in case III with γ-unstable nuclei (instability with respect to the equilibrium value of γ). Full integrability of the Hamiltonian suggests classical regularity and, in the quantum regime, Poisson statistics for the eigenvalues.

Alhassid *et al.* (1990) and Alhassid and Whelan (1991) checked these expectations. Using coherent states and

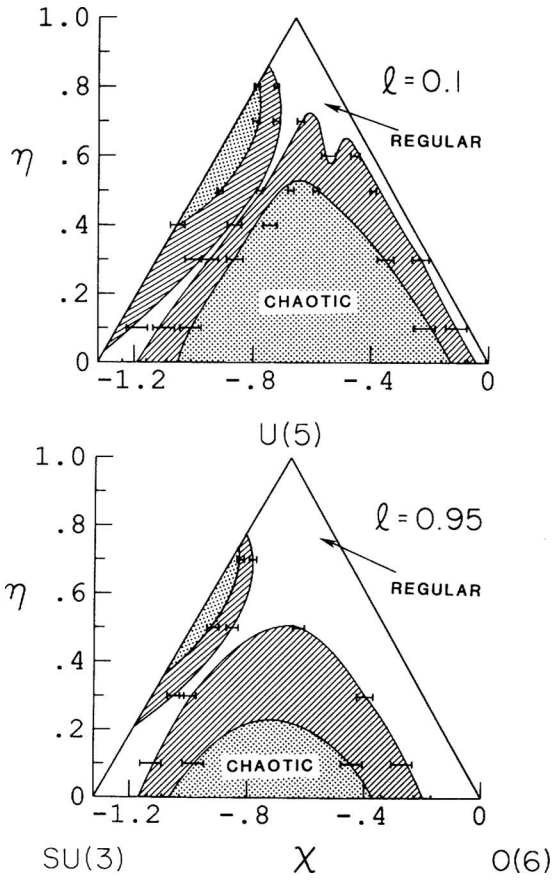

FIG. 24. Domains of regular or chaotic motion in the η-χ plane for two values of ℓ, the angular momentum per boson. The accessible parameter space has the shape of a triangle. Three domains in parameter space are separated by solid lines: Domains with nearly regular motion (fraction of chaotic phase-space volume $\leqslant 0.3$; white areas); domains with nearly chaotic motion (fraction of chaotic phase-space volume > 0.7; dotted areas); and the regions in between. From Alhassid and Whelan, 1991.

the limit $N \to \infty$, one reaches the classical limit [similarly as by Meredith *et al.* (1988)]. The behavior of the trajectories in phase space was studied for several values of the total angular momentum. For fixed $\vec{L}^2$ the parameter c_1 is redundant. Moreover, the Hamiltonian can be rescaled. This leaves two parameters: η [defined in terms of the negative ratio of c_0 and Nc_2, with the factor N originating in the classical limit of the quantum Hamiltonian (38)] with $0 \leqslant \eta \leqslant 1$ and χ with $-\sqrt{7}/2 \leqslant \chi \leqslant 0$. The results are shown in Fig. 24. The three symmetries in relation (39) correspond to the three corners of the triangles shown: Case I corresponds to $\eta=1$, case II to $\eta=0$ and $\chi=-\sqrt{7}/2$, and case III to $\eta=0$ and $\chi=0$. The three corners are surrounded by regions of no or weak chaos as expected. Chaos is strongest for small angular momenta and in the center and lower part of the triangle. They emphasized the existence of a narrow strip of nearly regular motion connecting the upper and left-hand corners of the triangle.

The quantum spectra were analyzed with the help of the NNS distribution and the Δ_3 statistic. The Porter-Thomas distribution was checked using $E2$ transition probabilities. As a result, the Bohigas-Giannoni-Schmit conjecture (see Sec. II.F) was confirmed again, this time for a system of interacting bosons. More specifically, all three fluctuation measures are close to the GOE values in the domains of parameter space where the classical motion is close to fully chaotic, and show significant deviations and a tendency toward Poissonian behavior in the domains where the classical motion is almost regular. To obtain good statistics, the results shown were for $N=25$ bosons and $J=2$ states. This is close to the angular momentum value $\ell=0.1$ shown in the upper part of Fig. 24. They stressed that for smaller, more realistic values of N, similar effects are seen. These IBM studies of chaos were extended to higher energies and spins by including broken-pair degrees of freedom (Alhassid and Vretenar, 1992). The regular behavior predicted for nuclei in the "arc of regularity," which separates vibrational and rotational motion (see Fig. 24), was recently confirmed experimentally (Jolie *et al.*, 2004).

In summary, collective models also display quantum chaos. Regular features dominate near the yrast line and at and near symmetries of the Hamiltonian. Chaos is strongest in regions of parameter space that are far removed from such symmetries. This is consistent with the analyses of data reviewed in Secs. III.C.2 and III.C.3.

C. Special issues

In Secs. IV.A.2, IV.B.2, and IV.B.3 we have shown that the dynamics of nuclei often produce spectral fluctuations of the GOE type and thus quantum chaos. In the present section, the emphasis is different. We address a number of complex situations in which we cannot test whether RMT applies. Rather, we postulate that it does and use RMT as a tool to model the physical system. This leads to results that are used in analyzing data.

1. Decay out of a superdeformed band

The potential energy of deformation $V(\beta,\gamma)$ introduced in Sec. IV.B.1 differs from the deformation energy of the liquid-drop model. The difference is due to the shell structure of nuclei. Nuclei with a completely filled major shell for neutrons and/or protons (see Fig. 18) are particularly stable. But major shells well separated from each other in energy exist not only for spherical nuclei. As the nucleus is being deformed, the energies of the single-particle states change, and new major shells emerge for certain values of the deformation parameters. This statement applies quite generally for single-particle potentials including those with a spin-orbit force. More generally, at fixed excitation energy the density of single-particle states of the shell model shows considerable fluctuations as a function of deformation. The same is true of the sum of the energies of all occupied single-particle states and, thus, of the deformation potential $V(\beta,\gamma)$. Beyond the smooth dependence on deformation parameters due to the liquid-drop model, $V(\beta,\gamma)$ therefore displays maxima and minima that re-

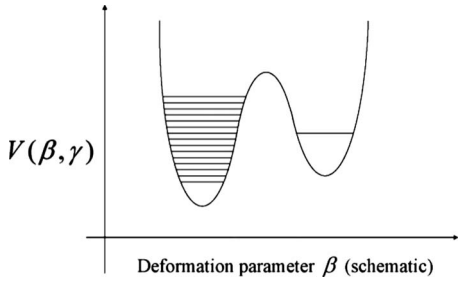

FIG. 25. The deformation energy $V(\beta,\gamma)$ for fixed total spin J_0 vs deformation (schematic). In some nuclei, $V(\beta,\gamma)$ may display a second minimum at large deformation. The level shown in the second minimum, a member of the SD band with spin J_0, may decay either via gamma emission to the next lower level in the SD band (not shown) or, via tunneling, mix with the ND states with spin J_0 located in the first minimum. The latter decay dominantly by statistical $E1$ emission.

flect the deformation dependence of the filled single-particle states of the shell model. For those values of the deformation parameters and for those mass numbers where a major shell is filled, the nuclear binding energy is expected to have a maximum and, consequently, the potential energy of deformation $V(\beta,\gamma)$ is expected to have a minimum.

Strutinsky (1966, 1967, 1968) realized that shell closures and, more generally, maxima and minima of $V(\beta,\gamma)$ are generic phenomena that are not limited to small deformations. His "shell-correction method" is based on the semiclassical periodic-orbit theory for independent-particle motion and allows the calculation of a correction to the deformation energy of the liquid-drop model. The correction is the difference between the ground-state energy calculated from the actual single-particle level density (with states filled up to the Fermi energy), and that obtained from a smoothed level density. The method of calculation and many of its results have been summarized by Brack *et al.* (1972) and by Brack and Bhaduri (1997). A particular prediction was that in certain nuclei and as a function of deformation, $V(\beta,\gamma)$ would display a second pronounced minimum (in addition to the absolute minimum defining the nuclear ground state). This is schematically shown in Fig. 25.

Following earlier evidence, the discovery of "superdeformed" rotational bands in ^{152}Dy (Twin *et al.*, 1986) and other medium-weight nuclei confirmed the existence of the second minimum. The moment of inertia of a very strongly deformed nucleus is larger than usual. A rotational band corresponding to an intrinsic state located in the second minimum can therefore be identified by its particularly large moment of inertia and the resulting narrow spacings of its members. The intensities of the $E2$ gamma transitions within a SD band show a remarkable feature: The intraband $E2$ transitions follow the band down with practically constant intensity. At some point, the intraband transition intensity starts to drop sharply. It either disappears abruptly or is much reduced in the next intraband transition(s) and then disappears. This phenomenon is referred to as the decay out of a SD band (Ragnarsson and Åberg, 1986; Herskind *et al.*, 1987). It is attributed to the mixing of the SD state(s) and the normally deformed (ND) states of the same spin and parity located in the first minimum; see Fig. 25. Calculations using the shell-correction method show that the barrier separating the first and the second minimum of the deformation potential depends on and decreases with decreasing spin J. Decay out of the SD band sets in at a spin value J_0 for which penetration through the barrier is competitive with the intraband $E2$ decay. Theoretical efforts aim at a quantitaive description of that process. We describe here one of the theoretical approaches, which is based on the use of random-matrix theory.

The first minimum of the deformation potential is typically a few MeV deeper than the second minimum. Therefore, the ND states populated by decay out of the SD band have a typical excitation energy of 3–4 MeV above yrast. These states are believed to decay largely via statistical emission of $E1$ gamma quanta. Such decay would only contribute to the background in the coincidence spectrometer used to detect the rotational bands. This view is consistent with the fact that no signal for the decay of the ND states has been found. In view of the total lack of spectral information on the ND states, a statistical model is used in the analysis of the data. It is assumed that the spectral fluctuation properties of the ND states can be modeled by the GOE. This is the view taken by Vigezzi *et al.* (1990a, 1990b) and Shimizu *et al.* (1992), and in most subsequent work on the subject; see, however, Døssing *et al.* (2004). It is the aim of these works to gain information on the barrier separating the first and the second minimum through the analysis of the decay data.

The quantity of central interest is the probability I_{out} for decay out of the SD band. A plausible formula for I_{out} was obtained by Vigezzi *et al.* (1990a, 1990b) and Shimizu *et al.* (1992) as follows. When one disregards the coupling of both the SD and ND states to the electromagnetic field, the resulting model for the Hamiltonian has the form of Eq. (24), with $H_{0\mu}$ the matrix elements for penetration of the barrier separating the SD state $|0\rangle$ and the N ND states $|\mu\rangle$ with $\mu=1,\ldots,N$. This is in fact a doorway model for the SD state. The difference from the usual doorway situation is that because of the barrier, the spreading width $\Gamma^{\downarrow}$ is small compared to or at best of the order of the mean level spacing d of the ND states. Let $|m\rangle$ with $m=1,2,\ldots,N+1$ denote the eigenstates of H and $c_m=\langle 0|m\rangle$ the amplitudes with which the SD state $|0\rangle$ is admixed into the eigenstates $|m\rangle$. It is assumed that $E2$ decay out of the next-higher state in the SD band populates the state $|m\rangle$ with probability $|c_m|^2$, and that the widths for decay of the state $|m\rangle$ back into the SD band or by statistical emission of $E1$ gamma rays are given by $|c_m|^2\Gamma_S$ and by $(1-|c_m|^2)\Gamma_N$, respectively. Here Γ_S is the width for electromagnetic decay within the SD band, and Γ_N is the common total decay width for $E1$ emission of the ND states (it has the same

value for every state $|\mu\rangle$). We then have (Vigezzi *et al.*, 1990a, 1990b; Shimizu *et al.*, 1992)

$$I_{\text{out}} = \sum_m |c_m|^2 \frac{(1-|c_m|^2)\Gamma_N}{(1-|c_m|^2)\Gamma_N + |c_m|^2\Gamma_S}. \tag{40}$$

To compare with the measured decay probability out of a SD band, the ensemble average of this expression was numerically simulated by putting E_0 in the middle of the GOE spectrum, diagonalizing a large number of random matrices of the form (24), and using the eigenfunctions to calculate the coefficients c_m. Repeating the procedure for different strengths of the barrier penetration matrix elements, one determines the actual strength by a fit to the data.

The arguments used to write down Eq. (40) imply a perturbative treatment of the coupling to the electromagnetic field. As a result, I_{out} depends on two dimensionless parameters, the ratio Γ_N/Γ_S and the ratio $\Gamma^{\downarrow}/d$ which determines the coefficients c_m. Thus, I_{out} is independent of the fine-structure constant. This is physically implausible because once the SD state is populated, the competition is between the intraband decay and the population of the ND states and thus between the electromagnetic and the strong interaction. More importantly, the analyses of data using the approach of Vigezzi *et al.* (1990a, 1990b) and Shimizu *et al.* (1992) yielded values of $\Gamma^{\downarrow}$ that were about two orders of magnitude smaller than Γ_N, putting a perturbative treatment of Γ_N into question. Weidenmüller *et al.* (1998) and Gu and Weidenmüller (1999) used the same statistical model (24) in a nonperturbative way. The amplitudes for intraband decay of the SD state and for $E1$ decay of the ND states were added as diagonal terms on the right-hand side of Eq. (24). An expression for the amplitude for decay out of the SD band was derived using that modified Hamiltonian. The ensemble average of that amplitude was calculated analytically. The resulting expression for the average probability for decay out of the SD band involves a threefold integral and depends on the dimensionless parameters Γ_N/d and $\Gamma_S/\Gamma^{\downarrow}$. The result was compared with that of Vigezzi *et al.* (1990a, 1990b) and Shimizu *et al.* (1992), and the limits of validity of the latter approach were determined. Analytical approximation formulas to the exact result were given to simplify the data analysis. Many data have been analyzed using either approach; see, for instance, Krücken *et al.* (2001), and references therein. A simplified treatment was developed by Stafford and Barrett (1999).

A few figures taken from Krücken *et al.* (2001) may serve as examples for the results obtained. Superdeformed bands occur not only for mass numbers around 150 (where they were first discovered) but also, for instance, in the lead region ($A \approx 200$). A case in point is the first SD band in ^{194}Hg. For spin $J=12\hbar$, one finds $\Gamma_S=0.097$ meV, $\Gamma_N=4.8$ meV, and $d=16.3$ eV. The analysis using the results of Vigezzi (1990a, 1990b) yields $\Gamma^{\downarrow}=37$ meV and that using Gu and Weidenmüller (1999) yields $\Gamma^{\downarrow}=25$ meV. Calculating the rms barrier penetration matrix element v from $\Gamma^{\downarrow}$ and using results for several values of J, one obtains a dependence on J roughly in agreement with the theoretical expectation $v \propto \exp(-\alpha J)$.

Decay out of a SD band continues to receive considerable attention; see, for instance, Sargeant *et al.* (2005), and references therein. Our aim here was to show how RMT is basically used in analyzing data.

2. Double giant dipole resonance

We recall the discussion of the giant dipole resonance (GDR) at the beginning of Sec. II.G. Action of the dipole operator on the nuclear ground state induces the dipole mode. That mode can be viewed as an oscillation of the center of mass of protons against that of neutrons. This simple intuitive picture is exact in the framework of two extremely opposite models of nuclear structure, namely, the harmonic-oscillator independent-particle model and a collective model using neutron and proton fluids. Therefore, the picture is expected to have general validity. If the oscillation is approximately harmonic, a repeated $E1$ excitation of the GDR should be possible and should lead to the double giant dipole resonance (DGDR). The DGDR does indeed exist and was first observed in a number of nuclei in the 1990s. For a review, see Bertulani and Ponomarev (1999). Compared to predictions of the harmonic picture, the measured cross sections for excitation of the DGDR were found to be larger by factors ranging from 1.3 to 2. The widths of the DGDR were found to be about 1.4 times larger than those of the GDR. This last fact is in keeping with some but not all theoretical estimates. These findings have attracted much theoretical attention. Anharmonicities of the Hamiltonian and nonlinearities of the external field were studied as possible causes for the discrepancies.

Here we focus on an explanation originally due to Carlson, Canto, Cruz-Barrios, *et al.* (1999), and Carlson, Hussein, de Toledo Piza, *et al.* (1999), which uses the Brink-Axel hypothesis. The Brink-Axel hypothesis postulates the existence of a giant dipole resonance built not only on the nuclear ground state, but also on every excited nuclear state as well (Brink, 1955; Axel, 1962). With the above picture for the GDR as an oscillation of the center of mass of protons against that of neutrons, the hypothesis is plausible. The hypothesis suggests an enhancement of the excitation cross section of the DGDR by the following mechanism. The GDR is a doorway state and mixes with the background states having the same spins and parities as the GDR. The mixing time is simply estimated as $\hbar/\Gamma^{\downarrow}$. If that mixing time is small or at most of the order of the time it takes to excite the DGDR from the GDR, then each of the background states admixed to the GDR mode may get excited into its own GDR. The contributions from the excitation of the background states would add to that of the GDR and lead to an enhancement of the cross section. With a GOE model for the background states as in Eq. (24), the average intensity for excitation of the DGDR in a collision between two heavy ions can be worked out using controlled approximations (Gu and

Weidenmüller, 2001). For realistic values of the parameters, it is found that the contribution of the background states is significant, and that the results of the calculations agree well with data on the reaction ^{208}Pb+^{208}Pb at 640 MeV/nucleon. The DGDR is, thus, another case in which RMT is successfully used to understand data. The use of RMT vindicates the Brink-Axel hypothesis.

3. Damping of collective modes and friction

Collective motion is due to the coherent motion of many nucleons. Examples are the rotational or vibrational motion of nuclei (Sec. IV.B.1) or the giant dipole resonance, an oscillation of the center of mass of neutrons against that of protons (Secs. II.G and IV.C.2). Other examples are encountered in heavy-ion collisions and induced nuclear fission. In the first case, the grazing collision of two heavy nuclei at energies of a few MeV per nucleon (at the Coulomb barrier) leads to a process known as deep inelastic scattering (Nörenberg and Weidenmüller, 1980; Weidenmüller, 1980): The kinetic energy of relative motion and the associated angular momentum are partly transformed into intrinsic excitation energy and spin of both fragments. At the same time, nucleons are transferred between the two reaction partners. As a result, the reaction mainly produces pairs of fragments in highly excited states with masses similar to those of the incident nuclei, but with considerably smaller kinetic energies. Similar processes occur at higher incident energies (Cassing and Nörenberg, 1985). The excitation energies of either fragment cannot be measured precisely. A phenomenological description of the process focuses attention on the collective degrees of freedom, i.e., on the relative coordinates of both fragments. These move under the influence of a conservative potential (due to the Coulomb force and the overlap of both nuclei) and of dissipative forces. The latter account for the transfer of energy and angular momentum into intrinsic degrees of freedom as well as for nucleon transfer between both reaction partners. In the simplest approximation, the relative motion is described classically and the dissipative forces are represented by a friction constant (Wilczynski, 1973). Induced fission is a somewhat similar process: Here the shape deformation leading to fission is identified as the collective degree of freedom. For fission to happen, that degree of freedom must overcome the fission barrier. Between the top of the fission barrier and the scission point, the fission degree of freedom gains kinetic energy. That energy is partly transformed into intrinsic excitation energy of the fissioning system. The process can again be described phenomenologically as involving dissipative forces acting on the fission degree of freedom (Grangé and Weidenmüller, 1980). The number of neutrons emitted prior to fission serves as a measure of the strength of that dissipation (Gavron *et al.*, 1986). In nuclear physics, dissipative processes typically arise in the context of nuclear reactions. On the other hand, the theoretical treatment usually does not refer to scattering processes.

The description of dissipative forces due to the interaction of a quantum system with its environment is a standard topic in nonequilibrium statistical mechanics. If the f collective degree(s) of freedom q_ν with $\nu=1,2,\ldots,f$ can be treated classically, the phenomenological description of the collective motion may use an equation of the type

$$\frac{d}{dt}\frac{\partial \mathcal{L}}{\partial \dot{q}_\nu} - \frac{\partial \mathcal{L}}{\partial q_\nu} = F_\nu(q,\dot{q}). \tag{41}$$

Here $\mathcal{L}(q_\nu,\dot{q}_\nu)$ is the classical Lagrangian, t is the time, and F_ν are the friction forces. To get the most general description, stochastic Langevin forces must be added to the friction forces. An equivalent description is in terms of a Fokker-Planck equation. If the classical approximation is not justified, Eq. (41) must be replaced by its quantum analog which typically involves the density matrix. Often it is justified to characterize the friction forces by a friction constant and the Langevin forces by a diffusion constant. We refer to these constants as transport coefficients. Calculating transport coefficients is the aim of a microscopic approach to these processes.

The canonical approach is that of Caldeira and Leggett (1983), who described the environment (the "heat bath") as an infinite set of harmonic oscillators. The nuclear case differs from the standard situation in statistical mechanics in several respects. First, the intrinsic degrees of freedom cannot be viewed as an infinitely extended heat bath. The total energy of the system (intrinsic plus collective degrees of freedom) is conserved, and the energy content of either subsystem is roughly the same. In other words, the nucleus is a mesoscopic system for which the thermodynamic limit is not appropriate (although some statistical description may still apply). Second, the coupling between the collective and the intrinsic degrees of freedom is typically very strong. The energy content of the interaction part of the Hamiltonian is not small compared to that of either subsystem. As a consequence, the usual Markov approximation often does not apply (Brink *et al.*, 1979). These facts must be taken into account as one works out the transport coefficients appearing in Eq. (41) or in the quantum analog of that equation from a microscopic approach.

The microscopic approach itself also encounters some difficulties. First, the definition of the collective degree(s) of freedom in terms of the coordinates of participating nucleons poses problems. Second, in nuclei dissipative processes typically involve the transfer of several MeV or even several ten MeV from the collective to the intrinsic degrees of freedom, perhaps together with the transfer of several ten units of angular momentum. The level densities in the fragments at the resulting excitation energies are very high. A detailed microscopic description of the intrinsic degrees of freedom is therefore not possible. Rather, one employs stochastic models of the random-matrix type. In such models, the coupling matrix elements between collective and intrinsic degrees of freedom are Gaussian-distributed random variables [in accord with the Porter-Thomas distribution in Eq.

(18)]. The mean coupling strength and the density of intrinsic states are estimated using simple nuclear models. As a result, the force acting on the collective degree(s) of freedom is random, and the transport coefficients are defined as ensemble averages involving that random force.

Calculating the transport coefficients as ensemble averages poses physical questions and technical difficulties quite different from those encountered in calculating the average of the strength function $\Sigma_\tau |\langle 0|\tau\rangle|^2 \delta(E-E_\tau)$ in Sec. II.G. That calculation leads to Eq. (25). In a time-dependent picture, Eq. (25) shows that the amplitude of the collective mode decays exponentially due to mixing with the background states. The decay width is given by the spreading width of Eq. (26). [To see that it is the *amplitude* of the collective mode that undergoes exponential decay, we note that the strength function can be expressed identically in terms of the Green's function as $-(1/\pi)\mathrm{Im}\langle 0|(E^+-H)^{-1}|0\rangle$.] In the case of transport coefficients, it is necessary to average *probabilities* (squares of amplitudes). Quantum mechanics implies that the sum of all occupation probabilities is conserved in time. Therefore, transport coefficients describe the redistribution in time of occupation probabilities caused by dissipative forces. Friction, for instance, implies that collective states at lower energy become occupied at the expense of states at higher energy. Averaging expressions that depend on squares of amplitudes is technically harder than averaging amplitudes.

The description of dissipative processes in heavy-ion reactions and of fission in terms of RMT has received much theoretical attention. Aside from reviews (Nörenberg and Weidenmüller, 1980; Weidenmüller, 1980) and the papers cited above, we mention the work of Agassi *et al.* (1977) and of Hofmann and Siemens (1977) and Hofmann *et al.* (2001). In general, the interaction of collective and microscopic degrees of freedom has been studied by Bulgac, Kusnezov, and collaborators [see Bulgac and Kusnezov (1996), and references therein]. There are other approaches to nuclear dissipation that do not use RMT but emphasize the chaotic aspects of single-particle motion; see Blocki *et al.* (1995), and references therein.

4. Fluctuations of binding energies

The masses of atomic nuclei are the keys to understanding many physical and astrophysical processes. For this reason, it is important to construct reliable theoretical models for the values of the nuclear masses or, equivalently, for the binding energy $B(A)$ as function of mass number A. (We suppress for simplicity the additional dependence of B on neutron number N or proton number Z.) This function is also needed to predict the masses of (as yet) unknown nuclei.

The standard approach to a global modeling of the function $B(A)$ starts from the liquid-drop model of the nucleus and considers in addition shell corrections (see Sec. IV.C.1), as well as corrections due to the pairing force (see Sec. IV.A.2). The latter lead to an odd-even staggering of $B(A)$. The resulting "semiempirical mass formula" contains about 30 parameters and is fitted to a large number of data. Years of painstaking work have culminated in a best fit (Möller *et al.*, 1995) that reproduces the data points very well but not exactly. The overall difference (root-mean-square value taken in a limited window of mass values) is of the order of 0.5 MeV and decreases with increasing A. Other approaches (Duflo and Zuker, 1995; Samyn *et al.*, 2004) have led to similar differences. The value of 0.5 MeV is obviously very small and of the order of 5×10^{-4} in comparison with the total binding energy, which for medium-weight and heavy nuclei is of the order of GeV. Nevertheless, that small value has attracted considerable attention.

Bohigas and Leboeuf (2002) suggested that there are two types of contributions to the shell correction for the nuclear binding energy. The first is due to the regular motion of nucleons in the mean field and is taken into account in terms of the Strutinsky shell correction method or, in the fits just mentioned, in terms of the semiempirical mass formula. The second is due to the (partly) chaotic motion of nucleons within the nucleus. Bohigas and LeBoeuf (2002) also evaluated that part within the mean-field approximation. They argued, however, that their final result for the fluctuations of the chaotic part is of much more general validity, and may be interpreted as arising from the residual interactions.

With $\rho(E)$ the density of single-particle states, the shell correction to the binding energy has the form $\int dE E\rho(E)$. Fluctuations of the binding energy are characterized by the variance of that expression, the average taken over a window of mass numbers and indicated by angular brackets. That variance can be expressed identically in terms of the form factor $K(\tau)$ as $\langle B^2(A)\rangle - [\langle B(A)\rangle]^2 = [\hbar^2/(2\pi^2)]\int_0^\infty d\tau K(\tau)/\tau^4$. The form factor is essentially the Fourier transform of the density-density autocorrelation function. For the chaotic contribution to the variance, $K(\tau)$ is approximated by the random-matrix result $K(\tau)=2\tau$. This expression applies for values of τ below the Heisenberg time, and for $\tau \geqslant \tau_{\min}$, where $\tau_{\min}$ is the period of the shortest periodic orbit in the system while $K(\tau)=0$ for $\tau < \tau_{\min}$. The value of $\tau_{\min}$ is estimated using free motion at the Fermi velocity over a distance typically given by the nuclear radius. This yields a result for the root-mean-square value of the fluctuation $\sigma(A)$ of the binding energy of $\sigma(A) = 2.78\ \mathrm{A}^{-1/3}$ MeV. That result is in reasonable agreement with the deviations of the data from the semiempirical mass formula.

The interpretation proposed by Bohigas and Leboeuf (2002) of the deviations of measured binding energies from the semiempirical mass formula as due to chaotic motion has caused much debate that will not be reviewed here. It implies that throughout the valley of stability the binding energies of all nuclei are correlated (Molinari and Weidenmüller, 2006; Olofsson *et al.*, 2006). Such correlations, while expected on dynamical grounds, are surprising from a statistical viewpoint.

V. RANDOM-MATRIX MODELS INSPIRED BY NUCLEAR-STRUCTURE CONCEPTS

In Sec. IV it was shown that, in the framework of standard nuclear models such as the shell model or the cranking model, chaos is a generic property of nuclei. However, these models differ from the GOE, the standard ensemble to model chaotic systems. To motivate the study of the random-matrix ensembles treated in the present section, we elucidate the difference between these nuclear models and the GOE, more precisely, between these models and a generic realization of the GOE. In doing so, we focus attention on the shell-model Hamiltonian (34); what will be said applies *mutatis mutandis* likewise to the Hamiltonian of the cranking model in Sec. IV.B.2. For simplicity, we disregard total spin and isospin. A more complete discussion for the *sd* shell including these quantum numbers may be found in Sec. V.B.

Without spin and isospin, the many-body eigenstates of the single-particle part of the shell-model Hamiltonian (34) are Slater determinants. These are multiply degenerate. The degeneracies are lifted by the residual interaction $V_{\rm res}$. The way this happens depends on the rank k of $V_{\rm res}$. If $V_{\rm res}$ is a pure two-body interaction ($k=2$), then $V_{\rm res}$ has nonvanishing matrix elements only between those pairs of Slater determinants that differ in the occupation numbers of at most two single-particle states. In the Hilbert space spanned by Slater determinants, the matrix of $V_{\rm res}$ then has many zeros. If $V_{\rm res}$ also contains three-body forces ($k=3$), the number of zeros is reduced because $V_{\rm res}$ now connects all Slater determinants that differ in the occupation numbers of at most three single-particle states. The systematic appearance of zeros in the matrix representation of $V_{\rm res}$ is completely removed only when $V_{\rm res}$ contains m-body interactions, where m is the number of valence nucleons. For a generic realization of the GOE, on the other hand, zeros do not appear systematically. This is why it is sometimes said that the GOE contains interactions of arbitrary rank.

When the first evidence for the validity of a RMT approach to nuclei became available in the 1960s, the question arose how that difference between the GOE and a realistic residual interaction would affect nuclear properties. Would the spectral statistics be the same? Later, other nuclear properties (such as the average level density) came into the focus of RMT. How would these depend on the rank of $V_{\rm res}$? To answer these questions, several noncanonical random-matrix ensembles were introduced. French and Wong (1970) and Bohigas and Flores (1971) defined and studied what became known as the two-body random ensemble (see Sec. V.B). Later Mon and French (1975) defined the embedded k-body random ensembles where the rank of the residual interaction is a free parameter (see Sec. V.A). Recently, constrained ensembles (where certain matrix elements of the GOE are suppressed) were introduced by Papenbrock *et al.* (2006) (see Sec. V.C). The present section is devoted to a review of these ensembles. The analytical treatment of the first two ensembles is much more difficult than that of the canonical ensembles of RMT because they lack the orthogonal invariance of the GOE. Therefore, a complete analytical theory of these ensembles does not exist. The analytical treatment of the constrained ensembles is still in its infancy.

A. Embedded ensembles

For the k-body embedded ensembles of random matrices [introduced by Mon and French (1975)], we confine ourselves to a brief account of the main features of the orthogonal case and refer the reader to several reviews (Brody *et al.*, 1981; Kota, 2001; Benet and Weidenmüller, 2003) for further details.

The embedded ensembles dispose of all the complexities due to the couplings of angular momentum and spin but retain the symmetries imposed by the exclusion principle. One considers m fermions in $l \geqslant m$ degenerate single-particle states (which carry no further quantum numbers) that interact via a random k-body interaction with $k \leqslant m$. To obtain an understanding of the transition from the two-body ensemble to the GOE, the parameter k is allowed to range from $k=1$ to $k=m$, although $k=2$ is the most interesting (i.e., realistic) case. The case $k=1$ is integrable and, therefore, somewhat exceptional.

Labeling the single-particle states with a running index $j=1,\ldots,l$, we introduce the usual fermionic creation operators $a_j^\dagger$ and define the creation operators for k fermions by

$$\psi_{k,\alpha}^\dagger = \prod_{s=1}^{k} a_{j_s}^\dagger, \tag{42}$$

where α stands for the set $j_1<j_2<\cdots<j_k$. The corresponding annihilation operators are defined by $\psi_{k,\alpha}=(\psi_{k,\alpha}^\dagger)^\dagger$. The random k-body interaction is

$$V_k = \sum_{\alpha,\gamma} v_{k;\alpha\gamma}\psi_{k,\alpha}^\dagger\psi_{k,\gamma}. \tag{43}$$

The matrix elements $v_{k;\alpha\gamma}$ are real and symmetric Gaussian-distributed random variables with zero mean values and a common second moment $\overline{v_{k;\alpha\gamma}v_{k;\alpha'\gamma'}}=v^2(\delta_{\alpha\alpha'}\delta_{\gamma\gamma'}+\delta_{\alpha\gamma'}\delta_{\gamma\alpha'})$. The Kronecker deltas represent the string $\delta_{j_1j_1'}\delta_{j_2j_2'}\cdots\delta_{j_kj_k'}$, etc. The interaction V_k lifts the degeneracy of the many-body states; the parameter v^2 sets the scale for the spectrum. Without loss of generality, we may put $v^2=1$.

The k-body embedded ensembles are then defined in terms of the three parameters k,l,m with $k\leqslant m\leqslant l$. The ensembles are jointly referred to as EGOE(k). In canonical RMT, universal results are obtained in the limit of infinite matrix dimension. For EGE(k), the same limit is obtained by taking $l\to\infty$. For fixed k, this can be done by imposing constraints on the ratio m/l. Brody *et al.* (1981) defined the dilute limit as $l\to\infty$, $m\to\infty$, $m/l\to 0$.

Central questions in the theory of the embedded ensembles are as follows: (i) What is the shape of the spectral density? (ii) What are the spectral fluctuation prop-

erties? (iii) Are these properties universal (i.e., independent of the assumed Gaussian distribution)? (iv) Are the spectra ergodic? (v) Can the embedded ensembles be usefully applied to real nuclei? If so, what are their predictions? Ideally, questions (i)–(iv) should be answered in the limit $l \to \infty$.

Partial answers to these questions have been obtained with a variety of methods. The moments method (Mon and French, 1975) evaluates moments of V_k in the limit $l \to \infty$. The distribution of Hamiltonian matrix elements being Gaussian, products of Hamiltonian matrices are averaged by Wick contraction involving all pairs of matrices. In the dilute limit $k \ll m \ll l$, $m/l \to 0$ for $l \to \infty$, only pairs of neighboring matrices are taken into account ("binary correlation approximation"). Numerical methods give some insight, although the extrapolation to large matrix dimension may pose problems. The study of the second moments of the many-body matrix elements of V_k reveals a duality symmetry between EGOE(k) and EGOE($m-k$).

For the spectral density, there is a gradual transition from the semicircular shape (which is attained for $k=m$) to the Gaussian shape (which applies for $k \ll m$). The transition sets in at $2k=m$. Less is known for the level statistics. It is clear that for $k=m$ the spectral fluctuations are Wigner-Dyson-like, and that for $k=1$ they are Poissonian. The cases $1<k<m$ have been much debated without firm analytical conclusion. Numerical evidence points toward Wigner-Dyson statistics for $k \geqslant 2$. Universality has not been addressed. Ergodicity has been proved for some observables in the limit $l \to \infty$, but the nonergodic contributions disappear very slowly with increasing l.

We turn to the applications of EGOE(2) to nuclei. These are based upon the binary correlation approximation (Kota, 2001). Moreover, it is stipulated that the suppression of spin and isospin quantum numbers does not limit the predictive power of EGOE(k) in nuclei. With that assumption, the EGOE(2) result for the spectral density explains why shell-model calculations with a large number of valence nucleons yield approximately Gaussian spectra. But a Gaussian spectrum results also for $k=1$ irrespective of m, so that spectra of approximately Gaussian shape are generically expected. EGOE(k) also predicts the distribution of transition strengths. For an operator O causing a transition from energy E_i to energy E_f, the transition strength distribution is defined as the ensemble average of the trace of $O^\dagger \delta(V_2-E_f) O \delta(V_2-E_i)$. This expression equals the square of the transition matrix element multiplied with the densities of the initial and final states. The average can be worked out and yields a bivariate Gaussian distribution. Comparison with shell-model calculations by Kota (2001) shows good agreement. Similarly, transition strength sums can be worked out in closed form. The same is true for the average occupation numbers of single-particle states, which were referred to in Sec. IV.A.2 and which also agree well with results of the shell model. The method can be extended to cases in which the Hamiltonian is the sum of a single-particle operator and V_2. It is then possible, for instance, to predict the onset of chaos versus the strength of V_2, again in good agreement with numerical calculations.

In summary, we see that EGOE(2) yields a number of results that are in good agreement with the shell model. That means, in turn, EGOE(2) is capable of making predictions that can reliably be used when shell-model calculations are not available. All this is in stark contrast to the GOE and is possible only because EGOE(2) takes account of an essential aspect of the shell model. On the other hand, it is difficult to obtain analytical results for EGOE(k) that are not based upon the binary correlation approximation. Perhaps most importantly, there still is no definitive analytical result on the spectral fluctuation properties of EGOE(k).

The embedded ensembles have recently been generalized to cover particles with spin [see Kota (2007)].

B. Two-body random ensemble

The two-body random ensemble (TBRE) addresses the following questions: Which nuclear properties obtained by diagonalizing the shell-model Hamiltonian (35) are generic (i.e., hold for most two-body interactions), and which are specific properties of a given interaction? And how does the residual interaction mix the states so as to produce chaos in nuclear spectra? To this end, the TBRE uses the actual form (35) of the shell-model Hamiltonian but replaces the matrix elements v_α of the actual two-body interaction by Gaussian-distributed real random variables with zero mean value and a common second moment [multiplied by the factor of 2 for the diagonal elements; see Eq. (45)]. In contrast to the embedded two-body random ensemble (see Sec. V.A), the TBRE obviously does take into account spin and isospin quantum numbers. It is time-reversal invariant. Moreover, the TBRE explores the properties of the residual two-body interaction uniformly in the space spanned by the variables v_α. Statements derived for the TBRE apply to almost all two-body interactions with the exception of a set of measure zero.

The TBRE was introduced by French and Wong (1970) and Bohigas and Flores (1971). They were mainly interested in the spectral fluctuation properties of the TBRE. The numerical results reported by French and Wong (1970) and Bohigas and Flores (1971) showed that the NNS distribution and the Δ_3 statistic of the TBRE agree with those of the GOE. These results were confirmed by later numerical studies and showed that chaos is a generic property of the TBRE. Interest in the TBRE was revived in 1998 by the work of Johnson *et al.* (1998, 1999). They showed that in even-even nuclei the TBRE predicted ground states with spin 0 and positive parity much more frequently than corresponds to their statistical weight, in spite of the fact that the matrix elements v_α are random. That finding caused substantial theoretical activity [see Zelevinsky and Volya (2004) and Zhao, Arima, and Yoshinaga (2004)], including studies of

bosonic systems interacting via a random two-body interaction. Here we confine ourselves to the nuclear-physics aspects of the TBRE. Papenbrock and Weidenmüller (2004, 2005, 2006, 2007) investigated the mechanism by which the TBRE mixes the shell-model configurations.

The TBRE contains the nondegenerate single-particle energies [first term on the right-hand side of Eq. (35)] as nonrandom parameters. The mixing of shell-model configurations in the TBRE depends on the mean strength of the two-body matrix elements measured in units of the spacing of the single-particle levels. Complete mixing occurs only when that ratio is large; see Sec. IV.A.2. For simplicity and clarity, theoretical studies of the TBRE focusing on chaos often assume that the single-particle energies are degenerate (in which case they can be put equal to zero by a shift of the energy scale). We follow that custom here and study the mixing of shell-model configurations in a "pure" TBRE. It has to be borne in mind, however, that the nondegeneracy of the single-particle levels tends to weaken the mixing found in that model.

1. Comparison GOE-TBRE

Before discussing specific properties of the TBRE, it is instructive to compare the TBRE with the GOE. In the GOE and with $N \gg 1$ the matrix dimension, the number of independent random variables is $N(N+1)/2$ and, thus, large compared to N. In the TBRE, on the other hand, the number $\mathcal{N}$ of independent random variables is typically small compared to the dimension $\mathcal{D}(J,T,\Pi)$ of the Hamiltonian matrix. We recall that in the *sd* shell, we have $\mathcal{N}=63$ while typically $\mathcal{D}\approx 10^3$ in the middle of the shell and for low values of J. In the *pf* shell, the corresponding figures are $\mathcal{N}=195$ and $\mathcal{D}\approx 10^4$–10^5. The complete mixing of the basis states and the ensuing validity of Wigner-Dyson statistics for the spectrum cannot be achieved by such a small number of random variables alone. In an essential way it is also due to the matrices $C_{\mu\nu}(JT\Pi;\alpha)$ appearing in Eq. (35). Therefore, studies of the TBRE must focus on the structure of these matrices; see Sec. V.B.2.

The GOE is mathematically accessible and formally attractive because it is orthogonally invariant, universal, and ergodic (see Sec. II.C). By construction, the TBRE is much more realistic than the GOE (if one includes the nondegenerate single-particle states of the shell model in the Hamiltonian) but probably lacks all these properties. It is not orthogonally invariant because the matrices $C_{\mu\nu}(JT\Pi;\alpha)$ are fixed by the shell model. An orthogonal transformation would change the chosen representation of these matrices in Hilbert space but would leave every realization of the TBRE unchanged. It is not clear whether the TBRE is universal (i.e., yields results that do not depend on the assumed Gaussian distribution of the matrix elements v_α). We are not aware of any paper addressing that question. The TBRE is not ergodic because the limit of infinite matrix dimension cannot be taken in a meaningful way (except for the case of a single j shell, where $j\to\infty$ is a meaningful limit that has not been explored yet). In spite of these shortcomings, the TBRE has attractive features; see below. In Sec. II.C it was pointed out that GOE spectra carry no information content. The TBRE produces spectra with Wigner-Dyson level statistics. At the same time, the TBRE does carry information content because the number of random variables is small compared to typical matrix dimensions. Ideally, it takes $\mathcal{N}$ data points to completely determine the values of the random variables in the TBRE; that number is typically small compared to the number of eigenvalues pertaining to fixed values of J, T, and Π. Again, this shows the important role played by the matrices $C_{\mu\nu}(JT\Pi;\alpha)$ in the TBRE. These matrices are fixed by the geometry of the shell model itself. At the same time, they are important for the strong mixing of the shell-model configurations. The choice of the residual interaction only determines the particular linear combination of the C's that forms the shell-model Hamiltonian $\mathcal{H}_{\mu\nu}(JT\Pi)$ in Eq. (35).

Properly speaking, the TBRE is not a single ensemble but a set of ensembles. Indeed, in every shell a given set of matrix elements $\{v_\alpha\}$ determines for all values of A pertaining to that shell the Hamiltonian matrices $\mathcal{H}_{\mu\nu}(JT\Pi)$ for all values of J, T, and Π. Taking v_α as random variables implies that all these matrices become Gaussian random-matrix ensembles. Since all these ensembles depend upon the same set $\{v_\alpha\}$ of random variables, they are correlated. Such correlations are the hallmark of the TBRE. Correlations of this type do not occur naturally within the GOE.

2. Structure of the matrices $C_{\mu\nu}(JT\Pi;\alpha)$

The discussion in Sec. V.B.1 has revealed the central role played by the matrices $C_{\mu\nu}(JT\Pi;\alpha)$ in the TBRE. As emphasized in Sec. IV.A.1, these matrices are completely determined by the coupling scheme chosen to construct the many-body states $|JT\Pi\mu\rangle$. They depend upon vector-coupling coefficients and on coefficients of fractional parentage and, thus, are given in terms of group-theoretical concepts. (The coefficients of fractional parentage give the decomposition of a state $|JT\Pi\mu\rangle$ for m nucleons in terms of the same states for $m-1$ nucleons.) The matrices $C_{\mu\nu}(JT\Pi;\alpha)$ are determined by the intrinsic symmetries of the shell model and are known completely. At the same time, these matrices are highly complex, and there is no analytical theory yet to describe their structure. We are confined to describing some of their properties and refer the reader for details to Papenbrock and Weidenmüller (2007).

To see how the nondiagonal elements of $V_{\rm res}$ mix the unperturbed configurations, we use the coupling scheme described above Eq. (35) and classify the many-body states in terms of the partitions $\{m_{\ell j}\}$ of m. For $m=12$ there are 41 such partitions in the *sd* shell. Each partition consists of a string of three non-negative integers that give the number of nucleons in each subshell. In that basis, the matrix elements of $V_{\rm res}$ attain block structure. Each block is labeled by a pair of partitions $\{m_{\ell j}\}$.

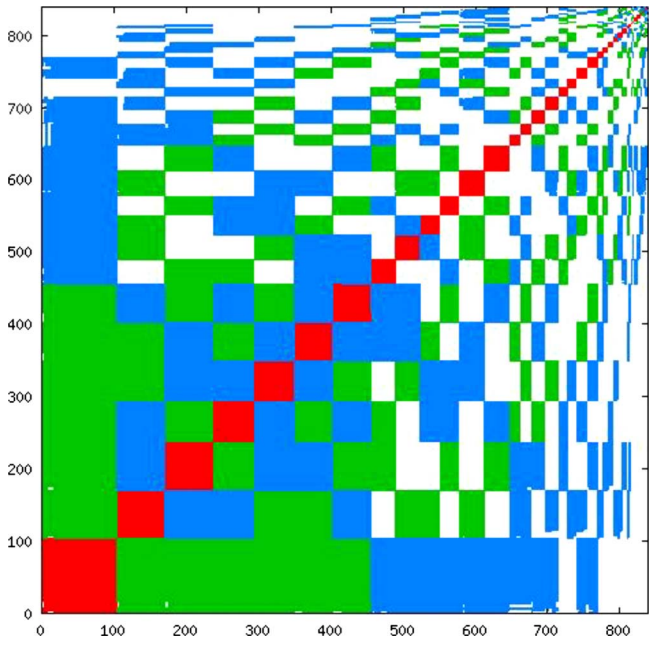

FIG. 26. (Color online) Block structure of the matrix of the shell-model Hamiltonian for the *sd* shell. Blocks in black, light gray, dark gray (online red, green, blue) indicate matrix elements that change the partition by zero, one, or two units, respectively, as explained in the text. White areas do not carry matrix elements. From Papenbrock and Weidenmüller, 2005.

The blocks come in four classes: (i) the partition $\{m_{\ell j}\}$ is unchanged (diagonal blocks arising from those two-body matrix elements that do not change partition although they may change the actual many-body basis state), (ii) the partition $\{m_{\ell j}\}$ is changed by adding unity to one of its elements at the expense of another element (the residual interaction lifts a single nucleon from one subshell to another), (iii) the partition $\{m_{\ell j}\}$ is changed by adding unity to two of its elements or two to one of its elements at the expense of one or two other elements (the residual interaction lifts two nucleons into different subshells), and (iv) the partition $\{m_{\ell j}\}$ is changed by moving more than two nucleons into different subshells. These blocks are empty because a two-body interaction cannot move more than two nucleons.

The block structure of the matrices $C_{\mu\nu}(JT\Pi;\alpha)$ (also displayed by Zelevinsky *et al.*, 1996) is shown here in Fig. 26 for $m=12$ and for the states with $J=0$, $T=0$ of the *sd* shell. Blocks in classes (i), (ii), (iii), and (iv) are shown in black, light gray, dark gray, and white (online red, green, blue, and white), respectively. It is obvious that the structure of the matrix is fundamentally different from that of a typical GOE matrix, where all states are coupled with each other. That fact implies that complete mixing of the shell-model configurations can never be the result of a single matrix $C_{\mu\nu}(JT\Pi;\alpha)$ alone. A linear combination of the type appearing in Eq. (35) is definitely needed. It is also obvious that the block structure shown in Fig. 26 is not restricted to the *sd* shell and is a generic property of the shell model.

The structure of individual matrices $C_{\mu\nu}(JT\Pi;\alpha)$ is governed by "geometric chaos" (Zelevinsky *et al.*, 1996). The many-body states $|JT\Pi\mu\rangle$ may be constructed by coupling first a pair of nucleons to given intermediate values of spin and isospin, by then vector-coupling a third nucleon to the resulting pair, etc. There are many different paths leading to the same total spin J and isospin T; their number determines the dimension $\mathcal{D}(J,T,\Pi)$ of the resulting Hilbert space. Each path corresponds to a different set of vector-coupling coefficients. Supposing that the vector-coupling coefficients are pseudorandom numbers, we expect that the states $|JT\Pi\mu\rangle$ also behave randomly. Several tests (Zelevinsky *et al.*, 1996; Zelevinsky and Volya, 2004) support this idea of geometric chaos. It is, therefore, reasonable to expect that the elements of the matrices $C_{\mu\nu}(JT\Pi;\alpha)$ behave randomly in those blocks where they do not vanish identically. This view is obviously not restricted to the *sd* shell but applies likewise to every major shell. Further insight into the mixing properties of the matrices $C_{\mu\nu}(JT\Pi;\alpha)$ is obtained by counting the number of matrices that yield nonvanishing contributions to a matrix element of the shell-model Hamiltonian $\mathcal{H}_{\mu\nu}(JT\Pi)$ and by calculating the inverse participation ratios for these matrices (Papenbrock and Weidenmüller, 2005). All this evidence points to strong mixing of shell-model configurations by the matrices $C_{\mu\nu}(JT\Pi;\alpha)$.

Although we are very far from a complete theory of the TBRE, the evidence presented makes it plausible that chaos is a generic property of the shell model. The matrices $C_{\mu\nu}(JT\Pi;\alpha)$ are both the fundamental building blocks of the TBRE and the agents for complete mixing of the shell-model configurations.

3. Another representation of the shell-model Hamiltonian

Can we gain further insight into the structure of the matrices $C_{\mu\nu}(JT\Pi;\alpha)$? Is it possible to define a quantitative measure for the information content of shell-model spectra? Why are spin-0 ground states dominant in the TBRE? These questions are answered by transforming the interaction part of the shell-model Hamiltonian $\mathcal{H}_{\mu\nu}(JT\Pi)$ in Eq. (35). This is done (Papenbrock and Weidenmüller, 2004) by diagonalizing for each set of quantum numbers $\{JT\Pi\}$ the real, symmetric, and positive-semidefinite matrix $S_{\alpha\beta}=\mathcal{D}^{-1}(JT\Pi)\mathrm{Tr}[C(JT\Pi,\alpha)C(JT\Pi;\beta)]$. We denote by $s_\alpha^2\geqslant 0$ the eigenvalues of $S_{\alpha\beta}$, by $s_\alpha\geqslant 0$ the roots of these eigenvalues, and by $O_{\alpha\beta}$ the eigenvector belonging to the eigenvalue s_α^2. We define the new random variables $w_\alpha=\Sigma_\beta O_{\alpha\beta}v_\alpha$ and, for $s_\alpha>0$, the matrices $B_{\mu\nu}(JT\Pi;\alpha)=(1/s_\alpha)\Sigma_\beta O_{\alpha\beta}C_{\mu\nu}(JT\Pi;\beta)$. By construction, the matrices $B_{\mu\nu}(JT\Pi;\alpha)$ are orthonormal with respect to the trace, $\mathcal{D}^{-1}(JT\Pi)\mathrm{Tr}[B(JT\Pi,\alpha)B(JT\Pi;\beta)]=\delta_{\alpha\beta}$. The shell-model Hamiltonian (35) takes the form

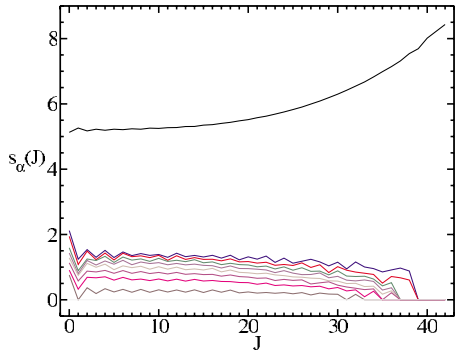

FIG. 27. (Color online) The square roots of the eigenvalues of the matrix $S_{\alpha\beta}(J)$ (see text) for the $j=19/2$ shell with six identical nucleons vs total spin J. From Papenbrock and Weidenmüller, 2004.

$$\mathcal{H}_{\mu\nu}(JT\Pi) = \delta_{\mu\nu}\sum_{\ell j}\varepsilon_{\ell j}m_{\ell j} + \sum_{\alpha} w_\alpha s_\alpha B_{\mu\nu}(JT\Pi;\alpha). \tag{44}$$

In the last sum over α, only terms pertaining to nonzero eigenvalues s_α^2 appear.

The form (44) of the shell-model Hamiltonian is instructive for several reasons. First, by adding further matrices we could enlarge the set $\{B(JT\Pi;\alpha)\}$ of orthonormal matrices to a complete set of $\mathcal{D}(JT\Pi)[\mathcal{D}(JT\Pi)+1]/2$ orthonormal real symmetric matrices. The linear combination of all these matrices with random coefficients would be equivalent to the GOE. The number of matrices $B(JT\Pi)$ is much smaller than $\mathcal{D}(JT\Pi)[\mathcal{D}(JT\Pi)+1]/2$, however. This shows once again that the TBRE is very different from the GOE; it is a constrained ensemble in the sense of Sec. V.C. Second, being obtained from the v_α by an orthogonal transformation, the new random variables w_α have the same Gaussian distribution as the former. However, not all w_α but only those pertaining to nonvanishing eigenvalues s_α^2 do appear in the sum in Eq. (44). At least one (and often several) eigenvalue s_α^2 always vanishes. That implies that one or several linear combinations of the v_α can never be measured (nor do they affect the shell-model spectrum). Third, those w_α that do appear in Eq. (44) are multiplied with the root factors s_α. The matrices $B(JT\Pi)$ are orthonormal. Therefore, the difficulty of determining the w_α in Eq. (44) from data increases with increasing smallness of the factors s_α. These root factors are derived from the matrix $S_{\alpha\beta}$ and reflect intrinsic properties of the shell model.

Papenbrock and Weidenmüller presented the distribution of the roots s_α for the case of a single j shell and for two nuclei in the *sd* shell. In Fig. 27, we show $s_\alpha(J)$ versus J for $n=6$ identical nucleons in the $j=19/2$ shell. Similar results have been found in all other cases (different nucleon numbers in the same shell and two nuclei in the *sd* shell). All roots are smooth functions of total spin J. One root is substantially bigger than the rest. The associated two-body operator is the monopole operator and essentially determines the centroid of the shell-model spectrum. These features can be understood semianalytically (Papenbrock and Weidenmüller, 2004). Identically vanishing eigenvalues are related to conserved quantum numbers. For instance, the matrix representation of the two-body operator $\vec{J}^2 - J(J+1)$ (with $\vec{J}$ the total spin operator) can be written as a linear combination of the matrices $C(JT\Pi;\alpha)$; that linear combination vanishes identically, and similarly for total isospin T.

4. Preponderance of spin-0 ground states in the TBRE

The discovery by Johnson *et al.* (1998) of the preponderance of spin-0 ground states used a specific version of the TBRE. That version favors neither a particle-particle nor a particle-hole representation, and they refer to it as the random quasiparticle ensemble. Following Johnson *et al.* (1998), we denote the two-body matrix elements $\langle j_3 j_4 st|V_{\rm res}|j_1 j_2 st\rangle$ appearing in Eq. (34) by $V_{\rho'\rho}$, where ρ and ρ' label the two-body states $|j_1 j_2 st\rangle$ and $|j_3 j_4 st\rangle$. The $V_{\rho'\rho}$ have zero mean values and second moments given by

$$\overline{V_{\rho'\rho}V_{\sigma'\sigma}} = \frac{v^2}{(2s+1)(2t+1)}[\delta_{\rho\sigma}\delta_{\rho'\sigma'} + \delta_{\rho\sigma'}\delta_{\rho'\sigma}]. \tag{45}$$

Here v^2 is a constant, i.e., independent of all the quantum numbers. The factor $1/(2s+1)(2t+1)$ guarantees that this a random quasiparticle ensemble. The single-particle energies $\varepsilon_{\ell j}$ in Eq. (35) are neglected.

Johnson *et al.* (1998) found that for several nuclei in the *sd* shell the probability of finding a ground state with spin 0 lies between 2/3 and 3/4, although the total fraction of spin-0 states is less than 10%. This result is known as the preponderance of spin-0 ground states. It holds for the random interaction (45). That interaction does not possess a strong pairing force (the agent usually held responsible for the preponderance of spin-0 ground states in actual nuclei). Other regularities were also observed (Johnson *et al.*, 1998, 1999; Zhao, Arima, Shimizu, *et al.*, 2004). We confine ourselves to the preponderance of spin-0 ground states. A large number of theoretical papers is devoted to this phenomenon. We confine ourselves to the two successful explanations that have been offered for the phenomenon and refer the reader to Zelevinsky and Volya (2004) and Zhao, Arima and Yoshinaga (2004) for further references.

The method used by Zhao and Arima (2001) and refined later [Zhao *et al.* (2002) and Zhao, Arima, and Yoshinaga (2004)] is based upon a simple counting procedure. They put one of the $\mathcal{N}$ different matrix elements of the residual interaction equal to (−1) and all others to zero and calculate the spectrum. The procedure is repeated $\mathcal{N}$ times, each time with a different nonzero matrix element. Let $\mathcal{N}_J$ be the number of times the ground state is found to have spin J. We have $\Sigma_J\mathcal{N}_J=\mathcal{N}$. The probability of finding a spin-0 ground state is then estimated as $\mathcal{N}_0/\mathcal{N}$. Comparing the results with an average over many diagonalizations of the TBRE, they found

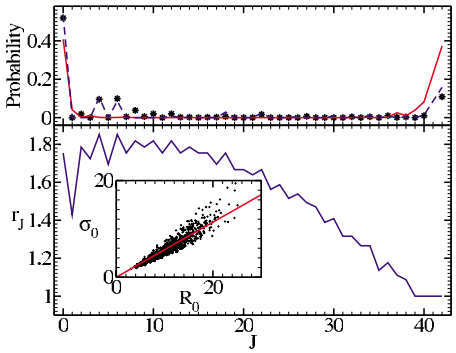

FIG. 28. (Color online) Six identical fermions in a $j=19/2$ shell. Inset: Spectral radius R_0 vs spectral width σ_0 (data points) and the linear fit (line). Bottom: Scaling factor r_J vs J. Top: Probability that the ground state has spin J (points), probability that spin J has the largest spectral width (solid line), and probability that the product $r_J\sigma_J$ is maximal (dashed line). From Papenbrock and Weidenmüller, 2004.

good agreement for a number of cases (four to six fermions in single j shells and two j shell systems, boson systems).

The analysis of Papenbrock and Weidenmüller (2004) used a two-step argument. (For simplicity, we replace the quantum numbers J,T,Π by the single symbol J.) First, the square of the width σ_J of the spectrum of levels with quantum number J is defined as the normalized variance of the shell-model Hamiltonian. Since shell-model spectra have approximately Gaussian shape (Mon and French, 1975), σ_J has a direct physical interpretation. From Eq. (44) we obtain $\sigma_J^2=\Sigma_\alpha w_\alpha^2(J)s_\alpha^2(J)$. The argument J on w and s serves as a reminder that both quantities depend on J. That dependence is weak, however, at least for the eigenvalues; see Fig. 27. More importantly, the spectral widths depend via w_α on the same random variables v_α and are, therefore, strongly correlated: They tend to be all large or all small for a given realization of v_α. The variances are biggest when many terms contribute almost uniformly to the sum over α; Fig. 28 shows that this is the case for σ_0. Altogether the correlations favor either σ_0 or the spectral width of the largest spin. Second, the quantity of interest is R_J, the largest (or smallest) eigenvalue of the spectrum of levels with spin J. (There is no distinction between the two because the v_α have random signs.) Numerical calculations show that the linear relation $R_J=r_J\sigma_J$ holds with r_J practically constant (i.e., independent of the realization of the v_α). For the states with $J=0$ this is shown for six identical nucleons in the $j=19/2$ shell in the inset in Fig. 28. The dependence of r_J on J is largely determined by $\mathcal{D}(J)$, the dimension of Hilbert space. Typically, $\mathcal{D}(J)$ decreases with increasing J and shows odd-even staggering. Both features are present in r_J; see Fig. 28. These tendencies of r_J suppress the competition of the spectral width belonging to the largest spin and favor R_0 over all other R_J; see Fig. 28. The explanation carries over to other cases including nuclei with an odd number of nucleons. In the nuclei ^{20}Ne and ^{24}Mg, it leads to a semi-quantitative agreement with numerical TBRE calculations (Papenbrock *et al.*, 2006).

The method of Papenbrock and Weidenmüller (2004) was improved by Yoshinaga *et al.* (2006). They considered, for instance, a single j shell with identical nucleons. The energy $E(J)$ of the lowest state of spin J was $E(J)=\mathcal{D}(J)^{-1}\,\mathrm{Tr}(\mathcal{H})-\Phi_J\sigma_J$. This equation differs from that of Papenbrock and Weidenmüller (2004) by inclusion of the trace of $\mathcal{H}$ and by the fact that an analytical form for the function Φ_J was proposed. The trace of $\mathcal{H}$ vanishes upon taking the ensemble average but, for each realization, fluctuates around zero. Inclusion of the trace in the equation for $E(J)$ removes the scatter of the points around the best linear approximation to r_J shown in Fig. 28. The function Φ_J was fitted and given analytically as $\Phi_J=\sqrt{0.99\ln\mathcal{D}(J)+0.36}$. Good agreement is obtained for $m=4$ to 6 fermions in several single j shells and systems with two j shells between TBRE results and the predictions based upon this approach. The method also works for bosons.

5. Correlations between spectra with different quantum numbers

As pointed out in Sec. V.B.1, the TBRE causes correlations between spectra carrying different quantum numbers (A,J,T,Π) but belonging to the same major shell. From the point of view of the shell model, this is not surprising: Switching from one realization of the TBRE to another is tantamount to using a different residual interaction; such a different choice of V_{res} is bound to affect the spectra of all nuclei in the shell. However, the existence of such correlations is surprising from the point of view of RMT and exceeds the traditional framework of the theory. Moreover, the statistical analysis of nuclear data has always assumed the absence of correlations between observables with different quantum numbers. That assumption is put into question by the TBRE.

Papenbrock and Weidenmüller (2006) displayed correlations in *sd*-shell nuclei between states in the same nucleus carrying different quantum numbers and between states with identical quantum numbers in different nuclei. The normalized cross-correlation functions had maxima of around 6–10 %. Similar figures result by calculating correlations in actual shell-model spectra by averaging over 17 *sd*-shell nuclei (Papenbrock and Weidenmüller, 2006).

6. Summary

The studies of the TBRE reviewed above suggest that chaos is a generic property of the shell model. The strong mixing is due to the matrices $C_{\mu\nu}(JT\Pi;\alpha)$ which, for every major shell, are determined by the geometry of that shell, by the number of valence nucleons, and by the quantum numbers $\{JT\Pi\}$. A complete theory of the TBRE would have to be based on the analysis of these matrices; such an analysis is not available yet. As a consequence, there is no analytical proof yet that TBRE

spectra do obey Wigner-Dyson statistics. TBRE and GOE are very different; in the TBRE there exist spectral correlations that are totally absent in the GOE.

C. Constrained ensembles

The spectral fluctuation properties of both the embedded ensembles and the TBRE are known only through numerical simulations. Such studies are necessarily confined to matrices of small dimensions N. A generic answer (valid for any N) can only be obtained analytically. A renewed attempt at such an answer was made by Papenbrock *et al.* (2006). They introduced and studied constrained Gaussian random-matrix ensembles. We review here the unitary case.

The starting point is a complete basis of N^2 orthonormal Hermitian matrices B_α in the N-dimensional Hilbert space. Orthonormality is defined in terms of the trace,

$$\langle B_\alpha | B_\beta \rangle = \mathrm{Tr}(B_\alpha B_\beta) = \delta_{\alpha\beta}. \tag{46}$$

We note that in contrast to Sec. V.B.3 we do not include the matrix dimension in the definition (46). Any Hermitian matrix H can be expanded in terms of that basis,

$$H = \sum_{\alpha=1}^{N^2} h_\alpha B_\alpha. \tag{47}$$

Taking the N^2 complex coefficients h_α in Eq. (47) as uncorrelated Gaussian-distributed random variables with zero mean value and a common second moment, one obtains the GUE. A constrained ensemble is obtained by requiring a subset $\{h_q\}$ of the expansion coefficients h_α in Eq. (47) to vanish identically. (It was shown in Sec. V.B.3 that the TBRE can be viewed as a constrained ensemble, and it is easy to see that the same statement holds for the embedded ensembles.) The resulting ensemble is not unitarily invariant, however. Unitary invariance is restored by integrating the constraining condition $\Pi_q \delta(\langle B_q | H \rangle)$ over the unitary group; see Sec. II.B. This yields the following probability density of the matrices H:

$$W(H) \propto \exp\left(-\frac{N}{2\lambda^2}\langle H|H\rangle\right) \times \int d\mathcal{U}\left(\prod_q \delta(\langle U B_q U^\dagger | H\rangle)\right). \tag{48}$$

The first factor on the right-hand side is the same as in Eq. (10). The second factor represents the constraints. It is unitarily invariant and, therefore, does not affect the eigenvector distribution. The eigenvalue distribution of the constrained ensemble differs from that on the right-hand side of Eq. (12) by the additional factor

$$F(E_1, \ldots, E_N) = \int d\mathcal{U}\left(\prod_q \delta(\langle B_q | U E U^\dagger \rangle)\right). \tag{49}$$

Here E is the diagonal matrix of eigenvalues.

In the GUE, quadratic level repulsion is a consequence of the Vandermonde determinant $\Pi_{\rho \le \sigma} |E_\rho - E_\sigma|$ appearing on the right-hand side of Eq. (12). Level repulsion is lifted by the constraints if and only if $F(E_1, \ldots, E_N)$ is singular whenever two eigenvalues coincide. Using Fourier transformation, one replaces each of the delta functions by an integral over a plane wave. The function $F(E_1, \ldots, E_N)$ can then be written as a Harish-Chandra-Itzykson-Zuber integral (Harish-Chandra, 1957; Itzykson and Zuber, 1980). Inspection of the result of the integration yields a sufficient condition for $F(E_1, \ldots, E_N)$ not to be singular. In its simplest form, that condition reads

$$N_Q < N(N-1)/2. \tag{50}$$

Here N_Q is the number of constraints. It is quite remarkable that the sufficient condition depends only on N_Q.

The result can be extended to the GOE and GSE. Moreover, other properties (spectral radius, distribution of matrix elements) of the constrained ensembles can be investigated and are seen to differ from those of the canonical ensembles. Relations can be established between the ensemble defined by the constraints on the set $\{h_q\}$ of matrix elements, and the one defined by the complementary set (all h_α but the set $\{h_q\}$ are constrained). Unfortunately, the condition (50) does not cover the physically interesting cases of the TBRE and the embedded ensemble with two-body interactions. The spectral fluctuation properties of these ensembles remain an open theoretical problem.

VI. SUMMARY AND CONCLUSIONS

Comparison of GOE predictions with data reviewed in Sec. III shows that there is good agreement on spectral fluctuations not only near neutron threshold but also in the ground-state domain. This is true also for the three nuclei with complete level schemes. Extensions of the GOE are used to successfully describe isospin mixing, and to test time-reversal invariance. Deviations from GOE predictions are found up to several 100 keV above yrast and in the case of symmetries. An enlargement of the data basis would be highly desirable. There is hope that the next generation of large-scale gamma detectors will contribute pertinent information on the interesting energy interval 500 keV to 1 MeV above yrast.

Studies of the spherical shell model, the Nilsson model, and the interacting boson model reviewed in Sec. IV show a joint tendency toward strong mixing of the unperturbed configurations and toward GOE fluctuation properties. This resolves the apparent dichotomy between Bohr's picture of the compound nucleus described in Sec. II and the independent-particle model. Typically, the GOE limit is not fully attained, however. For the *sd* shell, mixing is strongest for nuclei in the middle of the shell, but even here the spreading width of the unperturbed shell-model configurations located in the center of the spectrum is 20 MeV or so and, thus, smaller than the range of the spectrum.

Random-matrix ensembles patterned after nuclear-structure concepts were reviewed in Sec. V. The embedded two-body random ensemble possesses strong predictive power for average properties such as the shape of the spectrum or the distribution of transition strengths. This is true even though that ensemble disregards conserved quantum numbers such as spin or isospin. The two-body random ensemble is closest in structure to the shell model. The strong mixing of shell-model configurations is seen to be a generic feature of the shell model. At the same time, the two-body ensemble possesses features that go beyond the GOE such as the correlations between spectra with different quantum numbers. It would be intriguing to find such correlations experimentally.

Following the Bohigas-Giannoni-Schmit conjecture, we have identified chaos in nuclei with the occurrence of spectral fluctuations of the GOE type. Closer inspection has shown, however, that chaos in nuclei differs from that in few-degrees-of-freedom systems. The evidence presented shows that chaos is caused by the residual two-body interaction of the shell model. Shell structure is a typical feature of fermionic many-body systems. The residual interaction strongly mixes the shell-model configurations within a major shell, but leaves the overall shell structure largely intact. Evidence for this assertion comes not only from the success of shell-model calculations in the ground-state domain, but also from the success of the optical model for elastic scattering and from the existence of distinct maxima in the neutron strength function. The existence of regular features in nuclei also attests to the incomplete mixing of the shell-model configurations. We mention the regularities in the ground-state domain caused by the pairing force, collective motion, and doorway states.

The evidence presented in this review strongly supports the view that chaos is a generic property of nuclei. At the same time, we are far from having a complete theoretical understanding of chaos in nuclei. We lack an overall many-body theory that would permit the calculation of nuclear spectra from the nucleon-nucleon interaction within controlled approximations (except for the lightest nuclei). In contrast to few-degrees-of-freedom systems, there is also no theoretical framework such as the semiclassical approximation that would establish the connection between classical chaos and spectral fluctuation properties of the RMT type. On a more mundane level, the evidence presented above for chaos in the spherical shell model comes mainly from the *sd* shell. Although the arguments seem generic, it would be gratifying to have similar evidence in other major shells. Would the sizable correlations between spectra carrying different quantum numbers found in the two-body random ensemble persist with increasing shell size? Likewise, it is desirable to attain a deeper analytical understanding of how chaos arises within a major shell. Does the difference between the GOE and the two-body random ensemble entail other differences beyond those correlations? Also, the analysis of properties of the matrices $C_{\mu\nu}$ in Eq. (35) within a single j shell would be of substantial interest, coupled, if possible, with the proof of GOE spectral fluctuation properties for $j \gg 1$.

Chaos limits the predictability of spectral properties in nuclei in terms of simple models. For instance, the shell-model eigenfunctions become mixed ever more strongly as the excitation energy increases; see Sec. IV.A.2. Such strong mixing requires the presence of many matrix elements of the two-body interaction and cannot be modeled in simple terms. We are not aware of any attempts to formulate and quantify that limitation, however.

The way it is defined in this review, chaos is a statistical property of levels carrying identical quantum numbers. Regular dynamical features in nuclei typically relate several states carrying different quantum numbers. The coexistence of those two aspects of nuclear motion deserves deeper analysis. Hopefully, it would also shed light on the dynamical properties of other fermionic many-body systems.

ACKNOWLEDGMENTS

We owe thanks to many colleagues with whom we have discussed topics relating to chaos in nuclei over many years, and from whom we have learned much. Special and cordial thanks are due to those who made numerous valuable and thoughtful comments and suggestions: S. Åberg, Y. Alhassid, O. Bohigas, T. Friedrich, G. Garvey, T. Guhr, T. Papenbrock, A. Richter, T. H. Seligman, V. Zelevinsky, and Y. M. Zhao. We also thank R. Chankova, A. Chyzh, H. Friedrich, and J. F. Shriner, Jr., for assistance with the preparation. This work was supported in part by the U.S. Department of Energy Grant No. DE-FG02-97ER41042.

REFERENCES

Åberg, S., 1990, Phys. Rev. Lett. **64**, 3119.
Åberg, S., 1992, Prog. Part. Nucl. Phys. **28**, 11.
Abul-Magd, A. Y., H. L. Harney, M. H. Simbel, and H. A. Weidenmüller, 2004, Phys. Lett. B **579**, 278.
Abul-Magd A. Y., and H. A. Weidenmüller, 1985, Phys. Lett. B **162**, 223.
Adams, A. A., G. E. Mitchell, and J. F. Shriner, Jr., 1998, Phys. Lett. B **422**, 13.
Agassi, D., C. M. Ko, and H. A. Weidenmüller, 1977, Ann. Phys. (N.Y.) **107**, 140.
Agvaanluvsan, U., G. E. Mitchell, J. F. Shriner, Jr., and M. P. Pato, 2003, Nucl. Instrum. Methods Phys. Res. A **498**, 459.
Alhassid, Y., A. Novoselsky, and N. Whelan, 1990, Phys. Rev. Lett. **65**, 2971.
Alhassid, Y., and D. Vretenar, 1992, Phys. Rev. C **46**, 1334.
Alhassid, Y., and N. Whelan, 1991, Phys. Rev. Lett. **67**, 816.
Alhassid, Y., and N. Whelan, 1993, Phys. Rev. Lett. **70**, 572.
Alt, H., C. I. Barbosa, H.-D. Gräf, T. Guhr, H. L. Harney, R. Hofferbert, H. Rehfeld, and A. Richter, 1998, Phys. Rev. Lett. **81**, 4847.
Alt, H., H.-D. Gräf, H. L. Harney, R. Hofferbert, H. Lengeler, A. Richter, P. Schaardt, and H. A. Weidenmüller, 1995, Phys. Rev. Lett. **74**, 62.
Altland, A., and M. R. Zirnbauer, 1997, Phys. Rev. B **55**, 1142.
Arima, A., and F. Iachello, 1975, Phys. Rev. Lett. **35**, 1069.

Arvieu, R., F. Brut, J. Carbonell, and J. Touchard, 1987, Phys. Rev. A **35**, 2389.
Axel, P., 1962, Phys. Rev. **126**, 671.
Bae, M. S., T. Otsuka, T. Misusaki, and N. Fukunishi, 1992, Phys. Rev. Lett. **69**, 2349.
Balian, R., 1968, Nuovo Cimento B **57**, 183.
Balian, R., and C. Bloch, 1970, Ann. Phys. (N.Y.) **60**, 401.
Baltes, H. P., and E. R. Hilf, 1976, *Spectra of Finite Systems* (Wissenschaftsverlag, Mannheim).
Barbosa, C. I., T. Guhr, and H. L. Harney, 2000, Phys. Rev. E **62**, 1936.
Benet, L., and H. A. Weidenmüller, 2003, J. Phys. A **36**, 3569.
Berry, M. V., 1981, Ann. Phys. (N.Y.) **131**, 163.
Berry, M. V., 1985, Proc. R. Soc. London, Ser. A **400**, 229.
Berry, M. V., and M. Robnik, 1984, J. Phys. A **17**, 2413.
Berry, M. V., and M. Tabor, 1977, Proc. R. Soc. London, Ser. A **356**, 375.
Bertulani, C. A., and V. Yu. Ponomarev, 1999, Phys. Rep. **321**, 139.
Bilpuch, E. G., A. M. Lane, G. E. Mitchell, and J. D. Moses, 1976, Phys. Rep., Phys. Lett. **28**, 145.
Blocki, J., J. Skalski, and W. J. Swiatecki, 1995, Nucl. Phys. A **594**, 137.
Bohigas, O., and J. Flores, 1971, Phys. Lett. **34B**, 261.
Bohigas, O., and M. J. Giannoni, 1984, *Mathematical and Computational Methods in Nuclear Physics* (Springer, Heidelberg), p. 209.
Bohigas, O., M. J. Giannoni, and C. Schmit, 1984, Phys. Rev. Lett. **52**, 1.
Bohigas, O., R. U. Haq, and A. Pandey, 1983, in *Nuclear Data for Science and Technology*, edited by K. H. Böckhoff (Reidel, Dordrecht), p. 809.
Bohigas, O., and P. Leboeuf, 2002, Phys. Rev. Lett. **88**, 092502.
Bohigas, O., and M. P. Pato, 2004, Phys. Lett. B **595**, 171.
Bohigas, O., and H. A. Weidenmüller, 1988, Annu. Rev. Nucl. Part. Sci. **38**, 421.
Bohle, D., A. Richter, W. Steffen, A. E. L. Dieperink, N. Lo Iudice, F. Palumbo, and O. Scholten, 1984, Phys. Lett. **137B**, 27.
Bohr, A., 1951, Phys. Rev. **81**, 134.
Bohr, A., 1952, K. Dan. Vidensk. Selsk. Mat. Fys. Medd. **26**, No. 14.
Bohr, A., and B. Mottelson, 1969, *Nuclear Structure* (Benjamin, New York), Vol. 1 [also Vol. 2 (1975)].
Bohr, A., and B. R. Mottelson, 1952, K. Dan. Vidensk. Selsk. Mat. Fys. Medd. **27**, No. 16.
Bohr, N., 1936, Nature **137**, 344.
Bollinger, L. M., and G. E. Thomas, 1968, Phys. Rev. **171**, 1293.
Bollinger, L. M., and G. E. Thomas, 1970, Phys. Rev. C **2**, 1951.
Brack, M., and R. K. Bhaduri, 1997, *Semiclassical Physics* (Addison-Wesley, New York).
Brack, M., J. Damgaard, A. S. Jensen, H. C. Pauli, V. M. Strutinsky, and C. Y. Wong, 1972, Rev. Mod. Phys. **44**, 320.
Brink, D., 1955, D. Phil. thesis, Oxford University.
Brink, D., J. Neto, and H. A. Weidenmüller, 1979, Phys. Lett. **80B**, 170.
Brody, T. A., J. Flores, J. B. French, P. A. Mello, A. Pandey, and S. S. M. Wong, 1981, Rev. Mod. Phys. **53**, 385.
Brown, B. A., and G. Bertsch, 1984, Phys. Lett. **148B**, 5.
Brown, B. A., and B. H. Wildenthal, 1988, Annu. Rev. Nucl. Part. Sci. **38**, 29.
Bulgac, A., and D. Kusnezov, 1996, Phys. Rev. E **54**, 3468.
Bunakov, V. E., 1999, Yad. Fiz. **62**, 5 [Phys. At. Nucl. **62**, 1 (1999)].
Caldeira, A. O., and A. J. Leggett, 1983, Ann. Phys. (N.Y.) **149**, 374.
Carlson, B. V., L. F. Canto, S. Cruz-Barrios, M. S. Hussein, and A. F. R. de Toledo Piza, 1999, Ann. Phys. (N.Y.) **276**, 111.
Carlson, B. V., M. S. Hussein, A. F. R. de Toledo Piza, and L. F. Canto, 1999, Phys. Rev. C **60**, 014604.
Casati, G., F. Valz-Gris, and I. Guarneri, 1980, Lett. Nuovo Cimento Soc. Ital. Fis. **28**, 279.
Cassing, W., and W. Nörenberg, 1985, Nucl. Phys. A **433**, 467.
Caurier, E., G. Martinez-Pinedo, F. Nowacki, A. Poves, and A. P. Zuker, 2005, Rev. Mod. Phys. **77**, 427.
Caurier, E., G. Martinez-Pinedo, F. Nowacki, J. Retamosa, and A. P. Zuker, 1999, Phys. Rev. C **59**, 2033.
Chevalley, C., 1946, *Theory of Lie Groups* (Princeton University Press, Princeton).
Conway, J., 1990, *A Course in Functional Analysis* (Springer, New York).
Dembowski, C., B. Dietz, T. Friedrich, H.-D. Gräf, H. L. Harney, A. Heine, M. Miski-Oglu, and A. Richter, 2005, Phys. Rev. E **71**, 046202.
De Pace, A., A. Molinari, and H. A. Weidenmüller, 2007, Ann. Phys. (N.Y.) **322**, 2446.
De Shalit, A., and I. Talmi, 1963, *Nuclear Shell Theory* (Academic, New York).
Dias, H., M. S. Hussein, N. A. de Oliveira, and B. H. Wildenthal, 1989, J. Phys. G **15**, L79.
Dieperink, A. E. L., O. Scholten, and F. Iachello, 1980, Phys. Rev. Lett. **44**, 1747.
Dietz, B., T. Guhr, H. L. Harney, and A. Richter, 2006, Phys. Rev. Lett. **96**, 254101.
Døssing, T., B. Herskind, S. Leoni, A. Bracco, R. A. Broglia, M. Matsuo, and E. Vigezzi, 1996, Phys. Rep. **268**, 1.
Døssing, T., A. P. Lopez-Martens, T. L. Khoo, T. Lauritsen, and S. Åberg, 2004, in *The Labyrinth in Nuclear Structure*, edited by A. Braco and C. A. Kalfas (AIP, Melville, NY), p. 164.
Duflo, J., and A. P. Zuker, 1995, Phys. Rev. C **52**, R23.
Dyson, F. J., and M. L. Mehta, 1963, J. Math. Phys. **4**, 701.
Ellegaard, C., T. Guhr, K. Lindeman, J. Nygard, and M. Oxborrow, 1996, Phys. Rev. Lett. **77**, 4918.
Enders, J., T. Guhr, A. Heine, P. von Neuman-Cosel, V. Yu. Ponomarev, A. Richter, and J. Wambach, 2004, Nucl. Phys. A **741**, 3.
Enders, J., T. Guhr, N. Huxel, P. von Neuman-Cosel, C. Rangacharyulu, and A. Richter, 2000, Phys. Lett. B **486**, 273.
Fermi, E., E. Amaldi, O. D'Agostino, F. Rasetti, and E. Segre, 1934, Proc. R. Soc. London, Ser. A **146**, 483.
Fermi, E., E. Amaldi, O. D'Agostino, F. Rasetti, and E. Segre, 1935, Proc. R. Soc. London, Ser. A **149**, 522.
Flambaum, V. V., A. A. Gribakina, G. F. Gribakin, and M. G. Kozlov, 1994, Phys. Rev. A **50**, 267.
Frazier, N., B. A. Brown, and V. Zelevinsky, 1996, Phys. Rev. C **54**, 1665.
French, J. B., V. K. B. Kota, A. Pandey, and S. Tomsovic, 1985, Phys. Rev. Lett. **54**, 2313.
French, J. B., and S. S. M. Wong, 1970, Phys. Lett. B **33**, 449.
Garg, J. B., J. Rainwater, J. S. Petersen, and W. W. Havens, Jr., 1964, Phys. Rev. **134**, B985.
Garrett, J. D., J. Q. Robinson, A. J. Foglia, and H.-Q. Jin, 1997, Phys. Lett. B **392**, 24.
Gaudin, M., 1961, Nucl. Phys. **25**, 447.
Gavron, A., A. Gayer, J. Boissevain, H. C. Britt, J. R. Nix, A. J. Sierk, P. Grangé, S. Hassani, H. A. Weidenmüller, J. R.

Beene, B. Cheynis, D. Drain, R. L. Ferguson, F. E. Obenshain, F. Plasil, G. R. Young, G. A. Petitt, and C. Butler, 1986, Phys. Lett. B **176**, 312.
Grangé, P., and H. A. Weidenmüller, 1980, Phys. Lett. B **96**, 26.
Grossmann, C. A., M. A. LaBonte, G. E. Mitchell, J. D. Shriner, J. F. Shriner, Jr., G. A. Vavrina, and P. M. Wallace, 2000, Phys. Rev. C **62**, 024323.
Gu, J. Z., and H. A. Weidenmüller, 1999, Nucl. Phys. A **660**, 197.
Gu, J. Z., and H. A. Weidenmüller, 2001, Nucl. Phys. A **690**, 382.
Guhr, T., A. Müller-Groeling, and H. A. Weidenmüller, 1998, Phys. Rep. **299**, 189.
Guhr, T., and H. A. Weidenmüller, 1990a, Ann. Phys. (N.Y.) **199**, 412.
Guhr, T., and H. A. Weidenmüller, 1990b, Chem. Phys. **146**, 21.
Gurevich, I. I., and M. I. Pevsner, 1957, Nucl. Phys. **2**, 575.
Gutzwiller, M., 1990, *Chaos in Classical and Quantum Mechanics* (Springer, Berlin).
Haake, F., 2001, *Quantum Signatures of Chaos*, 2nd ed. (Springer, Berlin).
Hackenbroich, G., and H. A. Weidenmüller, 1995, Phys. Rev. Lett. **74**, 4118.
Hamoudi, A., R. G. Nazmitdinov, E. Shahaliev, and Y. Alhassid, 2002, Phys. Rev. C **65**, 064311.
Haq, R. U., A. Pandey, and O. Bohigas, 1982, Phys. Rev. Lett. **48**, 1086.
Harish-Chandra, 1957, Am. J. Math. **79**, 87.
Harney, H. L., 1984, Z. Phys. A **316**, 177.
Harney, H. L., A. Richter, and H. A. Weidenmüller, 1986, Rev. Mod. Phys. **58**, 607.
Haxel, O., J. H. D. Jensen, and H. E. Suess, 1949, Phys. Rev. **75**, 1766.
Heiss, W. D., R. G. Nazmitdinov, and S. Radu, 1994, Phys. Rev. Lett. **72**, 2351.
Herskind, B., B. Lauritzen, K. Schiffer, R. A. Broglia, F. Barranco, M. Gallardo, J. Dudek, and E. Vigezzi, 1987, Phys. Rev. Lett. **59**, 2416.
Heusler, S., S. Müller, A. Altland, P. Braun, and F. Haake, 2007, Phys. Rev. Lett. **98**, 044103.
Hofmann, H., F. A. Ivanyuk, C. Rummel, and S. Yamaji, 2001, Phys. Rev. C **64**, 054316.
Hofmann, H., and P. J. Siemens, 1977, Nucl. Phys. A **275**, 464.
Honma, M., T. Otsuka, B. A. Brown, and T. Mizusaki, 2002, Phys. Rev. C **65**, 061301(R).
Hussein, M. S., and M. P. Pato, 2000, Phys. Rev. Lett. **84**, 3783.
Iachello, F., and A. Arima, 1987, *The Interacting Boson Model* (Cambridge University Press, Cambridge).
Iachello, F., and I. Talmi, 1987, Rev. Mod. Phys. **59**, 339.
Imry, Y., 2002, *Introduction to Mesoscopic Physics*, 2nd ed. (Oxford University Press, Oxford).
Itzykson, C., and J. B. Zuber, 1980, J. Math. Phys. **21**, 411.
Johnson, C. W., G. F. Bertsch, and D. J. Dean, 1998, Phys. Rev. Lett. **80**, 2749.
Johnson, C. W., G. F. Bertsch, D. J. Dean, and I. Talmi, 1999, Phys. Rev. C **61**, 014311.
Jolie, J., R. F. Casten, P. Cejnar, S. Heinze, E. A. McCutchan, and N. V. Zamfir, 2004, Phys. Rev. Lett. **93**, 132501.
Koehler, P. E., J. L. Ullmann, T. A. Bredeweg, J. M. O'Donnell, R. Reifarth, R. S. Rundberg, D. J. Vieira, and J. M. Wouters, 2007, Phys. Rev. C **76**, 025804.
Kota, V. K. B., 2001, Phys. Rep. **347**, 223.
Kota, V. V. B., 2007, J. Math. Phys. **48**, 053304.
Krücken, R., A. Dewald, P. von Brentano, and H. A. Weidenmüller, 2001, Phys. Rev. C **64**, 064316.
Lane, A. M., and R. G. Thomas, 1958, Rev. Mod. Phys. **30**, 257.
Leboeuf, P., and J. Roccia, 2006, Phys. Rev. Lett. **97**, 010401.
Leviandier, L., M. Lombardi, R. Jost, and J. P. Pique, 1986, Phys. Rev. Lett. **56**, 2449.
Lewenkopf, C., and V. Zelevinsky, 1994, Nucl. Phys. A **569**, 183.
Liou, H. I., H. S. Camarda, and F. Rahn, 1972, Phys. Rev. C **5**, 1002.
Liou, H. I., H. S. Camarda, S. Wynchank, M. Slagowitz, G. Hacken, F. Rahn, and J. Rainwater, 1972, Phys. Rev. C **5**, 974.
Lombardi, M., O. Bohigas, and T. Seligman, 1994, Phys. Lett. B **324**, 263.
Lombardi, M., and T. H. Seligman, 1993, Phys. Rev. A **47**, 3571 (1993).
Lynn, J. E., 1968, *The Theory of Neutron Resonances* (Clarendon, Oxford).
Mahaux, C., and H. A. Weidenmüller, 1969, *Shell-Model Approach to Nuclear Reactions* (North-Holland, Amsterdam).
Martinez-Pinedo, G., A. P. Zuker, A. Poves, and E. Caurier, 1997, Phys. Rev. C **55**, 187.
Matsuo, M., T. Døssing, E. Vigezzi, and S. Åberg, 1997, Nucl. Phys. A **620**, 296.
Mayer, M. G., 1949, Phys. Rev. **75**, 1969.
Mayer, M. G., and J. H. D. Jensen, 1955, *Elementary Theory of Nuclear Shell Structure* (Wiley, New York).
McDonald, S. W., and A. N. Kaufman, 1979, Phys. Rev. Lett. **42**, 1189.
Mehta, M. L., 2004, *Random Matrices*, 3rd ed. (Academic, New York).
Meredith, D. C., 1993, Phys. Rev. E **47**, 2405.
Meredith, D. C., S. E. Koonin, and M. R. Zirnbauer, 1988, Phys. Rev. A **37**, 3499.
Mitchell, G. E., E. G. Bilpuch, J. F. Shriner, Jr., and A. M. Lane, 1985, Phys. Rep. **117**, 1.
Mitchell, G. E., and J. F. Shriner, Jr., 2001, Phys. Scr., T **90**, 105.
Molinari, A., and H. A. Weidenmüller, 2006, Phys. Lett. B **637**, 48.
Möller, P., J. R. Nix, W. D. Myers, and W. J. Swiatecki, 1995, At. Data Nucl. Data Tables **59**, 185.
Mon, K. F., and J. B. French, 1975, Ann. Phys. (N.Y.) **95**, 90.
Mottelson, B. R., 1992, Nucl. Phys. A **557**, 717.
Nature, 1936, Nature **137**, 351.
Neutron Cross Section, 1964, Sigma Center, Brookhaven National Laboratory BNL 325, Suppl. 2, Brookhaven, NY.
Nörenberg, W., and H. A. Weidenmüller, 1980, *Introduction to the Theory of Heavy-Ion Reactions*, 2nd ed. (Springer, Berlin).
Olofsson, H., Åberg, O. Bohigas, and P. Leboeuf, 2006, Phys. Rev. Lett. **96**, 042502.
Ormand, W. E., and R. A. Broglia, 1992, Phys. Rev. C **46**, 1710.
Pandey, A., 1981, Ann. Phys. (N.Y.) **134**, 110.
Papenbrock, T., Z. Pluhar, and H. A. Weidenmüller, 2006, J. Phys. A **39**, 9709.
Papenbrock, T., and H. A. Weidenmüller, 2004, Phys. Rev. Lett. **93**, 132503.
Papenbrock, T., and H. A. Weidenmüller, 2005, Nucl. Phys. A **757**, 422.
Papenbrock, T., and H. A. Weidenmüller, 2006, Phys. Rev. C **73**, 014311.
Papenbrock, T., and H. A. Weidenmüller, 2007, Rev. Mod. Phys. **79**, 997.
Percival, I. C., 1973, J. Phys. B **6**, L229.

Pieper, S. C., and R. B. Wiringa, 2001, Annu. Rev. Nucl. Part. Sci. **51**, 53.
Porter, C. E., 1965, *Statistical Theories of Spectra: Fluctuations* (Academic, New York).
Ragnarsson, I., and S. Åberg, 1986, Phys. Lett. B **180**, 191.
Raman, S., T. A. Walkiewicz, S. Kahane, E. T. Jurney, J. Sa, Z. Gacsi, J. L. Weil, K. Allart, G. Bonsignori, and J. F. Shriner, Jr., 1991, Phys. Rev. C **43**, 521.
Richter, A., 1995, Prog. Part. Nucl. Phys. **34**, 261.
Roccia, J., and P. Leboeuf, 2007, Phys. Rev. C **76**, 014301.
Rosenzweig, N., and C. E. Porter, 1960, Phys. Rev. **120**, 1698.
Sakhr, J., and N. D. Whelan, 2003, Phys. Rev. E **67**, 066213.
Samyn, M., S. Goriely, M. Bender, and J. M. Pearson, 2004, Phys. Rev. C **70**, 044309.
Sargeant, A. J., M. S. Hussein, and A. N. Wilson, 2005, in *Nuclei and Mesoscopic Physics*, edited by V. Zelevinsky (AIP, Melville, NY), p. 46.
Shimizu, Y. R., F. Barranco, R. A. Broglia, T. Døssing, and E. Vigezzi, 1992, Phys. Lett. B **274**, 253.
Shriner, J. F., Jr., E. G. Bilpuch, and G. E. Mitchell, 1989, Z. Phys. A **332**, 45.
Shriner, J. F., Jr., C. A. Grossmann, and G. E. Mitchell, 2000, Phys. Rev. C **62**, 054305.
Shriner, J. F., Jr., G. E. Mitchell, and E. G. Bilpuch, 1987, Phys. Rev. Lett. **59**, 435.
Shriner, J. F., Jr., G. E. Mitchell, and T. von Egidy, 1991, Z. Phys. A **338**, 309.
Soloviev, V. G., 1995, Nucl. Phys. A **586**, 265.
Sommermann, M., and H. A. Weidenmüller, 1993, Europhys. Lett. **23**, 79.
Stafford, C. A., and B. R. Barrett, 1999, Phys. Rev. C **60**, 051305(R).
Stephens, F. S., *et al.*, 2005, Phys. Rev. Lett. **94**, 042501.
Strutinsky, V. M., 1966, Yad. Fiz. **3**, 614 [Sov. J. Nucl. Phys. **3**, 499 (1966)].
Strutinsky, V. M., 1967, Nucl. Phys. A **95**, 420.
Strutinsky, V. M., 1968, Nucl. Phys. A **122**, 1.
Twin, P. J., B. M. Nyako, A. H. Nelson, J. Simpson, M. A. Bentley, H. W. Cranmer-Gordon, P. D. Forsyth, D. Howe, A. R. Mokhtar, J. D. Morrison, J. F. Sharpey-Schafer, and G. Sletten, 1986, Phys. Rev. Lett. **57**, 811.
Verbaarschot, J. J. M., and P. J. Brussard, 1979, Phys. Lett. **87**, 155.
Vigezzi, E., R. A. Broglia, and T. Døssing, 1990a, Nucl. Phys. A **520**, c179.
Vigezzi, E., R. A. Broglia, and T. Døssing, 1990b, Phys. Lett. B **249**, 163.
von Egidy, T., A. N. Behkami, and H. H. Schmidt, 1986, Nucl. Phys. A **454**, 109.
von Egidy, T., H. H. Schmidt, and A. N. Behkami, 1988, Nucl. Phys. A **481**, 189.
Watson, W. A., III, E. G. Bilpuch, and G. E. Mitchell, 1981, Z. Phys. A **300**, 89.
Weidenmüller, H. A., 1980, Prog. Part. Nucl. Phys. **3**, 49.
Weidenmüller, H. A., 1985, in *Nuclear Structure 1985*, edited by R. Broglia, G. B. Hagemann, and B. Herskind (Elsevier, Amsterdam), p. 213.
Weidenmüller, H. A., 1993, Phys. Rev. A **48**, 1819.
Weidenmüller, H. A., P. von Brentano, and B. R. Barrett, 1998, Phys. Rev. Lett. **81**, 3603.
Whitehead, R. R., A. Watt, D. Kelvin, and A. Conkie, 1978, Phys. Lett. B **76**, 149.
Wilczynski, J., 1973, Phys. Lett. B **47**, 484.
Wildenthal, B. H., 1984, Prog. Part. Nucl. Phys. **11**, 5.
Wilson, W. M., E. G. Bilpuch, and G. E. Mitchell, 1975, Nucl. Phys. A **245**, 285.
Yoshinaga, N., A. Arima, and Y. M. Zhao, 2006, Phys. Rev. C **73**, 017303.
Yoshinaga, N., N. Yoshida, T. Shigehara, and T. Cheon, 1993, Phys. Rev. C **48**, R509.
Zelevinsky, V., 2007, private communication.
Zelevinsky, V., B. A. Brown, N. Frazier, and M. Horoi, 1996, Phys. Rep. **276**, 85.
Zelevinsky, V., and A. Volya, 2004, Phys. Rep. **391**, 311.
Zhao, Y. M., and A. Arima, 2001, Phys. Rev. C **64**, 041301(R).
Zhao, Y. M., A. Arima, N. Shimizu, K. Ogawa, N. Yoshinaga, and O. Scholten, 2004, Phys. Rev. C **70**, 054322.
Zhao, Y. M., A. Arima, and N. Yoshinaga, 2002, Phys. Rev. C **66**, 034302.
Zhao, Y. M., A. Arima, and N. Yoshinaga, 2004, Phys. Rep. **400**, 1.